Czech Technical University in Prague
Faculty of Nuclear Sciences and Physical Engineering

Dissertation thesis

# Investigation of deformation processes in NiTi shape memory alloys by synchrotron x-ray diffraction

Prague 2017

Pavel Sedmák

# Bibliografický záznam

| | |
|---|---|
| Autor | Ing. Pavel Sedmák, České vysoké učení technické v Praze, Fakulta jaderná a fyzikálně inženýrská, Katedra materiálů |
| Název práce | Studium deformačních procesů ve slitinách s tvarovou pamětí NiTi pomoci difrakce |
| Studijní program | Aplikace přírodních věd |
| Studijní obor | Fyzikální inženýrství |
| Školitel | Prof. Dr. RNDr. Miroslav Karlík, České vysoké učení technické v Praze, Fakulta jaderná a fyzikálně inženýrská, Katedra materiálů |
| Školitel specialista | RNDr. Petr Šittner, CSc., Fyzikální ústav, Oddělení funkčních materiálů, Akademie věd, ČR |
| Akademický rok | 2016/2017 |
| Počet stran | 157 |
| Klíčová slova | Materiály s tvarovou pamäťou, martenzitická transformácia, NiTi, únava, termomechanické cyklovanie, LTSS, superelasticita, lokalizovaná deformácia, Rtg difrakcia |

## Bibliographic entry

| | |
|---|---|
| Author | Ing. Pavel Sedmák, Czech Technical University in Prague, Faculty of Nuclear Sciences and Physical Engineering, Department of Materials |
| Title of Dissertation | Investigation of deformation processes in NiTi shape memory Alloys by synchrotron x-ray diffraction |
| Degree Programme | Application of Natural Sciences |
| Field of Study | Physical Engineering |
| Supervisor | Prof. Dr. RNDr. Miroslav Karlík, Czech Technical University in Prague, Faculty of Nuclear Sciences and Physical Engineering, Department of Materials |
| Supervisor specialist | RNDr. Petr Šittner, CSc., Institute of Physics, Department of Functional Materials, Czech Academy of Sciences |
| Academic year | 2016/2017 |
| Number of pages | 157 |
| Keywords | Shape memory alloys, martensitic transformation, NiTi, fatigue, thermomechanical cycling, low temperature shape setting, superelasticity, localized deformation, x-ray diffraction |

# Abstrakt

Zliatiny s tvarovou pamäťou patria do skupiny funkčných materiálov, ktoré našli široké uplatnenie v mnohých inžinierskych aplikáciách, najmä v oblasti biomedicíny či ako jednoduché aktuátory. Schopnosť týchto zliatin zapamätať si tvar a vrátiť sa do pôvodného stavu po značnej deformácii, vychádza z bezdifúznej martenzitickej transformácie vyvolanej zmenou vonkajšieho napätia či teploty. Potenciál ich uplatnenia by bol oveľa väčší, keby bolo prepojenie martenzitickej transformácie a plasticity pri zvýšených teplotách, ovplyvňujúcich ich funkčnú stabilitu a únanovú životnosť, lepšie pochopené či úplne potlačené.

Pre úspešné uplatnenie týchto zliatin v inžinierskych aplikáciách vyžadujúcich cyklické zaťažovanie, musí byť vyriešený jeden z ich hlavných nedostatkov, ktorým je slabá funkčná a štruktúrna životnosť počas cyklického namáhania. V predkladanej práci som študoval procesy vedúce k degradácii funkčných vlastností NiTi zliatin a slabú únavovú životnosť. Skúmal som nestabilnú makroskopickú odozvu superelastických a aktuátorových NiTi drôtov, vystavených cyklickému mechanickému alebo termomechanickému namáhaniu. Experimenty zahrňovali vyhodnocovanie in-situ elektrického odporu drôtu, in-situ synchrotrónovú röntgenovú difrakciu, in-situ digitálnu obrazovú koreláciu povrchových deformácii a ex-situ TEM pozorovanie mikroštruktúry testovaných drôtov.

Boli uskutočnené experimenty cyklického superelastického ťahového namáhania tenkých NiTi drôtov s rôznymi mikroštruktúrami, s cieľom zistiť príčinu nestabilného chovania materiálu. Usúdil som, že funkčná únava je spôsobená postupným prerozdelením vnútorných napätí počas cyklovania vznikajúcich kvôli inkrementálnej plastickej deformácii sprevádzajúcej martenzitickú transformáciu v polykryštalickom materiále. Tieto vnútorné zmeny vedú k zmene napäťovo-deformačnej odozvy počas cycklického namáhania – k funkčnej únave. Miera nestability závisí na odolnosti NiTi mriežky voči plastickej deformácii.

S rovnakým zámerom boli uskutočnené experimenty tepelného cyklovania na dvoch typoch drôtov podrobených rôznym úrovniam konštantného vonkajšieho napätia. V práci je ukázané, že za nestabilnú tepelno-deformačnú odozvu je zodpovedný inkrementálny nárast plastickej deformácie prebiehajúcej spolu so spätnou martenzitickou transformáciou, nastávajúci v každom cykle počas ohrevu za podmienok obmedzujúcich rozmerové zmeny vzorky. Nárast plastickej deformácie nastáva keď napätie a teplota prekročia kritickú hranicu a kedy je martenzit ešte prítomný v mikroštruktúre vzorky. Drôt namáhaný v ťahu sa pri cyklickej tepelnej deformácii postupne predlžuje, ale nestráca svoje funkčné vlastnosti.

Pre overenie predpokladaného prepojenia plasticity a transformácie boli uskutočnené termomechanické experimenty za podmienok, ktoré toto prepojenie podporujú – ohrev/chladenie – pri podmienkach obmedzujúcich dĺžku NiTi drôtu. Zistil som, že ak je

deformovaný NiTi drôt ohrievaný za podmienok obmedzujúcich jeho dĺžku, prebieha v ňom spätná martenzitická transformácia prepojená s plastickou deformáciou dislokačným sklzom a dvojčatením. Inými slovami, pri ohreve NiTi drôtu obsahujúceho orientovaný martenzit pri izbovej teplote za podmienok obmedzujúcich jeho dĺžku, sa postupne mení na drôt obsahujúci plasticky deformovaný austenit s mikroštruktúrou obsahujúcou vysokú hustotu spletí dislokácii, stien domén, vnútorných deformácii a lamelárnych defektov identifikovaných ako {114} austenitické dvojčatá. Spätná martenzitická deformácia prepojená s plastickou deformáciou je interpretovaná ako unikátný TRIP deformačný mechanizmus pôsobiaci v NiTi zliatinách pri zvýšených teplotách a napätiach. Tento deformačný mechanizmus hrá kľúčovú úlohu v NiTi technológiách, najmä v prípade “shape setting”, aktuácie a tréningu pre jav dvojcestnej tvarovej pamäti.

V poslednej časti som skúmal lokalizovanú superelastickú deformáciu NiTi drôtu namáhaného v ťahu, ktorá prebieha pohybom makroskopických rozhraní (čelá martenzitických sklzových pásov) pri konštantnom ťahovom napätí. Tento jav je veľmi dôležitý, pretože ťahová skúška na NiTi drôtoch je všeobecne považovaná za základný test charakterizujúci funkčné vlastnosti materiálu. Uskutočnil som jedinečný experiment zameraný na charakterizáciu čela martenzitického sklzového pásu pomocou 3D-RTG mikroskopie na ID11 Beamline, ESRF. Podarilo sa mi určiť tenzory deformácie a napätia v ~15000 austenitických zrnách v okolí rozhrania a z nich charakterizovať makroskopické vnútorné deformačné a napäťové polia obklopujúce čelo konkávneho rozhrania. Lokálne napätia v zrnách na čele rozhrania sú rozložené takým spôsobom, že v zrnách, ktoré sa nachádzajú na čele rozhrania je oveľa vyššie šmykové napätie v porovnaní so zrnami ďaleko od rozhrania. V dôsledku toho tieto zrná transformujú spoločne zatiaľ čo v iných miestach drôtu sa nič nedeje. Pretože maximálna neelastická deformácia prostredníctvom martenzitickej transformácie je obmedzená kryštalografickými podmienkami transformácie, čelo rozhrania sa pohybuje pozdĺž drôtu pri konštantnom napätí. Mechanizmus, ktorým sa rozhranie pohybuje drôtom bol objasnený porovnaním experimentálnych dát s výsledkami MKP simulácie lokalizovanej deformácie použitím termomechanického modelu vyvinutého pre NiTi polykryštál. Zistili sme, že predpoklad často používaný v literatúre, že martenzitická transformácia v polykryštalickom NiTi drôte v ťahu nastáva pri konštantnom nominálnom ťahovom napätí nie je celkom správna. Napäťové stavy v transformujúcich zrnách sú veľmi vzdialené od ťahových a ekvivalentné napätia su oveľa vyššie ako nominálne napätie vypočítané zo sily pôsobiacej na drôt.

# Abstract

Shape memory alloys are functional materials that have already found many engineering applications, mainly as biomedical devices and simple actuators. The ability of SMAs to recover their original shape after large deformation originates from the diffusionless martensitic transformation driven by stress and/or temperature. However, their application potential could be much increased if concurrent martensitic transformation and plasticity taking place at elevated temperatures and affecting their functional stability and fatigue performance is prevented or better understood.

To successfully employ shape memory alloy elements in cyclic engineering applications, stable functional properties and good structural fatigue performance has to be guaranteed. In my thesis, I have studied the processes leading to a degradation of the functional properties of NiTi and poor fatigue performance. I investigated unstable macroscopic response of superelastic and actuator NiTi wires subjected to cyclic mechanical and thermomechanical loads. The thermomechanical loading experiments involved also evaluation of in-situ electric resistance of the wire, in-situ synchrotron x-ray diffraction, in-situ digital image correlation of surface strains and ex-situ TEM observation of microstructures in tested wires.

Cyclic superelastic loading of thin NiTi wires with different initial microstructure was investigated to reveal the origin of the cyclic instability. I have found that the gradual redistribution of internal stress upon cycling arises from incremental plastic deformation accompanying martensitic transformation within the constrained polycrystalline aggregate. It leads to a gradual change of stress-strain response upon cycling - functional fatigue. With decreasing matrix slip resistance, the rate of the cyclic instability increases.

Cyclic thermal loading tests on two types of NiTi actuator wires under various constant external loads was performed with the same purpose. I have found, that the instability of strain-temperature response is mainly due to the incremental plastic deformation taking place alongside the reverse martensitic transformation during the constrained heating when the oriented martensite is still present in the wire and the applied stress and temperature exceed a particular limit. There is no plasticity on cooling under stress. The cycled wire gradually elongates but does not lose its actuator functionality.

Thermomechanical loading experiments involving constrained heating/cooling after deformation in martensite state were performed to investigate in detail the coupled martensitic transformation and plasticity in NiTi wires. I have found that heating of a deformed NiTi wire under external constraint triggers a reverse martensitic transformation coupled with a plastic deformation due to dislocation slip and twinning. It was observed that a constrained NiTi wire containing oriented martensite at room temperature, becomes gradually converted into a plastically deformed austenitic wire upon heating with a new microstructure containing high

density of dislocation tangles, domain walls, internal strain and lamellar defects identified as {114} austenite twins. The reverse martensitic transformation coupled with plastic deformation was interpreted as a unique TRIP like deformation mechanism acting in NiTi shape memory alloys at elevated temperatures and large stresses. The mechanism is claimed to be very important for NiTi technology, particularly for the shape setting, actuation and two-way shape memory effect training.

Finally, I investigated the localized superelastic deformation of NiTi wires in tension proceeding via motion of macroscopic interfaces (martensite band fronts) under constant applied stress. This phenomenon is very important in SMA field since a tensile test on NiTi wire is generally considered as a basic test characterizing the functional properties. A unique experiment focused on the characterization of the martensite band front was performed by means of 3D-XRD microscopy using ID11 beamline at ESRF. I determined the strain and stress tensors in ~15000 austenitic grains within the martensite band front. From them I reconstructed the macroscopic internal stress and strain fields in the wire surrounding the nose cone shaped front. It was revealed that the local stresses in the grains ahead of the advancing front redistribute in such a way that the grains located at the buried conical interface experience much higher shear stresses compared to other grains far from the interface. Consequently, these grains transform collectively while very little is happening elsewhere in the wire. Because the maximum inelastic deformation via martensitic transformation is limited due to crystallography of the transformation, the martensite band front moves along the wire under constant applied force. Finite Element model of the localized deformation using a thermomechanical model of NiTi polycrystal was confronted with the experimental results to reveal the mechanism by which the front propagates through the wire. It was found that the assumption frequently adopted in the literature that the martensitic transformation in a polycrystalline NiTi wire loaded in tension takes place under nominal tensile stress is not quite correct – stress states in the transforming grains are very far from the tensile and equivalent stresses are much higher than the nominal stress calculated from the applied force.

# Table of Contents

# Acknowledgement

First, I would like to thank my supervisor specialist Dr. Petr Šittner for excellent guidance, support and motivation throughout the whole PhD studies. Gratitude goes also to my academic supervisor prof. Miroslav Karlík for leading my studies and motivating me to fulfil all academic duties.

I thank my fellow lab mates from the Department of Functional Materials of the Institute of Physics of the CAS for their support and stimulating discussions. Also, I would like to express my gratitude for their assistance with the complementary DIC, SEM and TEM measurements, which helped me to better understand what I measured.

Special thanks go to ID22 and ID11 ESRF beamline staff, namely Caroline Curfs, Andy Fitch, and Jon Wright, for all their support and assistance with the experiments and data analysis, which I could not make without them.

Last but not least, I would like to thank my family, my parents and my brother for supporting me throughout life, and my beloved wife, for all their love, help and tolerance during my PhD studies.

This work was financially supported by research projects of the Grant Agency of Czech Republic, P107/12/0800, 14-15264S and 16-20264S, SGS projects SGS13/222/OHK4/3T/14, SGS16/249/OHK4/3T/, FZU-ESRF PhD grant, proposals MA2133 and MA2900 and inhouse beamtime at ID22 and ID11.

# Symbols and abbreviations

## General symbols

| | |
|---|---|
| $A_f$ | Austenite finish temperature |
| $A_s$ | Austenite start temperature |
| d | spacing between crystallographic planes |
| I | Intensity of diffracted X-rays |
| $M_f$ | Martensite finish temperature |
| $M_s$ | Martensite start temperature |
| Q | Reciprocal lattice vector length |
| $2\Theta$ | X-ray scattering angle |
| $\varepsilon$ | Strain |
| $\varepsilon_t$ | Transformation strain |
| $\sigma$ | Stress |
| $\sigma_c$ | Critical stress to induce martensite |

## Abbreviations

| | |
|---|---|
| CV | Correspondence variants |
| CW | Cold work |
| DIC | Digital Image Correlation |
| EBSD | Electron backscatter diffraction |
| FWHM | Full width at half maximum |
| HPV | Habit plane variant |
| LTSS | Low temperature shape setting |
| MT | Martensitic transformation |
| SEM | Scanning electron microscopy |
| SMA | Shape memory alloys |
| SME | Shape memory effect |
| TEM | Transmission electron microscopy |
| XRD | X-ray diffraction |

# 1 Introduction

## 1.1 Problem statement

Shape Memory Alloys (SMA) belong to a class of functional materials due to their exceptional behaviour under thermomechanical loads originating from the reversible martensitic transformation (MT). Among these materials, NiTi-based alloys gained the greatest interest and thus the highest number of resulting applications. The origin of NiTi goes back to 1963, when it was discovered by Buehler et al [1] at Naval Ordnance Laboratory. The laboratory initials were included in its alias dictus and since then it is referred to as NiTinol. Soon after its discovery NiTi attracted great attention, partly because of the unique thermomechanical properties and partly because of its commercial availability and fast growing number of its technological and engineering applications in areas such as medical devices (stents, surgical instruments, endodontic instruments and many others) [2,3], industrial applications (various thermal actuators, couplings, microactuators) [3] in automotive and aerospace industry [2]. All these applications benefit from NiTinol's superior properties when compared to other shape memory alloys such as CuAlNi, CuZnAl, NiMnGa etc. In comparison to these SMAs, NiTi possesses the best ductility (they exhibit up to 50% elongation) while keeping high tensile strength. NiTi alloys also have high corrosive resistance, which is beneficial for their medical application [4].

In essence, SMA display two interesting properties; shape memory effect and superelasticity. The former is the ability of material to recover its previous shape upon heating when deformed below a critical transformation temperature $M_f$, while the latter is the ability of material to recover large strains beyond its elastic limit when deformed in an austenitic phase [5].

In the context of engineering applications of NiTi, the fatigue remains the biggest challenge, which prevents further grow of the technology. Fatigue of SMA is classified as structural and functional. The former is the same as in other conventional materials – nucleation and propagation of a crack, while the latter means degradation of functional properties.

Transformation between the parent high temperature cubic austenite and the product low temperature monoclinic martensite in NiTi is induced by increasing stress and/or decreasing temperature. For both stress (superelastic applications) and temperature (actuators) induced transitions, the functional fatigue causes unstable stress-strain (strain-temperature) response upon thermomechanical cycling. It is known that it is related to plastic deformation taking place simultaneously with the martensitic transformation. Nevertheless, despite its practical importance, the origin of the functional fatigue of NiTi on the microstructural level still remains to be clarified. In this respect, the high energy x-ray diffraction proved to be an excellent tool for investigating the evolution of the microstructure (phase fraction, defects, internal stress) upon cycling and studying thus the origin of the functional fatigue. When used in combination with macroscopic thermomechanical testing with in-situ electric resistivity evaluation supported by complementary techniques such as DIC, TEM or EBSD, the sources of the instable behaviour can be clarified as will be shown in this work.

This work is, nevertheless, dedicated primarily to my in-situ synchrotron X-ray diffraction studies of the functional degradation processes taking place in the thin NiTi SMA wires during cyclic thermomechanical loading. It was made as a part of the ongoing research of fatigue of NiTi wires in the group of Functional Department of IP ASRC, in the frame of the FACT (Fatigue of NiTiX High Temperature Shape Memory Actuators) GACR project. It was originally intended to study the functional fatigue of high temperature SMA. Due to the serious problems arising during production stage of high temperature NiTiHf wire samples by drawing process, mainly caused by the brittleness, which prevented drawing the wire samples, the goal of the work was deflected to a study of the functional fatigue of binary NiTi wires. Despite this fact, we believe that the processes causing the functional degradation of both high temperature NiTiX and NiTi SMA are qualitatively the same, but they are shifted to higher temperatures in case of high temperature NiTiX. Therefore, the combined plasticity-transformation processes responsible for the functional degradation can be studied on binary NiTi wires and the knowledge can be to some extent applied to high temperature shape memory alloys applications in the future.

## 1.2 Outline of the thesis

The main goal of this thesis is to investigate and reveal the processes responsible for functional fatigue of NiTi SMA wires subjected to various thermomechanical loading paths by means of in-situ synchrotron XRD particularly to thermal cycling under constant stress, superelastic cycling at constant temperature and recovery stress tests involving constrained heating/cooling after deformation in martensite state.

The first part of the thesis gives a theoretical background of the shape memory alloys, particularly NiTi alloys, their basic functional properties such as shape memory effect or superelasticity. State of art of the functional fatigue of NiTi shape memory alloys is discussed. Basic properties of NiTi wires, thermomechanical testing methods and a brief introduction to synchrotron x-ray diffraction are outlined.

The second part comprising chapters 2 and 3 presents the results of in-situ x-ray diffraction studies during thermomechanical loading experiments on NiTi wires under various constraints in two chapters. The former deals with thermal cycling on two types of actuator wires under constant stress, while the letter deals with unique experiments directly focusing on coupled martensitic transformation and plasticity, which is considered to be responsible for the functional fatigue of NiTi.

The third part consists of two attached publications presenting my work dealing with the superelastic mechanical loading of NiTi wires. First paper describes the macroscopic strain instability upon cyclic superelastic loading. Second paper is devoted to 3D XRD microscopy study of macroscopic austenite/martensite interface propagating along the wire during stress induced martensitic transformation.

The last part provides a summary of the achieved results, discusses achieved findings and outcomes, and outlines the directions for future research.

**List of included papers**

- Instability of cyclic superelastic deformation of NiTi investigated by synchrotron X-ray diffraction.
  P. Sedmak, P. Sittner, J. Pilch, C. Curfs, Acta Materialia 94 (2015), 257 – 270.

- Grain-resolved analysis of localized deformation in nickel-titanium wire under tensile load.
  P. Sedmak, P. Sittner, J. Pilch, L. Heller, J. Kopecek, J. Wright, P. Sedlak, M. Frost, Science 353 (6299) 94 (2015), 559 – 562.

## Comments on my contributions

While working on my thesis, I was a member of FMC research team at the Institute of Physics of the CAS lead by L. Heller. I have performed thermomechanical experiments, synchrotron x-ray measurements and related data analysis. My colleagues from the department (Ludek Heller, Lukas Kaderavek) performed complementary DIC measurements, colleagues from Institute of Physics CAS Jaromir Kopecek with J. Dluhos from TESCAN company performed 3D EBSD analysis, colleagues from the Institute of Thermomechanics CAS (Petr Sedlak, Miroslav Frost) proposed the finite element based constitutive model for localized deformation in NiTi, and our former colleague from the Institute for Nuclear Materials Science SCK•CEN (Remi Delville) performed TEM studies on NiTi wires subjected to the various thermomechanical loading paths.

## Papers not included in the thesis

- Evolution of internal stresses during cyclic superelastic deformation of NiTi investigated by X-ray synchrotron diffraction.
  P. Sedmak, P. Sittner, J. Pilch, C. Curfs, Materials Today: Proceedings 2 (2015), S731-S734.

- On the coupling between martensitic transformation and plasticity in NiTi: experiments and continuum based modelling.
  P. Sittner, P. Sedlak, H. Seiner, P. Sedmak, J. Pilch, R. Delville, L. Heller, L. Kaderavek, submitted to Progress in Materials Science, May 2017

## 1.3 Theoretical background and literature review

### 1.3.1 Shape memory alloys

SMAs are functional materials possessing superior properties such as shape memory effect and superelasticity. Both effects are driven by diffusionless martensitic phase transformation that occurs through a small reversible displacement of the atoms over very short distances. It can be induced both thermally and by applying external stress. High temperature parent phase with higher symmetry - austenite - transforms into low temperature phase with lower symmetry, called martensite. In this work we focus on martensitic transformation in NiTi SMA. From crystallographic point of view, there are three possible paths how a crystal lattice of NiTi alloy can change from B2 cubic austenite into B19’ monoclinic martensite; directly, via rhombohedral R-phase, or via B19 orthorhombic, depending on the chemical composition, thermal treatment, applied stress and/or temperature [5,6] as shown in Figure 1.

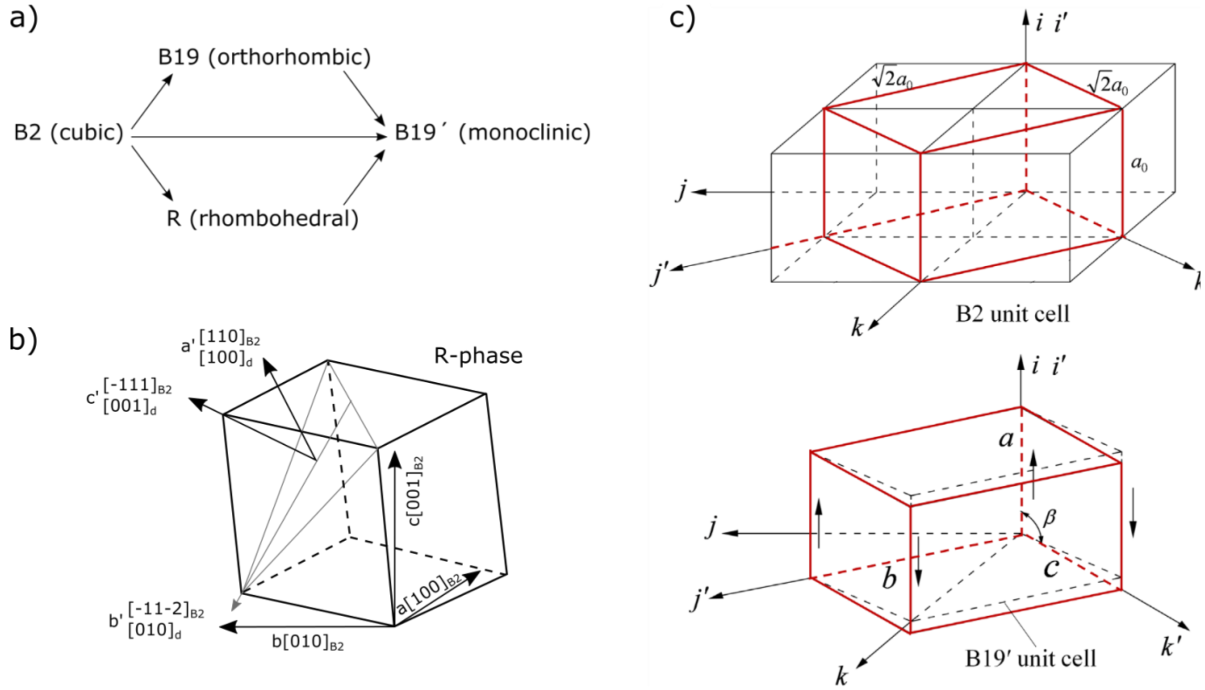

Figure 1. Three possible crystallographic transformation paths (a) of martensitic transformation in NiTi alloys depending on the chemical composition of B2 austenite [5]. Lattice correspondence between (b) B2 and R phase, (c) B2 and B19’ phase.

When martensite forms within the parent phase, the crystal structure difference from parent phase generates large strains around it, which cannot be accommodated elastically. Therefore, another deformation mode is necessary. In the MT field, this is the so-called lattice invariant shear in martensite, which allows the existence of mobile habit plane between austenite and martensite which is achieved via twinning or faulting [5]. Accommodation by twinning is shown in Figure 2. On the left hand side, there is an oriented single crystal of austenite, on the right hand side there is a martensite phase with the lattice invariant shear twinning and the undistorted plane between them is called habit plane. Close to each habit plane, the transformation strain of the martensite is considered as an invariant plane strain and the martensitic structure above this plane is called habit plane variant (HPV). HPV consists of a martensite matrix and its twin. The martensite matrix and its twin are called correspondence variant pairs (CVP) since they have the same lattice correspondence to the parent phase and are called the correspondence variant (CV). The lattice correspondence means that some crystallographic directions of the parent phase are in a strict relation with the crystallographic directions of the martensite phase.

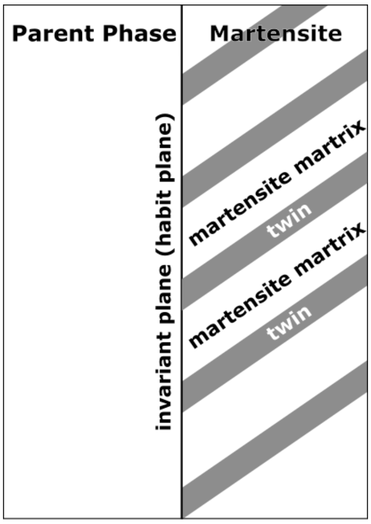

Figure 2. Martensitic transformation proceeds by a motion of habit planes [5] at which the strains are compatible due to the martensite microstructure on the right side.

The number of lattice correspondence variants depends on the symmetry of the parent and the product phase. The martensitic microstructure which forms during the thermally induced A ➔ M transformation, is largely governed by the crystallographic compatibility requirements at the mobile habit planes and mutual accommodation of the large transformation strains over the crystal (self-accommodation). In the case of the monoclinic NiTi martensite, there are 12 different CVs, derived from 6 crystallographically equivalent planes in the parent cubic austenite. These 6 planes form basal planes for a martensite CV, and on each of these planes there are 2 transformation shear directions.

The situation is, however, different when external stress is present during the martensitic transformation. Then large strains generated between the austenite and martensite crystal structure close to the habit plane may potentially become sources of dislocation defects and irreversible plastic strains. If the strain compatibility at the habit plane interfaces can be achieved under stress without dislocation defects, due to a special combination of lattice parameters in parent and product phase, less defects are created in the course of the transformation and the stress-strain-temperature responses of the NiTiX alloy become much more stable [7,8], as observed in case of NiTiCu SMA.

## Shape memory effect - SME

When a SMA sample is cooled down to a temperature below $M_s$ (onset of MT) in the absence of external stress, transformation occurs in a self-accommodating manner, i.e. martensite variants form in many different orientations as dictated by the habit plane crystallography and strain accommodation. The sample has the same shape in the parent phase prior to the transformation and in the martensite phase after the transformation. When such self-accommodated structure is deformed, the martensite variant twin to other orientation more suitably oriented with respect to the applied stress. Upon subsequent heating, the deformed sample transforms back to the austenite and returns back into its original shape. This phenomenon is known as the shape memory effect (SME). It is graphically shown in Figure 3a. Although it looks simple, it is not. Recall that the martensite microstructure detwinned by the previous deformation must twin again upon heating to form the mobile habit planes. In spite of many years of SME studies, is not yet very clear how this happens even in NiTi. It is only known that the deformation in martensite results in a temporary shift of the Af temperature in the first cycle after deformation.

The situation is different when the forward and reverse transformation occurs under symmetrical conditions as e.g. during superelastic stress-strain test or during the actuator test involving cooling/heating through the transformation range under constant applied stress.

Figure 3b shows a typical actuator test cycle under constant stress. The forward transformation starts at $M_s$, and finishes at $M_f$ temperature. Upon heating, a reverse transformation from martensite to austenite begins at $A_s$ and finishes at $A_f$ temperature. The total recovered strain and temperature hysteresis ($A_f$ – $M_s$) are defined in the Figure 3b. Transformation temperatures can be measured either by differential scanning calorimetry (DSC), electrical resistivity measurement or using the intercept method [9] from strain-temperature measurements.

It is essential that the material naturally remembers only its shape in the parent phase. The SME is thus one-way SME. However, it is also possible to modify the material microstructure so the it partially remembers both the parent and the martensite shapes. To achieve that, a special "training" is used. Typically, the alloy is repeatedly strongly deformed in the martensitic state or heated in restrained conditions [7]. During the transformation of such trained alloy, precipitates and lattice defects are present in the microstructure generating stress fields that facilitate the growth of certain martensite variants, and thus defining the shape of the sample in martensite state. This phenomenon is called two-way shape memory effect.

### Superelasticity

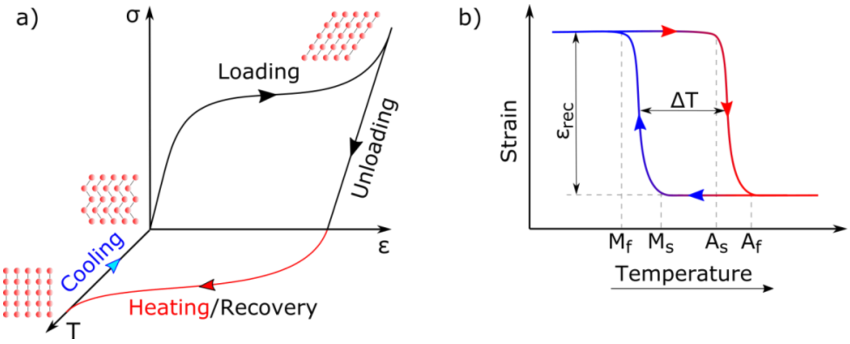

Figure 3. Stress-strain-temperature response due to a) shape memory effect, b) thermal cycle under constant applied stress.

If the SMA sample is deformed in the high temperature phase (at the temperature above $M_S$), it undergoes a stress-induced martensitic transformation into martensite phase when the stress reaches a critical value $\sigma_C$ (Figure 4). Upon unloading, the material transforms back to austenite, since martensite is unstable at such temperatures. Unlike the temperature induced transition, microstructure of the stress induced martensite contains the most favourable correspondence variants and the transformation proceeds always under stress. This creates problems with the strain compatibility at the moving habit planes and involvement of dislocation defects becomes likely, particularly at high temperature and large stress.

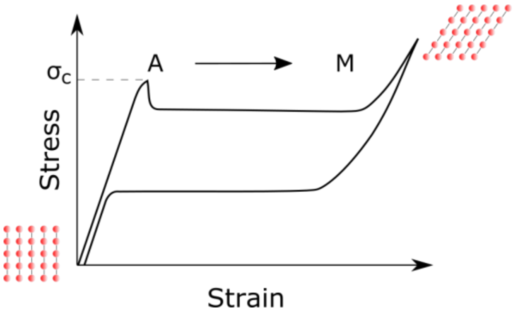

Figure 4. Superelastic stress strain response of NiTi wire in tensile test at constant temperature. The peak at the yield point is due to the nucleation of martensite bands of localized deformation somewhere in the center of the wire (not within the gripped part). The deformation of the wire proceeds in a localized manner by propagation of martensite band fronts under constant applied stress.

The critical stress for stress induced martensitic transformation $\sigma_c$ strongly increases with increasing temperature via Clausius-Clapeyron relation [5]:

$$\frac{d\sigma}{dT} = -\frac{\Delta H}{T_0 \varepsilon_t} \tag{1}$$

where $\sigma$ is plateau stress, $T_0$ test temperature, $\Delta H$ enthalpy (latent heat) and $\varepsilon_t$ is transformation strain. The slope $d\sigma/dT$ can be determined experimentally e.g. by measuring the superelastic curve at several different temperatures, and varies between 5-8 MPaK$^{-1}$ [10].

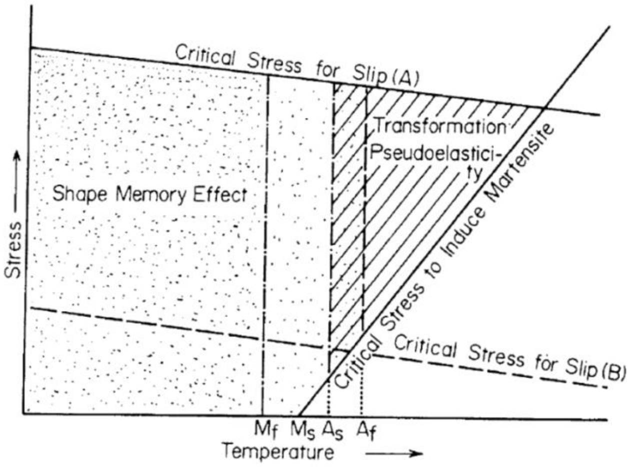

Figure 5. Schematic stress-temperature diagram of NiTi alloy suggesting temperature dependences of transformation stress and superelastic window, where superelasticity is observed [5].

Because of this, attention must be paid when choosing the test temperature for superelastic experiments. According to the state of the art knowledge, when the test temperature exceeds critical value $M_d$, material loses its functional properties and the deformation mode is plastic slip, as suggested in Figure 5. In reality, the situation is much more complex, since there is a wide temperature range where both martensitic transformation and plasticity occur side by side.

Other very important phenomenon is the localization of tensile deformation of NiTi into so-called martensite band fronts (MBF) [11], while the deformation is homogeneous in compressive loading. Upon tensile loading, when $\sigma_c$ is reached, MBF in which all the deformation is localized, nucleates and propagates along the length of the sample under constant force. The MBF is thus a macroscopic interface between the austenite and martensite band at which the macroscopic strains must be compatible similarly as in the case of the habit plane on the lattice level. The fact that the martensitic transformation in tension is localized significantly complicates the investigation of fatigue of NiTi. There are basically four possibilities for NiTi wire cycled in tension, as summarized in Figure 6.

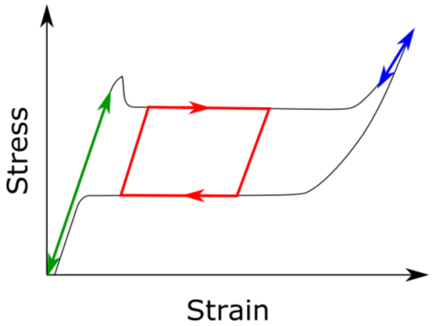

Figure 6. Testing NiTi wire in cyclic tension. Based on the shape of the hysteretic superelastic stress-strain response, one can perform following cyclic tests:

1. Cyclic loading in the elastic region of the austenite
2. Cyclic loading in the elastic region of the stress induced martensite
3. Full superelastic cyclic loading cycle involving the elasticity of both phases combined with the stress induced martensitic transformation
4. Cyclic loading in the plateau region where the reversible martensitic transformation occurs and the elastic loading is minimized

The fatigue performance of the wire in different cyclic tests is very different. During the elastic loading of austenite or martensite (green and blue color curves in Figure 6), material does not undergo any phase change and therefore no large strain gradients are expected. However, during a partial cycle in the plateau (red color), part of the material, which undergoes phase transformation, needs to accommodate large gradients of strain since nearly complete forward and reverse martensitic transformation takes place locally at the moving macroscopic interface even if only a small external strain amplitude is imposed. Due to the localized deformation, very small material volume transforms completely while the rest of the sample deforms only elastically. This is why the localization phenomena are very important. In my thesis, I tried to focus on nearly complete forward and reverse martensitic transformation in complete superelastic cycles to simplify the analysis of the in-situ x-ray diffraction studies. I also deal with the strain localization phenomenon in a special experiment using 3D x-ray diffraction method (3D-XRD experiment).

### 1.3.2 Functional and structural fatigue

Fatigue of materials originating from the cyclic mechanical loading has been studied for a very long time [12]. From the structural point of view, there are many factors affecting fatigue properties of a material such as grain size, inclusions, stress-strain state, matrix slip resistance, surface roughness, phase transformations and many others [12]. Fatigue still remains the biggest challenge which prevents SMA materials from being successfully employed in engineering applications. In the field of SMA, fatigue is classified as structural and functional. The former is the same as in other conventional materials - nucleation and propagation of cracks, while the latter means degradation of functional properties – variation of stress-strain responses upon cycling. Another speciality of SMAs is that we need to investigate thermomechanical fatigue, since large reversible strain brought about by cyclic variation of temperature are utilized in engineering applications.

If MT is completely reversible, there would be no functional fatigue and the applied stress should decide about the lifetime as it is common for structural fatigue of metals, i.e. millions of cycles up to several percent of strains (~6% for NiTi) in mechanical or thermomechanical cyclic loading shall be achievable. For high frequencies, heat produced by the cyclic MT will have to be taken away from the material to prevent significant stress increase due to rising temperature. If that goal is met, a wide range of SMA engineering applications so far hindered by poor fatigue performance of NiTi could be realized. But the field is not there yet.

This work is dedicated to the functional fatigue of NiTi; therefore, no comprehensive study of the structural fatigue will be provided here. However, there are many studies dealing with the structural fatigue of SMA materials, starting with the first by Melton [13], later Myiazaki et al. [14] introduced rotary-bending testing of fatigue life. Reinoehl [15] described the influence of carbide particles, and there are quite recent review studies by Kang [16] and Eggeler [17].

For both stress (superelastic applications) and temperature (actuators) induced martensitic transformations, the functional fatigue brings about accumulation of defects and internal stress in the material. This leads to unstable stress-strain-temperature response upon thermomechanical cycling. Although the transformation interacts with both stress and temperature, there is a difference in that it is driven by increasing stress in the former and decreasing temperature in the latter. This brings about significant differences in fatigue performance. The stress induced transformation is typically localized in a sharp macroscopic interface propagating along the specimen, while the transformation is macroscopically homogeneous when it is induced thermally. Whether this is a source of much poorer superelastic fatigue performance compared to thermomechanical cycling at low stresses or there are other phenomena involved is not clear yet. It is clear from the above that before we can solve the structural fatigue problem of NiTi, we need to get rid of functional fatigue or at least minimize the damage caused by it. To find out the exact mechanism of the functional fatigue remains to be discovered. In this respect, the high energy x-ray diffraction proved to be an excellent tool for investigating the microstructure evolution (phase fraction, defects, internal stress redistribution) upon cycling and revealing the origin of the functional fatigue.

Near equiatomic NiTi based SMA materials offer many potential superelastic and actuator applications. While there are already many superelastic applications [2], the actuator applications have been lacking behind until recently.

Compact NiTi actuators operating upon thermally induced martensitic transformation are promising for automotive and aerospace applications. Usually, they are used under constant stress or against biased spring. The stability of such device upon repetitive cycling needs to fulfil the operational requirements. As it was observed in many experiments, the strain stability depends on loading conditions, mainly on the applied stress and maximum temperature and applied constraint. Over the years, SMA scientists performed many studies using various approaches to characterize the unstable behaviour during the actuation manifested by a gradual change in thermomechanical response, accumulation of the irrecoverable strains and shift of transformation temperatures and hysteresis. There are numerous studies describing the effects of thermomechanical cycling on the functional stability from the macroscopic point of view. Most of the studies devoted to microstructural mechanisms responsible for the instability are quite recent.

Early works on the thermal cycling of NiTi alloys were performed by Miyazaki [18] who reported decreasing $M_s$ temperature with increasing number of cycles, later Matsumoto [19,20] explained this behaviour by formation of R phase prior to the transformation into B19’. Transformation temperature evolution was also the subject of the recent studies by Pelton [21] and Bowers [22] employing DSC and TEM techniques to explain the evolution of microstructure by appearance of R-phase and stabilizing the austenite phase due to dislocation density accumulation. From the macroscopic point of view, the instability was studied by Saikrishna et al. [23] who reported the relation between the microstructure and the stability of NiTi samples, NiTi actuators under various thermomechanical paths were studied by Mammano et al. [24] and Padula et al. [25], who explained the effect of overloading and overheating. Wagner et al [26] studied the effect of maximum upper temperature during thermal cycling. They suggested that not only the incremental plastic deformation accumulation upon cycling, but also Ni-rich precipitates $Ni_4Ti_3$ that are formed at elevated temperatures and contribute to a degradation of the functional properties. It depends however, very much on the initial chemical composition and thermal treatment of the material. Efforts have been made to improve the fatigue behaviour by Mertmann [27], applying a training to a sample whereby stabilizing the thermomechanical response, by Casati [28] studying the effect of electric heating methods improving the lifetime by changing the shape of the electric power pulse used for heating the sample or by Saikrishna [29,30] applying the overloading cycles interposed between the actuation cycles improving the lifetime. However, poor knowledge about the in-situ microstructure evolution inside SMA materials upon cycling brought the scientists to employ both in-situ neutron and x-ray diffraction methods to bridge the gap between the macroscopic instability and the microstructural changes. In-situ neutron diffraction upon thermal cycling was employed by Ye et al. [31,32] to investigate the instability under several stress levels, and quite recently by Benafan [33] to study the macroscopic instability with various prestrain conditions of the sample. Similarly Jones et al. [34,35] used in-situ synchrotron characterization of the microstructure evolution under several constant stress levels. They all reported similar conclusions such as significant martensite texture evolution, decrease of the transformation temperatures and increase of the irreversible strain, and depending on the initial conditions of thermomechanical cycling, change in the transformation strain. Martensite texture evolution was due to several martensitic variants selection upon cycling [33] which also explained increase in reversible strain. Two way shape memory effect created upon cycling was attributed to martensite stabilization by dislocations along twins ([36,37]) which also causes the transformation temperature change and increase of irrecoverable strains.

Superelastic fatigue is considered to be a problem because it affects the performance of NiTi elements in engineering applications [2,17] (superelastic members, vibration damping members or actuators) and because it is responsible for fatigue degradation and preliminary failure of NiTi [38]. Effect of the functional fatigue on practical applications can be partially reduced by stabilizing the cyclic responses by training [27], but the limited fatigue life remains to be a serious problem for the SMA technology. The link between functional [17] and structural fatigue [38] can be possibly understood in terms of dissipation energy based criteria [39] for structural fatigue (the more energy dissipated during the cyclic stress induced martensitic transformation, the shorter the fatigue lifetime). It is however not clear which phenomenon has the leading role in a functional fatigue; strain localization [40], transformation strain [41], transformation stress [42], surface finishing [43], inclusions [44] or growing evidence on the role of environmental effects in superelastic fatigue [45]. The last one cannot be safely considered as a general controlling mechanism of the Nitinol fatigue, particularly for the superelastic deformation in fluids. It has been known from early days of the Nitinol research that the instability of cyclic superelasticity is due to the plastic deformation by dislocation slip accompanying the stress induced martensitic transformation and accumulation of residual martensite [46,47].

Recent studies [17,38,45,48,49] were performed to find out how the accumulation of dislocation defects is related to functional and structural fatigue and how they can be linked together. What is the difference between dislocations created by thermal [50] and mechanical [48] cycling? How is the dislocation slip activity upon cycling related to the microstructure of NiTi wires [51]? Does the incremental slip occur during the forward or reverse transformations [52]? Does the slip occur in the austenite or in the martensite phase [52,53], at the propagating austenite/martensite interface [54] or elsewhere in the polycrystal in parallel to the transformation [55]? What are the actual stress and strain conditions at the propagating martensite band front, where all the deformation/transformation proceeds in a highly coordinated localized manner?

To answer at least a few of these questions, several experiments with various thermomechanical paths were performed in this work, giving the experimental evidence on the relation between martensitic transformation, dislocation slip, deformation instability, microstructure evolution and conditions on the moving martensite/austenite interface.

## 1.4 Materials and methods

### 1.4.1 NiTi wires

Transformation temperatures of NiTi wires, whether they exhibit superelastic or shape memory behaviour at given temperature, are given mainly by its chemical composition [5], as shown in Figure 7:

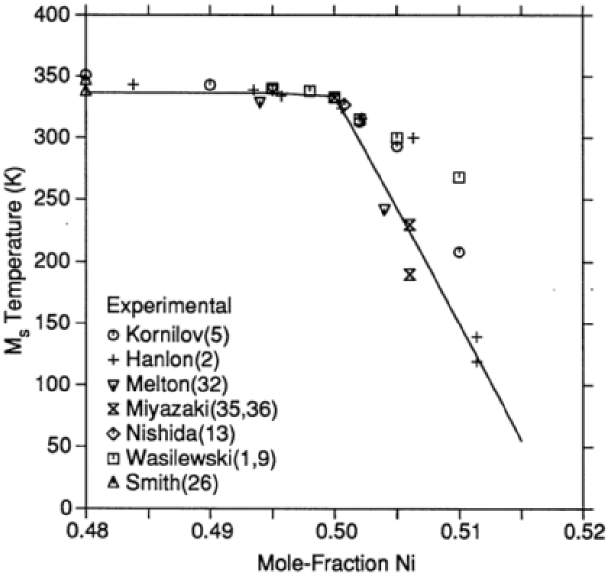

Figure 7. Dependence of martensite start temperatures on chemical composition of NiTi alloy [5].

NiTi wires investigated in this work are commercially available products from Fort Wayne Metals and Dynalloy companies. They are produced by extrusion into bars from ingots, followed by hot-working and final cold drawing process through a drawing die. Reduction of the wire diameter during the final cold drawing process, so-called cold work (CW), can achieve 10-90%, but commercial products usually have CW in the range 35- 50% [56]. Microstructure characterized by strong {111}<100> texture [36,57] along the wire axis is created during the extrusion and hot working processes. The texture significantly affects the superelastic properties of the wire, since the transformation strains for single crystals depend on the orientation (10.7% along <111>, 8.4% along <110> and 2.7% along <100> [46]). On the other hand, grain size and defect density in the wire depend on cold work and heat treatment. After cold working, a NiTi wire does not exhibit any functional properties due to a highly deformed microstructure. Final heat treatment is necessary to adjust its microstructure and functional properties [58,59]. Wires can be heat treated in the company, usually by continual heat treatment process, or custom heat treated by engineers to obtain desired microstructures and/or shapes.

### Shape memory wires

Fort Wayne Metal NiTi#5 and Dynalloy Flexinol 90C shape memory wires with no additional heat treatment were used for thermal cycling experiments. Thermomechanical response of Flexinol 90C and NiTi#5 actuator wires is shown in Figure 8. While Flexinol 90C wire is stable upon thermal cycling under 200MPa, NiTi#5 wire exhibits significant ratcheting. Chemical composition and precipitate content of NiTi#5 and Flexinol 90C wire are rather similar. The difference lies in the training/post processing given to Flexinol 90C wire after the production stage. Zero strain for actuator wires was set at high temperature in austenitic state, therefore stress-strain curves in Figure 8 do not start from zero strain.

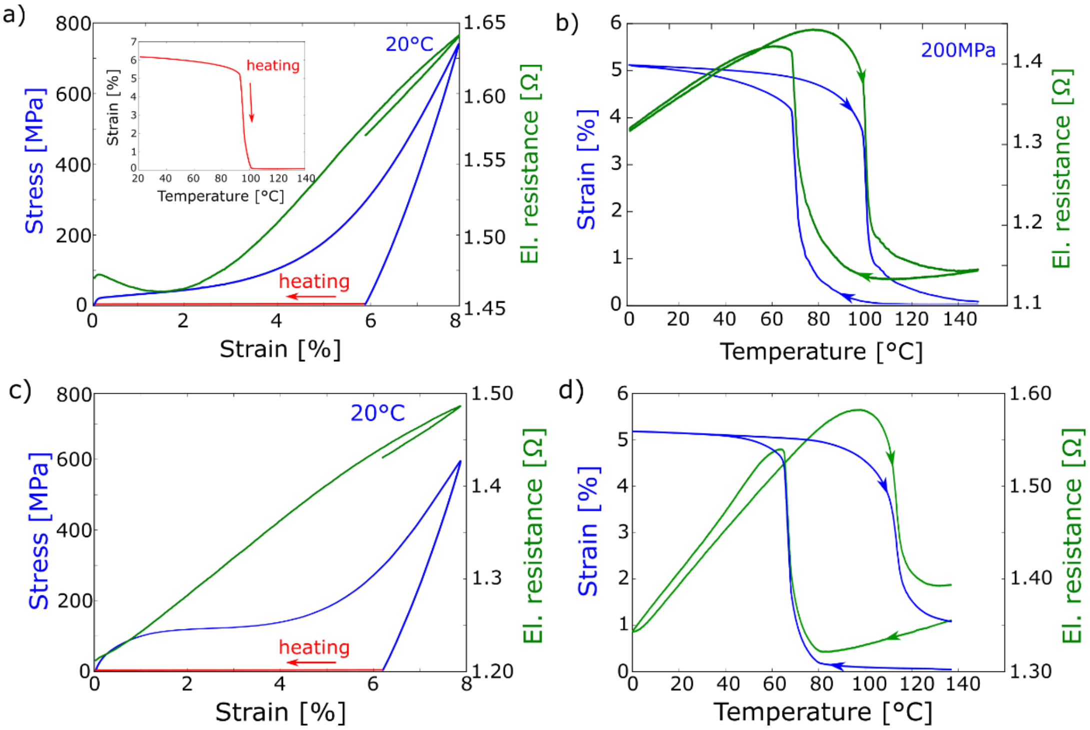

Figure 8. Mechanical and electrical resistance response of the shape memory wires Flexinol 90C (a,b) and NiTi#5 (c,d) in tensile test at room temperature (a,c) and actuator test involving heating/cooling under constant stress level 200MPa (b,d).

### Superelastic wires

Fort Wayne Metals Ni-rich NiTi#1 cold worked custom heat treated NiTi wires were used for superelastic tensile cycling experiments. Special heat treatment developed at the Department of Functional Materials of IP ASCR called the Final thermomechanical treatment by short electric current pulse (FTMT-EC) [58] was applied to all NiTi#1 wires used for the superelastic experiments. This treatment enabled to prepare a desired final microstructure of the wire, with controlled parameters such as degree of recovery/recrystallization and grain size. Functional properties of the superelastic straight annealed NiTi#1 are shown in Figure 9.

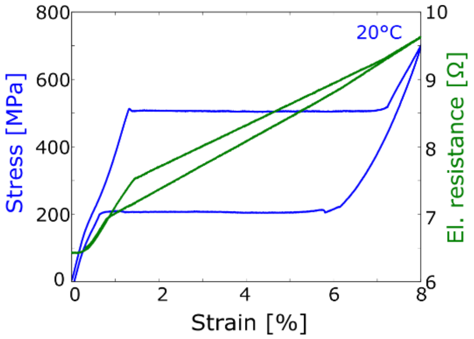

Figure 9. Stress-strain-electric resistance response of superelastic NiTi#1 SA wire at room temperature. The yield point peak is missing since the martensite band front nucleated within the gripped part of the wire.

All wires were annealed with the same electric pulse parameters (electric power pulse P = 125W per 100mm wire length in the Peltier chamber with a controlled temperature); the only difference was the annealing time. From now on, the superelastic wire microstructure will be referred to according to its annealing time in ms, e.g. 12ms wire for the wire annealed with 125W per 100mm, for 12ms. As mentioned in the preceding section this work links previous research [48,59] to new in-situ studies on 15ms and 16.5ms wires. In these studies [48,59], superelastic cycling of thin NiTi wires annealed by short electric pulsed with different annealing times (12, 14, 16, 18ms) were investigated by means of TEM and XRD. It was found that functional properties and stability of the wires dramatically change with annealing time. Wires with the annealing time of 12 and 14ms show the best functional response and stability, while 16ms and 18ms wires show significant ratcheting and change in the functional properties during first few cycles. To complement these results with 15ms and 16.5ms wires, new wires for more detailed synchrotron experiments were prepared. 15ms and 16.5ms wires exhibit "intermediate" functional stability where one can follow the microstructural changes in a few cycles without need of performing hundreds of cycles (as in the case of 12ms wire) and without complete rebuilding of the microstructure in very few first cycles, as typical for the 18ms wire. This microstructure tuning is essential since the synchrotron beamtime is very limited.

To grip the wires into the deformation machine, sample ends were compressed in the stainless steel capillaries with inner diameter of 0.18mm for 0.1mm wires, and inner diameter of 0.25mm for 0.2mm wires (Figure 10). The capillaries were mounted in the grips of the stress rig. A complete overview of the samples and experiments used for this thesis is given in Table 1.

Figure 10. NiTi wire clamped in steel capillaries.

Table 1. Overview of the samples used for the experiments

| Sample | Experiment type | Sample diameters |
|---|---|---|
| NiTi#5 shape memory wire | Thermomechanical experiments | 50mm, Ø 0.2mm |
| Flexinol 90C shape memory wire | Thermomechanical experiments | 50mm, Ø 0.2mm |
| Flexinol 90C shape memory wire | Low temperature shape setting | 50mm, Ø 0.2mm |
| NiTi#1 superelastic wire | Superelastic cycling at constant temperature | 50mm, Ø 0.1mm |
| NiTi#1 superelastic wire | Study of the martensite band front | 50mm, Ø 0.1mm |

### 1.4.2 Uniaxial tensile testing

Dedicated tensile loading frame (MITTER, developed at the Department of Functional Materials of IP ASCR, Figure 11) was used for both cyclic tensile deformation and cyclic actuator testing. It enables thermomechanical testing with in-situ recording of stress-strain-resistivity response. It is equipped with Peltier furnace to provide both constant temperature environment and sample heating/cooling by convection. The furnace was built to be compatible with in-situ synchrotron XRD experiments. It has a small hole on one side, where an incident beam enters the furnace and hits the sample, and a wide-angle exit window on the other side for diffracted x-rays. It is also equipped with a power pulse control unit used for the FTMT-EC method, i.e. fast Joule heating of the wire with defined heating profile and also for the repetitive heating during actuation tests.

The tensile loading is provided by linear motor operated either in strain or force control mode; precise strain measurement is provided by optical sensor with the 50nm resolution. It measures the position of one of the jaws of the stress rig. The error in strain measurement might be introduced by thermal expansion, deformation of the load cell etc., however when measuring large (several %) deformations of 50 mm long wire, the error becomes negligible. Strain control mode enables very low strain rates (~$10^{-4}$ $s^{-1}$) necessary to prevent the increase of the temperature by the latent heat released during forward transformation which needs to be radiated out of the sample. This is a necessary condition for single martensite band front formation and propagation [60,61]. If the strain rate is high, the local temperature at the martensite band front is increased by latent heat which cannot dissipate from the sample. According to the Clausius-Clapeyron relation, transformation stress at the martensite band front is increased and it is energetically more favourable to form another martensite band front rather than to propagate the first one.

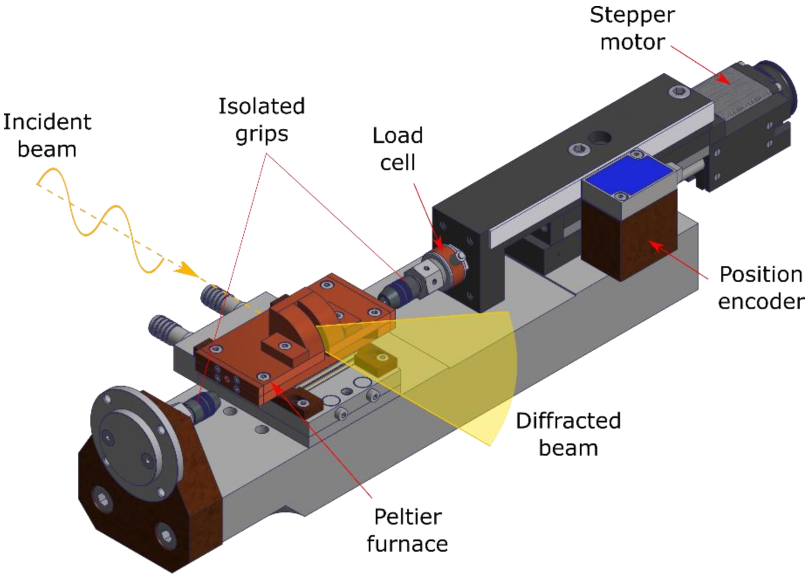

Figure 11. MITTER testing rig used for thermomechanical experiments on thin NiTi wires.

### 1.4.3 Synchrotron X-ray diffraction

X-ray diffraction (XRD) techniques are based on elastic scattering of incident photons on crystal lattice of the studied material and recording diffracted intensity vs. 2Θ angle in a specific range depending on the energy of incident beam using a detector placed behind the sample. The XRD technique has proven to be an excellent tool for investigating the evolution of microstructure in cyclically deformed materials. The most widespread diffraction technique is a laboratory XRD. The experiments performed in this work used high energy synchrotron XRD at ESRF source in Grenoble.  While the low energy laboratory x-rays diffract in the surface layer, the high energy x-rays penetrate through the bulk and can be thus used to probe the variation of the microstructure in a representative volume of the material.

Synchrotron radiation is created by bending the path of electrons traveling at high speed (close to the speed of light) using magnetic field. At the first stage, electrons are emitted by electron gun and accelerated by linear accelerator (LINAC). In the next stage, they travel to the booster synchrotron which increases their speed a little more so they reach final energy of several GeV (6GeV for ESRF) and finally enter the storage ring. Here, they travel around a closed orbit, which is built by a set of a straight sections and set of bending magnets serving to curve their trajectory. In the straight sections of the storage ring, insertion devices such as wigglers and undulators (devices with an alternating array of magnets producing alternating magnetic field along the electron path) are placed to produce synchrotron radiation in a more efficient way than from bending magnets. Each time the path of an electron is changed, it loses a certain amount of energy by emitting photons in form of synchrotron radiation. This radiation is emitted tangentially to the curved path aiming towards a beamline. Desired energy/wavelength is chosen using monochromator crystals and the beam can be further focused (e.g. in-vacuum transfocator) and its size defined by defining slits. Comparing to laboratory source, the biggest advantage of synchrotron radiation is higher energy (10-140keV), flux and brilliance which implies much higher penetration depth, shorter measurement times and better spatial properties of the beam respectively.

In this work, the experiments were performed at ID22 and ID11 ESRF beamlines. High resolution powder diffraction beamline ID22, allowing for high resolution measurements using 1D detector was employed for the measurements of cyclic superelastic deformation and cyclic actuator experiments. NiTi austenite and martensite peaks often overlap in the course of martensitic phase transformation, thus the high resolution ID22 diffractometer was necessary to overcome this problem. ID22 is mainly dedicated to powder and polycrystalline sample measurements. The biggest advantage of ID22 is the high resolution in 2Θ angle, which is necessary when following small changes of peak parameters upon cycling. It is achieved by using 9 detectors preceded by 9 Si 111 analyser crystals 2° apart, measuring diffracted intensity as a function of 2Θ (Figure 12). After a beam strikes the sample it is scattered towards the Si 111 analyser crystals. If the Bragg condition is met on one of the analyser crystals, detector records a signal.

Crystal structure and properties of the examined material are obtained from the whole diffraction pattern fitting by Pawley, Rietveld or a single peak fit, depending on required information. Each diffraction pattern consists of a set of observed diffraction peaks. Each single peak is described by its 2Θ position (or equivalently by d-spacing or Q range), its width (full width at half maximum FWHM) and its intensity. Position of a peak provides information about the unit cell parameters and the elastic strain (macrostress), intensity provides information about the crystal structure, phase content of the material and preferred orientation and finally FWHM is a convolution of the instrument parameters, crystalline size and microdeformation (plastic deformation). All this information was utilized to follow the deformation processes taking place in the NiTi polycrystal microstructure subjected to cyclic thermomechanical loading.

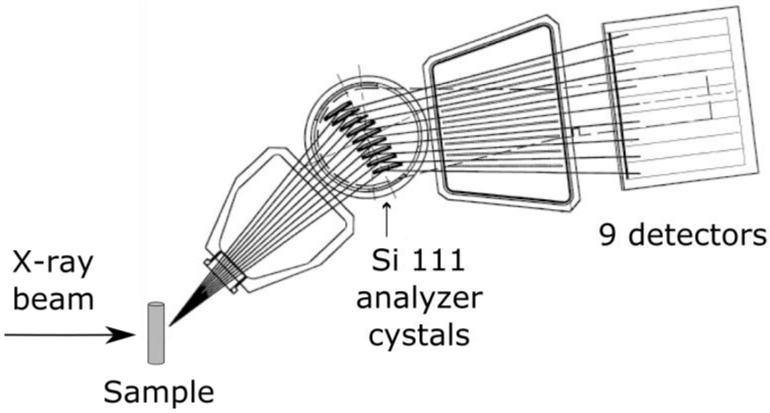

Figure 12. ID22 ESRF beamline detector setup with analyzer crystals.

Pawley fit is used as a first step for crystal structure analysis. It serves to find and refine unit cell parameters together with instrument parameters by identifying as many hkl indexes as possible from the data set and assigning them to the peak positions – indexing. The intensity of the individual peaks is a free parameter in this fit. All possible space groups are then calculated from unit cell parameters. Obtained parameters are used as an input into the Rietveld fit which serves for crystal structure solution. In Rietveld fit the intensities and peak widths (FWHM) are determined by crystal structure of the examined material. On the other hand, if the crystal structure is known, and a multiphase material is to be observed, volume phase fraction can be calculated from the diffraction pattern. This is very useful when studying martensitic transformation in NiTi upon temperature change, or phase fraction evolution upon cycling.  Both of the aforementioned methods are based on the least-square method, minimizing the difference between measured and calculated diffraction pattern. Single peak fit is used to analyze observed reflections separately. Refined parameters are peak area, position and peak shape function parameters. This technique can be applied to calculate individual lattice strains from peak positions and peak broadening upon cycling. For particular hkl reflection, lattice strain $\varepsilon_{hkl}$ is evaluated using Equation 2. from the stress free position $d_{0hkl}$ and the position $d_{hkl}$ measured under stress:

$$\varepsilon_{hkl} = \frac{d_{hkl} - d_{0,hkl}}{d_{0,hkl}} \tag{2}$$

3D XRD microscopy technique at ID11 material science beamline was used to measure the topology and the strain distribution within the martensite band front. 3D XRD technique combines conventional single crystal XRD rotation method and 2D detector enabling an analysis of polycrystalline samples. 3D XRD methods were developed [62–64] over the last 15 years at synchrotron sources as a technique for grain resolved crystallographic analysis of polycrystalline materials under load. Although they have been already used in many experiments [64–68], our study on localized deformation in tension (paper II) was the first ever application to NiTi. The combination of a rotation and a use of 2D detector gives rise to many diffraction peaks for each single grain in studied polycrystal, resulting in 3D information about the center of mass position, crystallographic orientation, size and elastic strain averaged over a single grain volume (Figure 13).

Data analysis is based on searching for single diffraction spots (interconnected regions on 2D detector) above defined threshold value recorded on a 2D detector. Identified peaks are then merged over all rotations around the wire axis into one 3D file containing all observed diffraction vectors. It is followed by indexing procedure, i.e. assigning the scattering vectors to the individual austenite grains. The result of such analysis provides the information about the center of mass position, orientation, size and elastic strain of each individual detected grain. 3D XRD method and associated data analysis are described in more detail in the paper II.

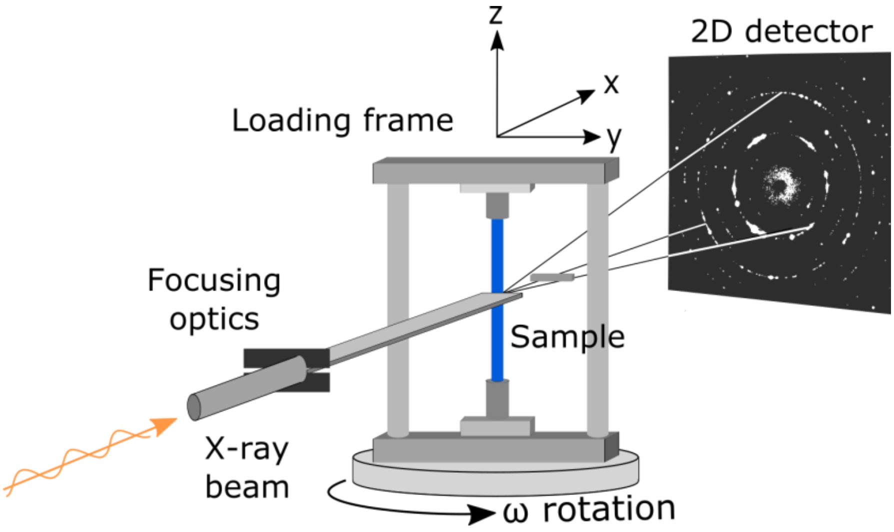

Figure 13. Setup for 3D synchrotron x-ray diffraction experiment at ID11 beamline at ESRF.

There is a principal difference in the diffraction techniques of the two above mentioned setups. The first difference is in the probed volume. The size of the beam at ID22 beamline is usually large enough (depending on the grain size of the probed material) to irradiate the sample volume containing many grains, i.e. the obtained information is averaged over a large number of grains. On the other hand, the 3D XRD microscopy setup at the ID11 beamline operates with a beam (often focused), the size of which can be tuned depending on the grain size of the material so that spotty diffraction patterns are recorded on 2D detector. Another difference is the grain size dependence for the two methods. For ID22, small grain size is necessary to obtain a good statistics giving meaningful results, for ID11 minimum grain size is necessary to obtain distinguishable spotty diffraction pattern on 2D detector.

The average sample grain size for ID22 measurements ranged from hundreds of nm up to 5µm, while for ID11 measurements minimum grain size necessary to obtain a spotty diffraction pattern was 5µm. The samples were annealed in such way, that only direct transformation from B2 austenite into B19' martensite is considered, without R-phase transformation. Stress free unit cell parameters at ID22 beamline were defined as $a$ = 3.015Å for space group *Pm-3m* B2 cubic austenite, and as $a$ = 2.883Å, $b$ =4.166Å, $c$ = 4.633Å, $\gamma$ = 96.5° for space group *P1121/m* B19' monoclinic martensite.

# 2 Thermomechanical loading experiments

This part of the thesis concerns cyclic thermomechanical loading experiments on NiTi actuator wires. The experiments on superelastic NiTi wires were published in Paper I (section 4).

Thermomechanical cycling experiments under various conditions mapping the macroscopic instability of NiTi actuators have been a subject of many studies in the literature (as described in the chapter 1.3.2). However, until quite recently, it was not well understood which microscopic processes are causing the cyclic instability of the strain-temperature response. The most relevant and comprehensive study was probably performed by Benafan et al [33]. They have studied thermomechanical cycling of shape memory NiTi samples under various constant tensile stresses using in-situ neutron diffraction technique. Their results provide information on the evolution of phase fraction, texture, internal strain and peak shape during the thermal cycling. They observed texture evolution towards oriented martensite with a selection of variants providing maximum transformation strain. They also observed peak broadening in austenite representing a defect accumulation during cycling. After several cycles, the peak broadening saturated, indicating the equilibrium between defect generation and its annihilation.

Similar study on two types of NiTi shape memory actuator wires is presented in the next section. The evolution of microstructure upon thermomechanical cycling was studied by in-situ synchrotron x-ray diffraction capable of penetration through the bulk of the thin wires supplemented with in-situ electric resistance measurements. Although the results are consistent with the Benafan's work, there are essential differences pointed out below.

## 2.1 Materials and methods

Thermal cycling experiments were performed on Fort Wayne Metals actuator NiTi#5 and Dynalloy actuator Flexinol 90C wire, both with diameter $d = 0.2$mm. Samples were mounted on the loading frame MITTER and installed on ID22 diffractometer in a vertical position (axial geometry – diffracting planes are roughly perpendicular to the loading direction) and XRD data were acquired in the $2\Theta$ range 0 – 30°. Energy of the x-rays was 31keV ($\lambda \sim 0.4$Å), with the beam size 1.5x1mm, irradiating the wire volume of $31.4 \times 10^6 \mu m^3$. Given that the grain size of both wires is under 100nm, statistics of the diffraction data from such samples was very good. For the sake of efficient use of the synchrotron beam time, the samples were not cycled in-situ at the beamline, but five samples from NiTi#5 and Flexinol 90C wires were thermally cycled in advance in the FMC laboratory for 1, 10, 50, 100 and 500 thermal cycles under constant applied stress of 200MPa (thermomechanical response of the first 100 cycles is shown in Figure 14). Thermal cycling was achieved by joule heating controlled by electric power pulses with a linear heating ramp, holding time at the maximum temperature and a linear cooling ramp with holding time at the 0 power. The upper cycling temperature was set to 200°C giving the total temperature range 20 - 200°C in one thermal cycle. The goal of the XRD measurements was to capture the microstructure evolution over the course of thermal cycling. Analysis of diffraction patterns helps to determine the evolution of the peak parameters such as peak positions, intensity and FWHM, defining the phase fraction and microstructure variation upon cycling. Full pattern Rietveld refinement could not have been used due to the problems with a strong texture and its variation upon cycling. Pawley fit was used instead to index the diffraction patterns and a single peak fitting procedure was applied afterwards to obtain the evolution of peak positions, integrated intensities and FWHM upon cycling for both austenite and martensite phase.

## 2.2 Thermal cycling experiments

During the XRD data acquisition, diffraction patterns were measured in three distinct thermomechanical states; i) at room temperature at 20MPa (denoted as cold strain, representing martensite strain), ii) at elevated temperature at 20MPa (~200°C, denoted as hot strain) used for upper limit of thermal cycling, and iii) after cooling back to room temperature at 20MPa stress. Because the thermomechanical response of Flexinol 90C wire under 200MPa stress was very stable upon cycling (Figure 14c), almost no evolution of the diffraction pattern was observed, therefore most of the attention will be paid on the NiTi#5 wire. Figure 15 shows the diffraction patterns of the NiTi#5 wire in 0, 1st, 10th, 50th, 100th and 500th cycle in the three distinct thermomechanical states (see Table 2).

Table 2. Overview of the XRD measurements on the actuator wires

| Sample | **NiTi#5 actuator wire** | **Flexinol 90C actuator wire** |
|---|---|---|
| XRD taken in the cycle N: | 0, 1, 10, 50, 100, 500 | 0, 1, 10, 50, 100, 500 |
| Thermomechanical state during XRD measurement | 1) 20MPa/20°C<br>2) 20MPa/200°C<br>3) 20MPa/20°C | 1) 20MPa/20°C<br>2) 20MPa/200°C<br>3) 20MPa/20°C |

1) Virgin wire (for both NiTi#5 and Flexinol 90C) prior to any thermomechanical load at room temperature was in the martensitic state.
2) In the second state, as the wire is heated to elevated temperature, it undergoes a reverse phase transformation from martensite to austenite phase.
3) Finally, in the third measured state after cooling back to room temperature, the wire transforms back to martensite.

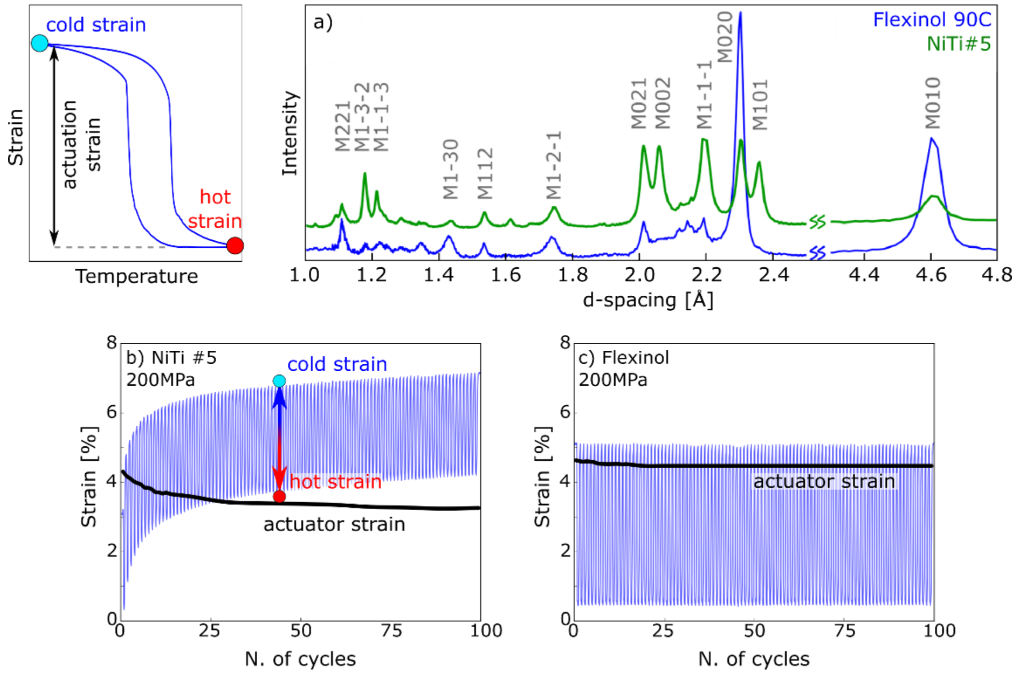

Figure 14. Thermal cycling under 200MPa of NiTi#5 and Flexinol 90C wire. a) Diffraction patterns of virgin NiTi#5 and Flexinol 90C wires before cycling at 20MPa. Evolution of hot and cold strain upon cycling of NiTi#5 (b) and Flexinol 90C (c) wires. Note the differences in diffraction patterns and in stability of actuator responses.

In the ideal case, where no plastic deformation and defects are generated upon cycling, one would expect stable macroscopic response and therefore no change of the microstructure upon thermal cycling. This was nearly the case of the Flexinol 90C wire cyclically loaded under 200MPa constant stress (Figure 14c), where essentially no evolution of strain-T response or of diffraction patterns was observed. Small change in actuator strain was observed in the first 25 cycles, then it became stable. Nevertheless, if the level of constant applied stress for cyclic thermal deformation is increased, cyclic strain-temperature response of the Flexinol 90C wire becomes unstable as well. Such case is discussed in the next paragraph – Flexinol 90C – overloading tests.

In the case of NiTi#5 wire under 200MPa, the macroscopic response is rather unstable (Figure 14b), cold strain continuously increased from 4.8% in the beginning of cycling, it became linear after 50 cycles and continued to increase thereafter. After 100 cycles, actuator strain completely stabilized at 3.2% and approached a saturated state. In other words – the wire gradually became longer but the actuator strain remained the same.

### NiTi#5 - Evolution of diffraction patterns during thermal cycling under 200MPa

Diffraction patterns of virgin NiTi#5 and Flexinol 90C wires are shown in the top part of Figure 14. Diffractogram of NiTi#5 wire is typical for self-accommodated martensite, while that of Flexinol 90C wire resembles diffractogram observed under tensile stress. It is due to the two way SME imprinted to the Flexinol 90C wire by production/training. The peak intensities in the diffraction pattern of the monoclinic martensite phase in NiTi#5 wire (Figure 15a,c) are strongly affected by the preferential selection of martensite variants (texture) with respect to the wire axis upon cycling. Texture is completely different in stress free state and under applied tensile stress.

To simplify the interpretation of the results, three measured thermomechanical states will be discussed separately. The overall evolution of the diffraction patterns during thermal cycling in virgin state and after 1st, 10th, 50th,100th and 500th cycle for three states is shown in the Figure 15. Results from the single peak fit analysis are plotted in the Figure 16.

The evolution of the diffraction patterns at room temperature (Figures 15a and 16a) provides the information on texture variation and defect accumulation during cycling. Note the increase of the relative intensities of several martensite peaks (M020, M1-30) on the expense of other peaks; however, the variation is very strong mainly in the first few cycles. FWHM increases for the most of the peaks, indicating defect accumulation mainly due to plastic deformation, although the mechanism and the stage of the thermal cycle at which dislocations are produced remains unclear. The variation of the relative lattice strain is very small indicating almost no internal stress redistribution among the families of the grains, which is most likely due to constant stress constraint applied during cycling.

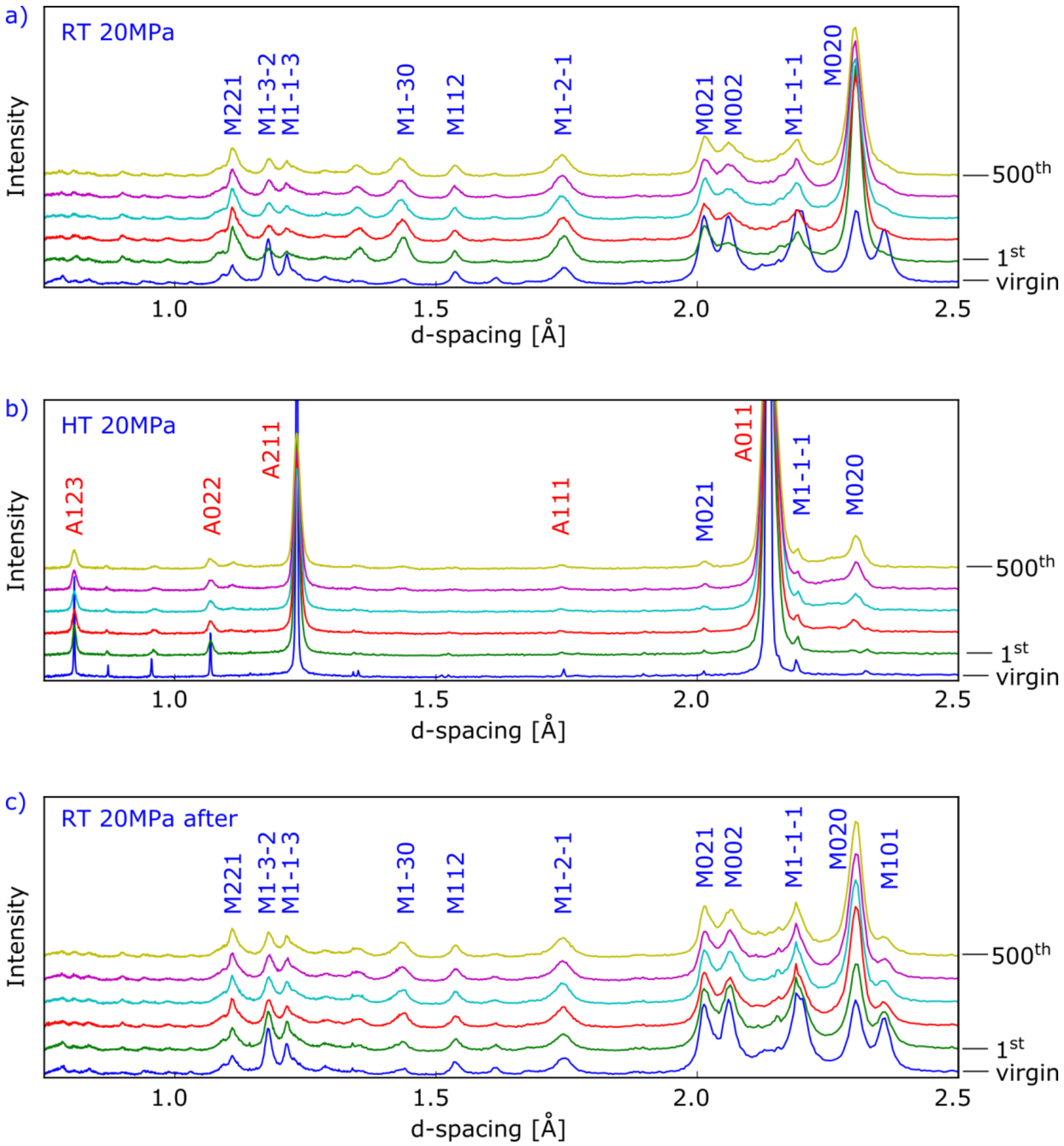

Figure 15. Evolution of diffraction patterns of NiTi#5 at a)20MPa at room temperature, b) 20MPa at high temperature and c) 20MPa cooled back to room temperature for virgin wire and after 1, 10, 50, 100 and 500 thermal cycles.

The evolution of the diffraction patterns at high temperature (Figures 15b and 16b) provides the information about the austenite microstructure evolution. The microstructure at elevated temperature is expected to be fully austenitic, but it is clear from the Figures 15b and 16b that this is the case only in the first few cycles. Relative intensity of austenite peaks decreases at the expense of increasing intensity of appearing martensite peaks upon cycling. Similarly, to previous case, FWHM significantly increases upon cycling and there is very little variation of lattice strain (peak positions).

Finally, for the unloaded state at room temperature (Figures 15c and 16c), a significant texture evolution occurs indicating appearance of a two-way shape memory effect in the microstructure upon cycling. Note that mainly reflections M010, M020 and M221 are significantly increasing on the expense of other reflections. In accordance with the two previous thermomechanical conditions, strong increase of FWHM and very little change in the relative lattice strain is observed.

a) RT 20MPa

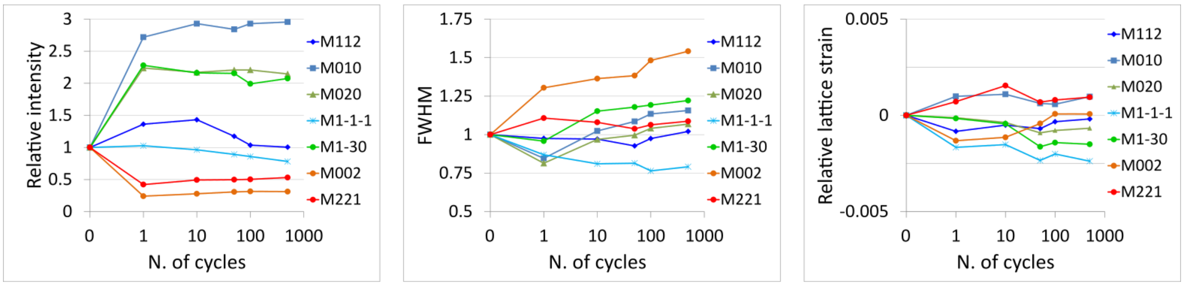

b) HT 20MPa

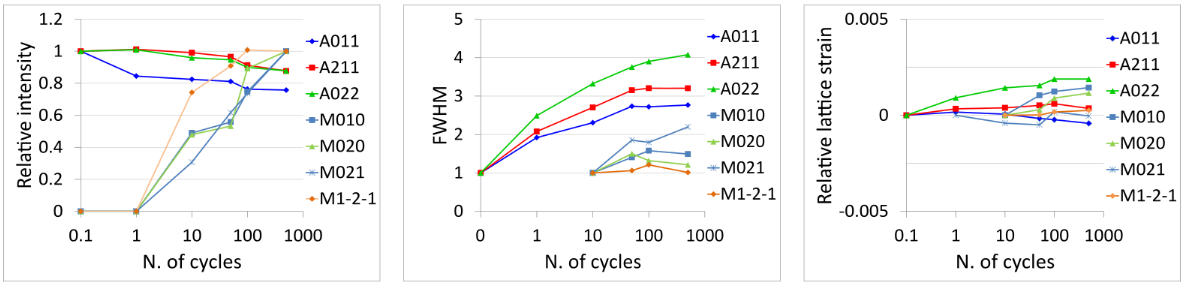

c) RT 20MPa after

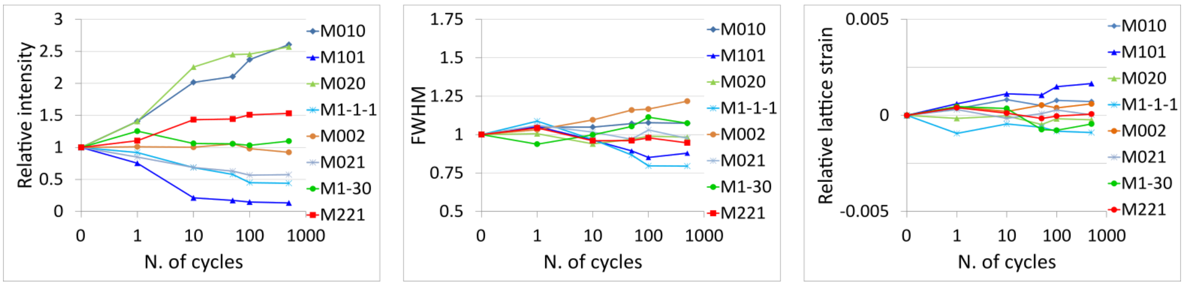

Figure 16. NiTi#5 wire: Evolution of the relative intensity, FWHM and relative lattice strain of selected reflections upon thermal cycling for three temperature-loading conditions: a) at RT under 20MPa, b) at elevated temperature under 20MPa and c) at RT under 20MPa.

Figure 16 provides complete information on the analysed diffraction results. The above discussed significant changes of peak intensities and widths in all three thermomechanical states up to 500th cycle are clearly visible. It appears that the wire microstructure continuously evolves as it gradually adapts to the imposed stress-temperature cycling. Thermomechanical response becomes more stable, however, the drift of both cold and hot strain due to plastic deformation continues up to last measured 500th cycle.

In spite of the continuing hot and cold strain drifts after 50cycles, transformation strain (Figure 14) becomes stable. In other words – the wire gradually becomes longer but the actuator strain remains the same. The different macroscopic responses of the Flexinol 90C and the FWM

NiTi#5 wires originate from their different microstructures. Flexinol 90C wire shows very stable behaviour, where the FWHM increase upon cycling is negligible at 200MPa stress level. The strengthened microstructure of the Flexinol 90C wire is less prone to plastic deformation upon thermal cycling. At higher applied stress levels, however, the strain-temperature response of the Flexinol 90C wire becomes unstable too.

Thermomechanical and in-situ XRD results from thermal cycling experiments on the NiTi#5 and the Flexinol 90C wires are not sufficient to complete the story behind the unstable behaviour of NiTi actuators and cannot be used to fully explain all microstructural changes. Only general conclusions on the texture evolution, defect accumulation and incomplete martensitic transformation could be elaborated from the presented results.

**Flexinol 90C - overloading tests**

When compared with NiTi#5, Flexinol 90C wire is very stable under 200MPa stress during thermal cycling. If the applied stress is increased, however, the strain instability occurs in the same way as for NiTi#5 wire. Higher stress level promotes the processes responsible for the instable behaviour, which are qualitatively the same as in the case of 200MPa, but much faster, more pronounced, and easier to follow by observing macroscopic strain-resistance-temperature response or by in-situ x-ray diffraction.

Therefore, overloading thermal cyclic tests (100 cycles) on Flexinol 90C wire were performed under four different levels of applied constant stress; 200, 500, 800 and 1000 MPa, without collecting diffraction data. Results are shown in the Figure 17. With increasing stress level, the transformation temperatures are shifted to higher values according to Clausius-Clapeyron relation (equation 1) and transformation strain in the first thermal cycle first increases from 4.6% (200MPa) to 4.8% (500MPa) and then decreases (magenta lines in Figure 17b). For both 200MPa and 500MPa, transformation strain decreases upon cycling, gradually stabilizes for 200MPa case, while it remains decreasing for 500MPa. The decrease of the transformation strain in the first thermal cycles for 800 and 1000MPa is due to the combination of insufficient heating temperature and plastic slip occurring at higher stress levels resulting in significant irrecoverable strain and therefore it is irrelevant to discuss the evolution of transformation strain for these two stress levels.

Beside the macroscopic thermomechanical response and the in-situ x-ray/neutron diffraction, the evolution of the microstructure can be studied by measuring the variation of the electric resistance response during thermal cycling. Common behaviour of the electric resistance in NiTi wires during thermally induced martensitic transformation can be described as follows (see Figure 9). In the first stage of heating (starting from martensite), electric resistance naturally increases with rising temperature, with a slope specific for martensite phase. Upon further heating, electric resistance reaches a maximum around $A_s$ temperature. It is because of two concurrent mechanisms taking place in the microstructure get into equilibrium; electric resistance growth due to rising temperature, and electric resistance drop due to the onset of martensitic transformation (electric resistance of austenite is lower than electric resistance of reoriented martensite). When all martensite transforms back to austenite, another process outweighs; thermal expansion of austenite, which causes the growth of electric resistance after reaching its minimum.

Electric resistance was only measured during the heating phase of the experiments, when the joule heating was triggered, because the testing machine was not properly calibrated for low values of the electric current. However, even such partial electric resistance data still provide valuable information about microstructure evolution.

Note the behaviour of the electric resistance during the first 10 actuation cycles at different stress levels in Figure 17c for 800MPa and in Figure 17d for 200MPa. At 200Mpa, the response is very stable throughout the cycling. At 800MPa (for NiTi actuators extremely high stress), the electric resistance behaviour changes rapidly during the first 10 thermal cycles (for 1000MPa the response is completely changed in the very first cycle). Instead of reaching a maximum value (at $A_s$ temperature) followed by a drop, the electric resistance reaches a maximum but gradually changes the slope of the drop, until the 10th cycle, where it stays on the plateau. With increasing number of cycles, the electric resistance response stabilizes. Such strange evolution of the electric resistance response during thermal cycling suggests that under high stresses the martensitic transformation is accompanied with dislocation slip having a strong influence on material stability.

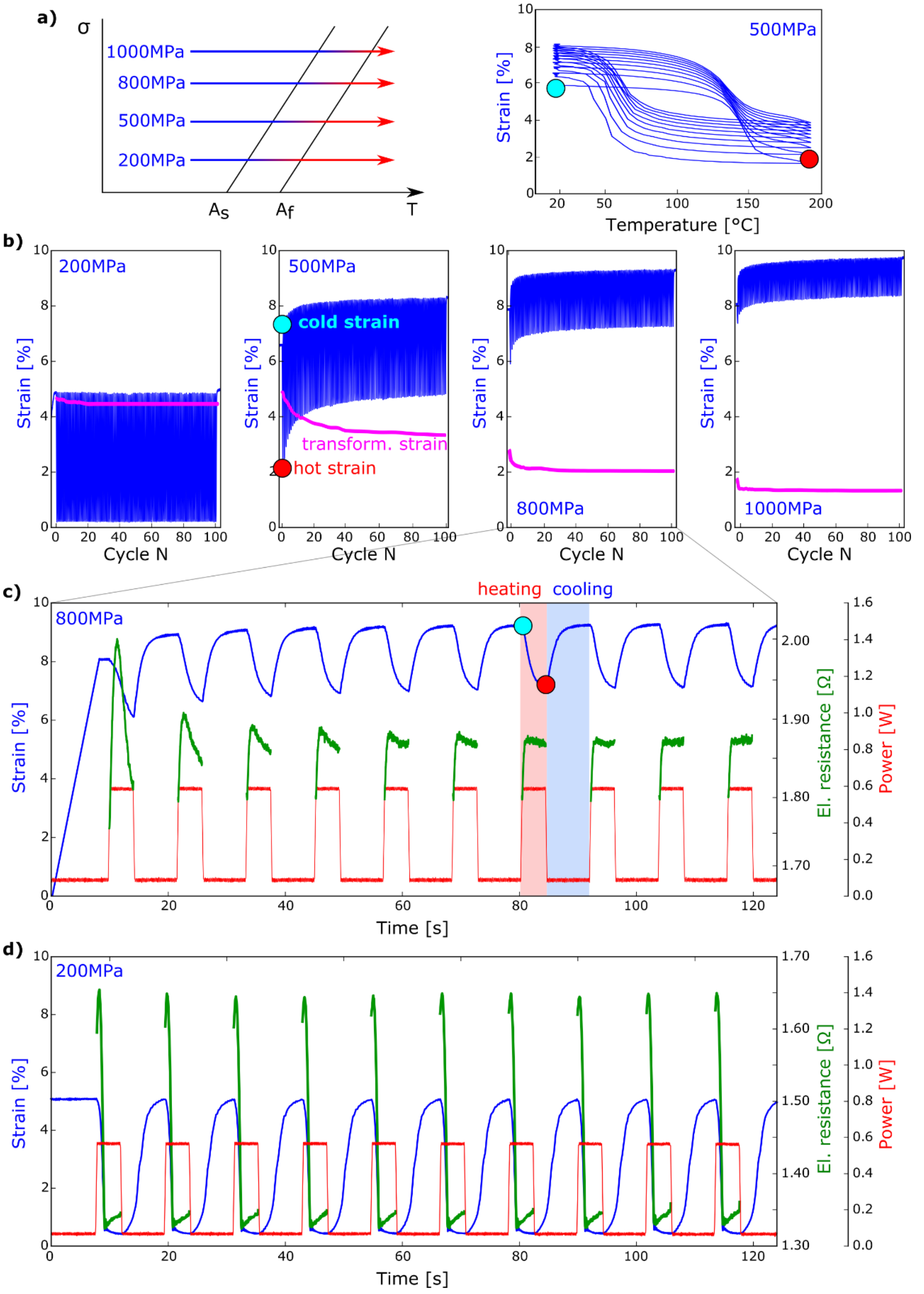

Figure 17. Thermal cycling of Flexinol 90C wire under constant applied stress. a) strain-temperature response during cycling under 500MPa. b) strain-No of cycles response in first 100 thermal cycles under different applied stresses, strain-time responses in first 10 thermal cycles under 800MPa (c) and 200MPa (d) stresses with electric resistance evolution [111].

## 2.3 Conclusions

From the macroscopic strain - electric resistance - temperature response observed experimentally upon thermal cycling and supported by in-situ synchrotron x-ray diffraction results, following conclusions can be drawn. During the thermal cycling of NiTi#5 wire under 200MPa, the texture evolves towards the oriented martensite. Consistent with the previous observation in the literature, defects gradually accumulated in the microstructure, which was evidenced by the observed peak broadening, and a two-way shape memory effect was gradually introduced. Austenite texture at high temperature remained almost unchanged throughout the cycling. However, martensite reflections started to appear at high temperature indicating martensite stabilization by the dislocations created by cycling. In which stage of the thermal cycle are the dislocations generated, however, cannot be deduced from these results. It was assumed that the newly formed dislocations produce stress field capable of keeping martensite in the microstructure above the $A_f$ temperature. It was assumed that these dislocations formed upon heating, when the oriented martensite transforms back to austenite. We call this process Low Temperature Shape Setting (to be discussed in detail in the following part of the thesis).

During the thermal cycling of Flexinol 90C wire under elevated stress levels, significant drift of both hot (austenite) and cold (martensite) strain was observed, resulting into accumulation of irrecoverable strain. Note that even under such drastic conditions as 1000MPa of constant stress, macroscopic thermomechanical response of the wire plastically deformed in the first cycle gets stabilized resulting into a small incremental increase of irrecoverable strain and much smaller but stable transformation strain upon further cycling. It means that the material completely rebuilt its internal microstructure, but the functional properties remained.

In-situ electric resistance measurement was employed to follow the microstructure evolution upon cycling, but it is not very well understood at the moment because of two facts. Firstly, electric resistance was measured only in the heating stage (when the joule heating power pulse was triggered), because it was not calibrated properly. Secondly, a strange evolution of the behaviour under higher stresses (800MPa, 1000MPa) was observed. One of the explanation for this abnormal behaviour was insufficient heating temperature leading to incomplete transformation.

The peculiar behaviour of the electric resistance at higher actuation stress levels was attributed to a low temperature shape setting mechanism described in the following chapter. This mechanism is suspected to be responsible for the unstable strain-temperature behaviour and changes in the microstructure projected also into electric resistance behaviour. The change of the electric resistance behaviour also confirms that besides martensitic transformation, plastic slip is present during the reverse martensitic transformation, responsible for a drastic increase of electric resistance above $A_s$ temperature. It also indicates that maximum damage occurs when the material is overheated in martensitic state.

Nevertheless, if properly understood, the in-situ electric resistance measurement serves as a very good complementary method to study the microstructure evolution upon thermal cycling.

# 3 Low temperature shape setting of NiTi

Deformation/transformation processes occurring in NiTi wires subjected to heating under external constraint were systematically studied in unique thermomechanical loading experiments presented in this section. The evolutions of tensile stress, strain and electric resistance of the wire measured during constrained heating/cooling tests are reported and analyzed with the help of the supplementary information provided by the application of various in-situ and ex-situ methods. The key method is the in-situ electric resistance measurement which provides information on the microstructure evolution during the test. In-situ synchrotron x-ray diffraction method allowed for determining the temperature and stress ranges, where the oriented martensite transforms into deformed austenite recorded during the constrained heating. Digital image correlation (DIC) observation of surface strains confirmed that plastic deformation is coupled with the reverse martensitic transformation and localized to martensitic regions only. Transmission electron microscopy (TEM) investigation of microstructures in the treated wires gave us detailed information on the lattice defects involved. A unique incremental-step thermomechanical experiment helped us to find out how the functional properties of the wire evolve during the constrained heating.

The obtained experimental results are interpreted in terms of the reverse martensitic transformation coupled with the plastic deformation via dislocation slip and twinning, which is understood as a deformation mechanism of NiTi, specific for high temperature - high stress conditions. According to the available literature, the dislocation slip can be easily nucleated at the propagating habit plane interface in NiTi in thermally [21,50] and mechanically [48,54] driven martensitic transformations. Combined transformation and plasticity appears also during isothermal heavy deformation of NiTi at ambient temperatures [84,85] as well as upon deformation at high temperatures [86].

Besides of the fact that this deformation mechanism offers a unique opportunity to shape set NiTi alloys at temperatures as low as 100°C - 300°C, it also plays a key role in actuation (it is responsible for the strain drift observed during the thermal cycling under stress and causes malfunction of embedded prestrained NiTi elements exposed to accidental overheating) and very likely also in fatigue of NiTi. Based on the knowledge of this TRIP like deformation mechanism, microstructure of the NiTi wire can be purposely manipulated and TWSME up to 4% can be imprinted to NiTi via single heating/cooling run under external constraint.

## 3.1 Introduction

In the following section, experiments dealing with the reverse martensitic transformation in NiTi subjected to a constrained heating after a deformation in the martensite state are discussed. NiTi shape memory alloys deformed and heated under the external constraint, which prevents the oriented martensite phase from returning back to the parent austenite phase, show peculiar stress-strain-temperature behaviours due to martensitic transformation coupled with plastic deformation due to dislocation slip and twinning. In the literature, thermomechanical loading tests investigating such NiTi behaviour include: i) recovery stress tests under fixed length [69,70], ii) thermal cycling under dead load [33] and iii) thermal cycling under general constraint, where the constrained length of the wire varies linearly with force and/or temperature [24,71]. Stress-strain-temperature responses observed in such tests can be either fully recoverable [69] or not. For a conventional NiTi wire, unrecovered strains appear after heating/cooling when maximum temperature reached upon constrained heating exceeds 100°C under stresses of several hundreds of MPa. Upon the constrained heating, the deformed martensitic wire transforms back to the austenite while the stress rises and falls. After cooling and unloading, the wire becomes several percent longer suggesting that irrecoverable deformation processes took place when the oriented martensite transformed to austenite upon heating. This is the principle of the shape setting of an already superelastic NiTi wire or it occurs when an actuator wire is overloaded/overheated during thermal cycling.

Conventionally, the term “shape setting” describes a heat treatment of a constrained cold worked NiTi, made with the purpose to give it a new shape and functional properties [72,73]. Typical conditions used for shape setting of a cold worked superelastic NiTi correspond to heat treatment at 400 °C -500 °C in a constrained shape using a fixture in environmental furnace for several minutes. Cold worked NiTi can also be shape set by Joule heating [74–76]. Mallard et al [51,59] recently proved, that a cold worked NiTi can be shape set using an electric power pulse lasting only a few milliseconds, with very similar results.

While investigating the shape setting of cold worked and annealed thin NiTi wires, it was found that the required heat treatments are rather different in both cases. To shape set a cold worked NiTi wire, it must be heated up to at least 400°C [48,74]. Superelastic NiTi wires, however, could be shape set at relatively low temperatures below 250°C [77,78] without modifying their functional properties. This was a breakthrough, since it enabled a technology for shape setting of hybrid NiTi/polymer textiles without damaging the integrated polymer fibres [79,80]. However, there are many issues that must be carefully considered when applying this technology. Functional properties are somehow different after shape setting of already annealed wires, the new shape is not set exactly as required and sometimes it is not set at all. These problems have been known in the industry. Engineers employ various tricks to deal with them; use different mandrels than actually required, to compensate the shape differences, perform the constrained heating slowly, in a step wise manner, or apply various conditioning pretreatments prior to the shape setting of an annealed NiTi. These tricks frequently do help but not always, since the physical origin of the problems remains unclear. We believe the knowledge on the physical processes occurring in NiTi subjected to the constrained heating we obtained from the experiments reported below are very relevant for the shape setting and actuation research.

There is rather limited data in the literature concerning the stress-strain-temperature behaviour of NiTi involving large stresses up to 1500MPa and high temperatures 20°C-400°C. Although the martensitic transformation is present under such conditions, the behaviour is not reversible since the inherently present plastic deformation cannot be recovered upon heating. In a typical shape setting experiment [58,70,81] on a superelastic or actuator NiTi wire deformed to ~5% in tension, constrained and heated, the tensile stress starts to increase with increasing temperature but reaches a maximum and decreases upon further heating. As the wire is longer and austenitic after the shape setting [58,81], it is obvious that the stress induced martensite was converted to plastically deformed austenite while going through the stress maximum [58]. Yan and Van Humbeeck [70] investigated evolution of the tensile stress of NiTi thin wire subjected to constrained heating up to 300°C, isothermal holding and cooling. They observed the above mentioned stress maxima on the stress-temperature curves recorded during the constrained heating but did not pay attention to them since they were particularly interested in stress relaxations observed during the isothermal holdings at high temperatures.

Surprisingly, there are only a few research reports in the literature dedicated to the investigation of the microstructure evolution during the shape setting of NiTi (constrained heating) which would tell us what happens in the wire when it passes through the stress maximum in such experiments. Malard et al [74] analyzed the evolution of microstructure of a cold worked NiTi wire subjected to short electric pulses by in-situ synchrotron x-ray diffraction. They found that the cold work microstructure passes through a sequence of recovery and recrystallization processes during a few milliseconds long Joule heat pulses, which can be precisely controlled to achieve required microstructure and functional properties of the wire. Yu et al [82] investigated the evolution of microstructure of a heavily cold-drawn amorphous NiTi wire by synchrotron x-ray diffraction during continuous heating in a furnace.

They reported structural relaxations via atomic rearrangements occurring in the amorphous phase much below the crystallization temperature. Benafan et al [83] investigated the microstructure evolution during shape setting of an annealed soft nearly equiatomic NiTi bar by in-situ neutron diffraction. They found that the martensite transformed to the austenite between 100°C - 200°C and stresses relaxed upon further heating to 450°C. Unfortunately, no neutron diffraction spectra were recorded between the 100°C - 200°C, where the martensite transformed to the austenite. They reported that the shape setting can be performed repeatedly and the functional behaviour prior and after each shape setting treatment are comparable.

In this work, experiments similar to Benafan's [83] and Yan's [70] are performed. When analyzing the results, the attention was paid particularly to the deformation/transformation process, which converts the oriented martensite into the plastically deformed austenite during the constrained heating. This process will be further on called "*Low Temperature Shape Setting /LTSS/*". The term was introduced earlier while working on the development of the shape setting technology for NiTi hybrid medical textiles [80].

## 3.2 Materials and experimental procedures

**NiTi wires**

The experiments were performed on Fort Wayne Metals superelastic NiTi wires #1 (Ti-50.8at%Ni) with diameter *d* = 0.1 mm and Dynalloy actuator wires Flexinol 90C with diameter *d* = 0.2 mm. The superelastic NiTi wires were used in cold worked state, straight annealed state as supplied by the SMA provider or in special annealed state (heat treatment of cold worked wire by electropulse method [48]) with initial microstructure and functional properties set as desired for the LTSS experiments. All superelastic wires are in austenitic B2 phase at room temperature. The wires show excellent functional properties and strength approaching 1500MPa (Figure 18). Flexinol 90C wire is in martensitic B19' phase at room temperature ($A_f$ temperature upon stress free heating is 90°C), with minor fraction of R-phase. Flexinol 90C wire is trained (thermomechanical cycling by supplier) and shows two-way shape memory effect. During the measurements, the zero strain was always set at high temperature in austenitic state (above 90°C). Therefore, the stress-strain curves for Flexinol 90C wire do now start at 0% strain.

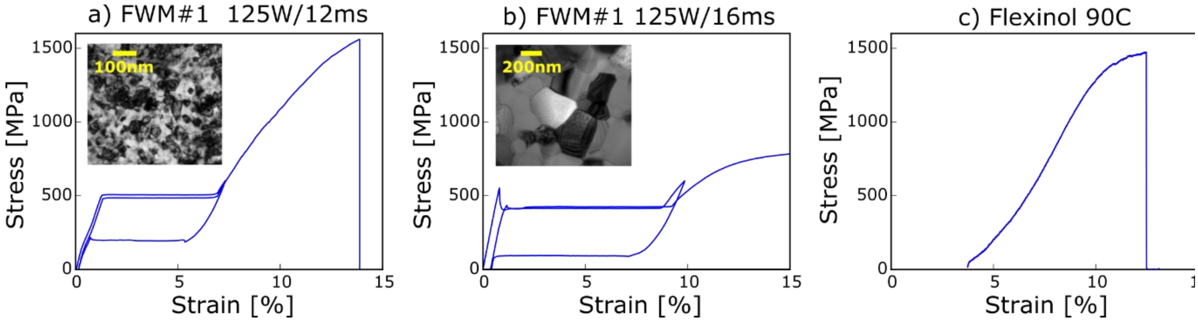

Figure 18. Functional response of NiTi wires at room temperature. a) FWM #1 superelastic wire, b) 125W/16ms electropulse treated cold worked FWM#1 superelastic wire, c) Flexinol 90C trained actuator wire r. Microstructures observed by TEM in NiTi wires are inserted in (a) and (b). Microstructure of the Flexinol 90C (c) is very similar to (a) [111].

### Thermomechanical testing

Dedicated thermomechanical loading rig MITTER equipped with Joule heating (see chapter 1.4.2) was used to perform the thermomechanical LTSS tests. It was programmed to perform the stepwise thermomechanical LTSS test (Figure 22) and linked to the control system of the beamline. X-ray diffraction patterns (2Θ angular range 0–30°) were measured during the stopovers of the programmed constrained heating test (46 equidistant temperature steps from 20°C to 400°C). Thin superelastic and actuator NiTi wires with a range of different starting microstructures were subjected to thermomechanical loading tests involving constrained heating up to temperature ~500°C. Stress, strain, temperature and electric resistance of the wire were continuously recorded.

### In-situ synchrotron X-ray diffraction

To find out the temperature range of LTSS processes during constrained heating, in-situ synchrotron x-ray diffraction experiment was performed at high resolution powder diffraction beamline ID22 at ESRF. The ID22 beamline (Figure 19) uses monochromatic x-ray beam and high resolution point detector to record a diffraction signal with a very high angular precision in determination of diffracted intensity as a function of 2Θ position (or d-spacing). High angular resolution is needed for analysis of the overlapping B2 and B19’ reflections in diffraction patterns measured during the constrained heating of NiTi wires exposed to LTSS treatments.

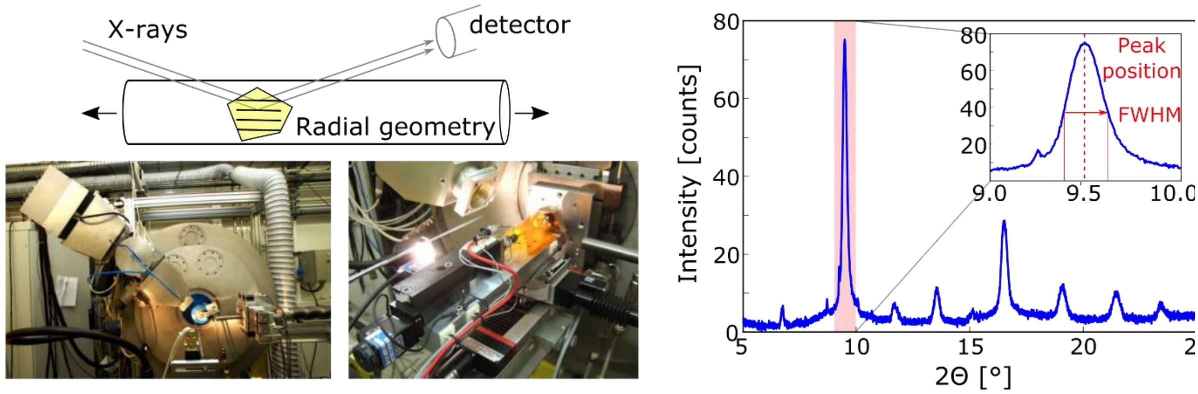

Figure 19. Set up of the in-situ synchrotron x-day diffraction experiment on ID22 diffractometer with installed MITTER rig (left) and introduction to the data analysis (right). Radial geometry of the in-situ diffraction experiment with diffracting lattice planes roughly parallel to the load axis is suggested by the schematic picture.

In the experiments, x-ray energy was set to 31keV (0.4Å) with a beam size of 1x1 mm irradiating NiTi wire volume of 7.85x10$^6$ or 31.4x10$^6$ μm$^3$ in case of 0.1mm or 0.2mm wire diameter, respectively. Since the grain size of the straight annealed FWM #1 and Flexinol 90C NiTi wires is below 100 nm and that of the 125W/16ms electropulse treated NiTi wires is less than 500nm [51], the statistics of x-ray diffraction data was very good. The MITTER stress rig was mounted on the x-ray diffractometer in axial geometry for superelastic NiTi#1 wires (wire was positioned in a vertical direction with the tensile axis lying roughly perpendicular to diffracting planes) or in radial geometry for actuator wires (wire was positioned in a horizontal direction with the tensile axis lying roughly parallel to diffracting planes).

## TEM characterization of microstructures

Thin foil specimens for TEM investigations of microstructures were prepared from the LTSS treated superelastic 125W/16ms NiTi wires as well as from the same wire subjected to additional 125W/ 12ms electropulse treatment. A cross-sectional surface of the cut wire was carefully polished. Longitudinal or transversal slabs were extracted from the center of the wire using the focused ion beam (FIB) technique and subsequently thinned to electron transparency. TEM observations were carried out in a FEG TECNAI F20-ST and CM30 Ultra-Twin operated at 200 kV and 300 kV, respectively. Microstructures of the wires prior and after the tests were analyzed by TEM in order to learn about lattice defects and deformation mechanisms involved.

## 3.3 Thermomechanical loading experiments

First, the basic low temperature shape setting tests performed on thin NiTi#1 superelastic and Flexinol 90C actuator wires with four different initial microstructures (Figure 20) will be discussed below to introduce the reader the constrained heating experiments on different types of NiTi wires. Starting microstructures and initial loading states of the samples subjected to LTSS tests are listed in Table 3.

Table 3. Initial microstructures and loading states of the NiTi wires subjected to LTSS tests.

| **Figure 20** | **sample** | **initial microstructure (at 0MPa)** | **initial loading state - (phase)** |
|---|---|---|---|
| a,b | NiTi#1 | austenitic | 450MPa / 1% - (austenite) |
| c,d | NiTi#1 | cold worked | 0MPa / 0.1% - (cold worked) |
| e,f | NiTi#1 | austenitic | 580MPa / 7% - (reoriented martensite) |
| g,h | Flex. 90C | martensitic | 700MPa / 7% - (reoriented martensite) |

The constrained heating/cooling tests up to 500-700°C were performed by Joule heating using controlled electric power pulses. Macroscopic σ-T and ρ-T responses (Figure 20) recorded during the constrained heating tests represent the observed material behaviour. Figures 20a-d show such responses for fully annealed superelastic NiTi wire in austenite state (Figures 20a,b) and a cold worked NiTi wire (Figures 20c,d) during constrained heating/cooling by electric pulse up to 700°C. Note that the stress and electric resistance responses of cold worked and austenitic wires are very different. The difference is only in the material state of the wire prior the test. While the response of the fully annealed austenitic wire (Figures 20a,b) is nearly linear and perfectly reversible on heating/cooling (thermal dilatation and electric resistance variation of a metal), the responses of cold worked wire are non-linear, hysteretic and irreversible since its microstructure significantly evolves during the constrained heating while it undergoes recovery and recrystallization processes. There is a stress maximum stress of the order 500-600MPa at temperature ~400°C upon the constrained heating. The stress maximum and temperature at which it is observed do not depend on the applied heating rate and prestrain. The austenitic NiTi wire cannot be shape set at all in spite of 500MPa starting stress and maximum temperature as high as 700°C. In order to shape set the cold worked wire (Figures 20c,d), temperature higher than 400°C must be reached since the microstructure of the cold worked wire starts to recrystallize beyond the 400°C temperature [74]. The recrystallization process is driven mainly by the internal energy stored in the crystal defects and internal stress of the cold worked wire, the stress is not so important.

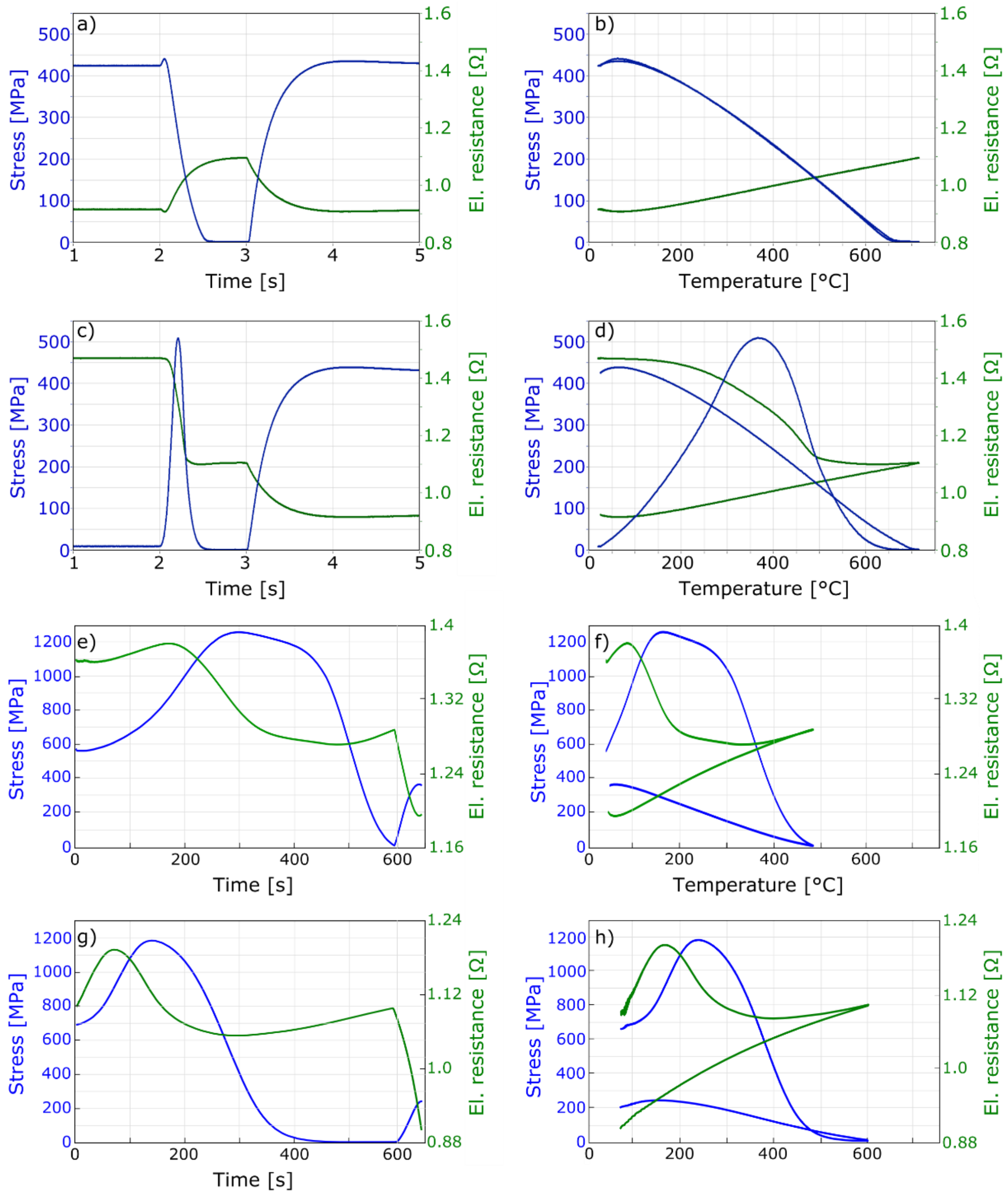

Figure 20. Stress and electric resistance responses recorded of NiTi wire subjected to electropulse heating/cooling under external constraint (controlled electric power in the heat pulse, length of the wire fixed): a,b) fully annealed superelastic wire in austenite state (prestrain 1%, stress 420MPa), c,d) cold worked NiTi wire (prestrain 0.1%, stress 10MPa), e,f) straight annealed superelastic NiTi wire deformed beyond the end of the stress plateau (prestrain 7%, stress 580MPa) and g,h) Flexinol 90C NiTi wire deformed beyond the end of the stress plateau (prestrain 7%, stress 640MPa) [111].

Figures 20e-h show constrained heating responses for fully annealed wires in martensite state. Figures 20e,f show a response of the superelastic straight annealed NiTi wire deformed beyond the end of the stress induced transformation plateau (580MPa). Figures 20g,h show response of the Flexinol 90C NiTi wire deformed in martensite state till 640MPa beyond the end of the reorientation plateau. Both wires are in the oriented martensitic state when the constrained heating starts. Compared to the cold worked NiTi wire (Figures 20c,d), the maximum stresses reached upon the constrained heating of annealed NiTi wires (Figures 20e-h) are much higher and are attained at much lower temperature. This is where the term Low Temperature Shape Setting /LTSS/ comes from [80]. As will be explained further below, while the cold worked wire is deformed plastically during the recrystallization process (dynamic recrystallization) upon the constrained heating, the oriented martensite in annealed wires is converted to plastically deformed (longer) austenite by the LTSS deformation/transformation process.

Figure 21 presents results of similar constrained heating tests on straight annealed FWM NiTi#1 superelastic wire. Since the wire deforms via propagation of martensite bands of localized deformation [88], it can be prestrained in tension to ~500MPa in a way, that it is:

- deformed elastically only up to 1.2% strain so it is in austenite (R-phase) when the heating starts (Figure 21a),
- deformed up to 4% strain so that martensite band covers a part of the wire only when the heating starts (Figure 21d)
- deformed up to 7% strain so that it is fully martensitic when the heating starts (Figure 21g).

Superelastic stress-strain responses of the wire prior and after the constrained heating/cooling are compared in the right column (Figures 21c,f,i). If the wire is heated in austenitic state (a-c), the response of stress and electric resistance during the constrained heating/cooling is completely reversible. The stress remains high upon heating because of the R-phase. Neither dimensions nor superelastic properties of the wire are affected by the constrained heating/cooling (Figure 21c). In contrast, the heat treated martensitic wire shows hysteretic irreversible stress and electric resistance response during the constrained heating/cooling (Figure 21h). After the heating/cooling, it is 4.7% longer and shows different superelastic response than prior the test (Figure 21i). The superelastic stress-strain response of heat treated partially deformed wire (Figure 21f) exhibits only partial shape setting (only 2% nonrecovered strain) and peculiar superelastic curve with two stress plateaus.

Note that, although the length of the wire remains constant during the heating/cooling test, the wire becomes longer but fully austenitic and functional after cooling and unloading (Figure 21g,i). This suggests that the oriented martensite must have been converted to plastically deformed longer austenite during the constrained heating/cooling. In other words, the wire was shape set at relatively low temperature below 300°C within the LTSS temperature range (Figure 21h).

A possible explanation of such experimental results in Figures 21d-f (prestrain 4%) is that the wire was shape set (plastically elongated) only in the parts, where the martensite band existed during heating and that the microstructure of the heated wire became heterogeneous after cooling/heating. This explanation would rationalize the curious superelastic curve with two stress plateaus in Figure 21f. Direct experimental evidence supporting this assumption, however, was missing. It will be further discussed in the chapter 3.7.

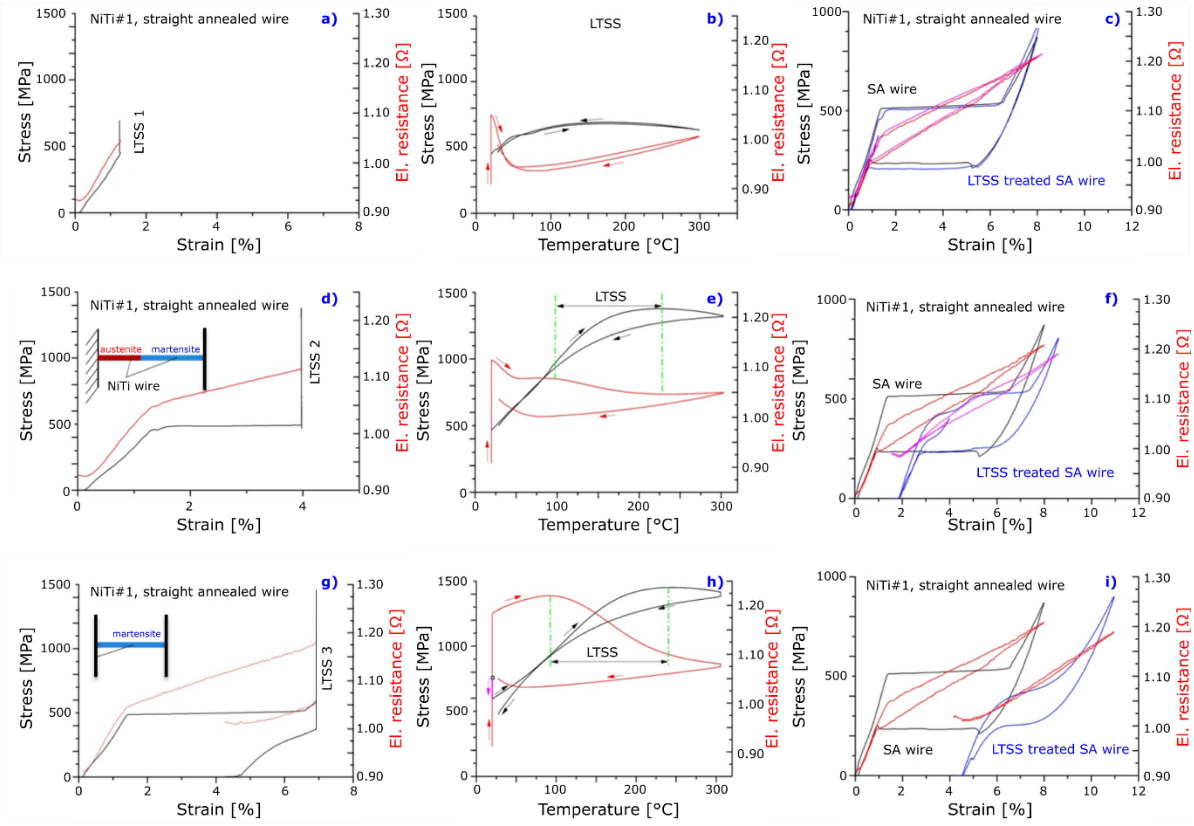

Figure 21. Stress and electric resistance responses recorded on straight annealed superelastic NiTi wire (FWM #1 wire) subjected to electropulse heating/cooling under external constraint in: a-c) austenite state (1% prestrain), d-f) mixed austenite + martensite band state (4% prestrain), g-i) stress induced martensite state (7% prestrain). The experiments consist in prestraining at room temperature to various strains (a,d,g), constrained heating/cooling to 300 °C (b,e,h) followed by unloading at room temperature. Superelastic stress-strain responses prior and after the LTSS treatment are mutually compared in (c,f,i). The LTSS temperature range where plastic deformation occurs is denoted in e,h [111].

## 3.4 In-situ synchrotron x-ray diffraction LTSS experiment

In order to find out at which temperature and stress the oriented martensite transforms to austenite upon the constrained heating, in-situ synchrotron x-ray diffraction experiment was performed at the high resolution powder diffraction beamline ID22 at ESRF (Figure 19). In-situ synchrotron x-ray diffraction experiments were performed on: i) straight annealed superelastic NiTi wire, ii) superelastic NiTi wire (125W/16ms electropulse treated) with special recrystallized microstructure and iii) Flexinol 90C NiTi actuator wire. MITTER stress rig adapted for in-situ synchrotron x-ray diffraction experiments was used to perform the thermomechanical tests. NiTi wires were prestrained beyond the end of the stress plateau (presumably resulting in oriented martensite everywhere in the wire) and subsequent constrained heating/cooling was run up to preselected maximum temperature. X-ray diffraction patterns (2Θ range 0-30°) were recorded during the stopovers in the program of the thermomechanical test (equidistant steps of ~7°C from 20°C to 400°C) while the evolving stress, strain, temperature and electric resistance of the heated wire were continuously recorded.

The key in-situ diffraction experiment on the Flexinol 90°C actuator wire was performed using the MITTER tester programmed to run incremental constrained heating test with 46 incremental heating steps (Figures 22,23) for diffraction measurements to be carried out during the stopovers at constant temperature. The program consists of:

1. Heating the wire to 100°C under 5MPa, setting the strain to zero and cooling to 20°C
2. Loading to 7% strain at 20°C in a position control and constraining length of the wire
3. Heating to pre-set $T^{LTSS}$ temperature by electric power (heating rate ~1°C/s)
4. Holding for 600s at the $T^{LTSS}$ temperature while measuring the diffraction pattern
5. Continue by step 3 with incrementally increased $T^{LTSS}$ temperature ($\Delta T \approx 7°C$)

The obtained x-ray diffraction data provide key structure specific information on the microstructure evolution in the NiTi wire subjected to constrained heating. The evolutions of integrated intensities, positions and widths (FWHM) of individual reflections were analyzed. The irradiated gauge volume is considered to represent the whole wire as the physical processes taking place in the fully deformed, constrained and heated NiTi wire are considered to be homogeneous. Volume fractions of austenite and martensite phases in the heated wire were determined employing a full diffraction pattern fit by Rietveld refinement for Flexinol 90C wire and using single peak fit to extract individual intensities for superelastic wires using TOPAS5 software (R-phase not considered). Peak positions and peak widths (FWHM) carrying the information about defects and internal stresses in austenite and martensite phases were determined from single peak fit analyses of individual reflections for both Flexinol 90C and superelastic wires.

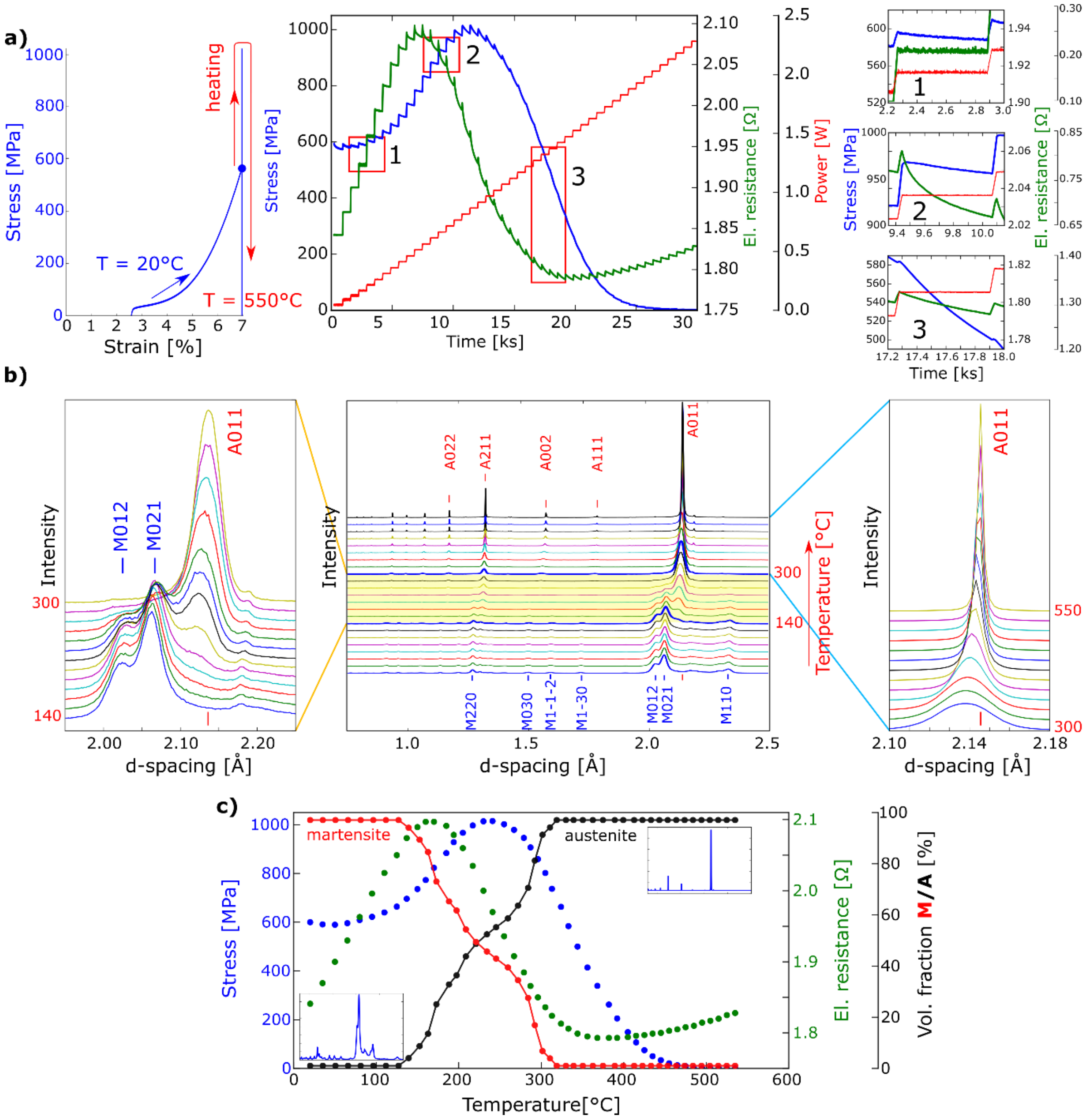

Figure 22. In-situ incremental synchrotron x-ray diffraction LTSS experiment on Flexinol 90C actuator wire: The wire is deformed at room temperature to 600MPa, constrained at 7% strain and heated in a step wise manner to 300C(a). Stress and electric resistance of the wire are continuously recorded (b) and X-ray diffraction patterns (c,d,e) are recorded in radial geometry during 10 minutes long stopovers. Volume fraction of austenite and martensite phase in the wire (b) is evaluated by quantitative phase analysis of complete diffraction patterns (c,d,e) using Rietveld analysis [111].

Results of the in-situ experiment on the Flexinol 90C actuator wire are mainly discussed here (Figures 22, 23). Since the heating was stepwise in time (Figure 22a right), the experimentally recorded stress-electric resistance-temperature response reflects the heating steps and holding time at stopovers (while recording the diffraction patterns). Variations of stress and electric resistance during the heating steps and holding times (relaxations) were evaluated. The diffraction patterns recorded during stopovers upon constrained heating clearly document that reverse martensitic transformation takes place upon the constrained heating (Figures 22, 23). Detailed look on the left side of Figure 22b shows emerging austenite 011A reflection growing and broadening next to the disappearing martensite reflections 012M and 021M, suggesting the progress of the reverse martensitic transformation and microstructure hardening with increasing temperature. The detail on the right side of Figure 22b shows decrease of the width of the 011A austenite reflection suggesting microstructure recovery upon further heating. Phase volume fractions of austenite and martensite phases were determined by the Rietveld analysis of the whole recorded diffraction patterns (Figure 22b middle). The obtained x-ray diffraction results are presented together with the evolving electric resistance and stress in Figure 22c. It clearly shows a gradual change of the oriented martensite into the austenite phase upon heating in the temperature range 150°C – 300°C, where maxima of both electric resistance and stress are observed.

Further information on the microstructure evolution upon heating was obtained from the analysis of the evolution of individual reflections (Figure 23). The intensities of the martensite and austenite reflections decrease and increase, respectively, as shown in Figures 23b,c reflecting the progress of reverse martensitic transformations in particularly oriented grains. The widths (FWHM) of diffraction peaks evolving during the constrained heating (Figures 23d,e) reflect another aspect of the microstructure evolution upon heating. The peak broadening reflects an increase of the density of lattice defects and internal strain within the microstructure while decreasing FWHM reflects microstructure recovery and/or recrystallization. The widths of martensite peaks (Figure 23d) remain constant on heating up to ~150 °C and sharply increase with increasing temperature above ~200 °C until they disappear. The austenite peaks emerge already broadened (Figure 23d) when they appear in the diffraction patterns upon heating and their widths at first increase reach a maximum and then significantly decrease upon further heating. Note that different peaks reach maxima at very different temperatures. Figures 23f,g show evolutions od increments and relaxations of electric resistance (f) and stress (g) upon heating. They provide additional information on microstructure evolution which will be further discussed in chapter 3.8.3.

In conclusion, the in-situ synchrotron x-ray diffraction experiment shows that the oriented martensite in the constrained wire gradually transforms to the austenite upon constrained heating within the LTSS temperature range and that the wire microstructure hardens until the end of the LTSS temperature range and recovers later upon further heating.

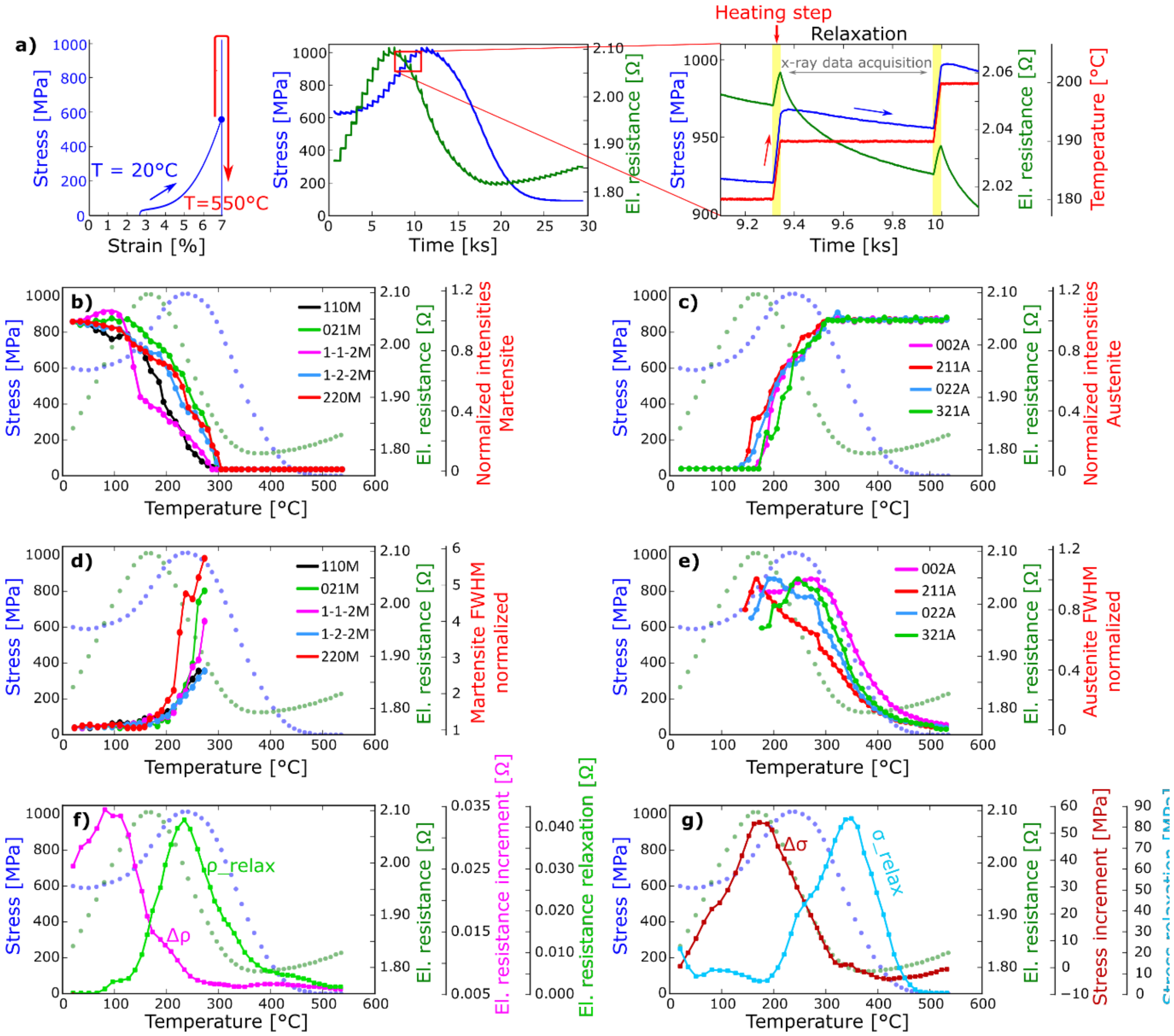

Figure 23. In-situ incremental synchrotron x-ray diffraction LTSS experiment on Flexinol 90C actuator wire: Normalized integrated intensities of selected martensite (b) and austenite (c) reflections evolving during the constrained heating. FWHM peak widths of several reflections of martensite (d) and austenite (e), increments and relaxations of electric resistance (f) and stress (g) are shown with superimposed electric resistance and stress of the wire continuously recorded during the constrained heating [111].

## 3.5 Ex-situ LTSS experiment

The reverse martensitic transformation was confirmed and the temperature range, where the oriented martensite was converted into austenite, was determined from the in-situ x-ray diffraction experiment. However, there was limited information about the plastic deformation and generation of lattice defects upon heating. In which the stage of the constrained heating does it occurs? Also, it was unclear how the functional properties of the wire evolved during the constrained heating. To find out that, we performed a unique ex-situ incremental LTSS experiment on the Flexinol 90C wire (Figures 24 - 26). This ex-situ experiment in fact mimics the constrained heating conditions of the in-situ synchrotron x-ray experiment without x-rays but includes thermomechanical subtests for evaluating the functional properties after each heating step. A complex thermomechanical schedule was programmed and executed using the MITTER tester.

The program involves:

1. Heating the wire to 100°C, setting strain to zero and cooling to 20°C under 5MPa
2. Loading to 7% at 20°C in position control and constraining the wire length
3. Heating to the pre-set $T^{LTSS}$ temperature by electric power (heating rate ~1°C/s)
4. Holding 150s at this temperature
5. Cooling to 20°C
6. Unloading to 5MPa at 20°C in position control
7. Heating from 20°C to 150°C under constant stress 5MPa using Peltier chamber.
8. Cooling from 150°C to 90°C under constant stress 5MPa using Peltier chamber.
9. Loading at 90°C till 650MPa in position control.
10. Unloading at 90°C till 5MPa in position control.
11. Heating from 90°C to 150°C under 5MPa constant stress
12. Cooling from 150°C to 20°C under 5MPa constant stress
13. Continue by step 2 using $T^{LTSS}$ increase by ~7°C

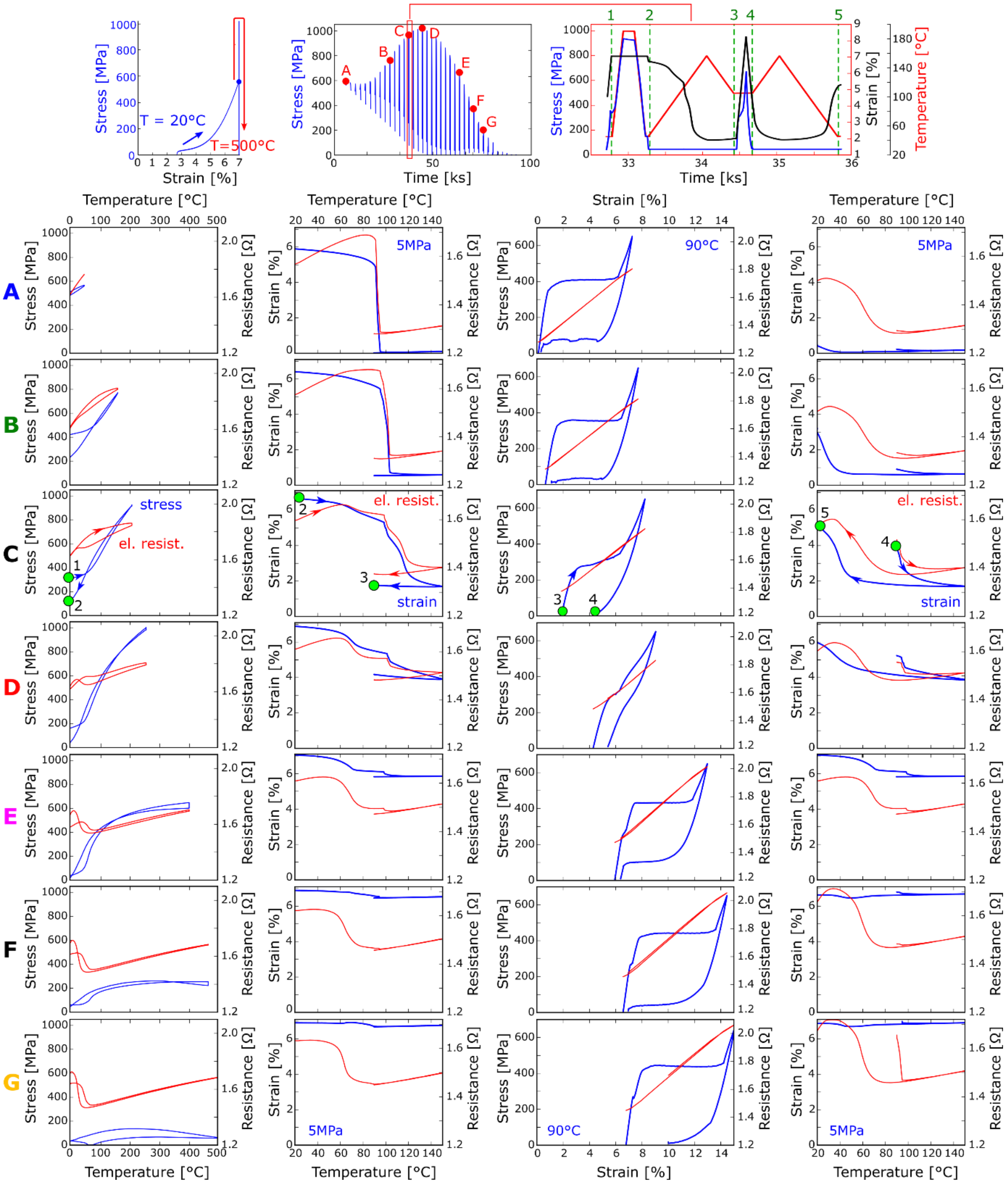

Figure 24. Ex-situ incremental LTSS experiment on Flexinol 90C actuator wire: This experiment (see test schedule and topside schema) basically simulates the in-situ LTSS experiment but, instead of recording x-ray data in stopovers, a prescribed sequence of thermomechanical loads (1-5) is performed in each step. Functional stress-strain-electric resistance-temperature responses recorded in selected material states A-G are shown in four columns. From the left: Col.1: constrained heating/cooling step to the pre-set $T^{LTSS}$ temperature, Col.2: heating/cooling to 90°C under constant stress 5MPa, Col.3: loading/unloading up to 650MPa at 90°C in position control, Col.4: heating/cooling to 20°C under 5MPa constant stress [111].

The irreversible plastic deformation processes are expected to proceed only during the constrained heating steps (program step 2) or potentially during the 150s holdings (program step 3) at the peak temperature $T^{LTSS}$ (stress increments during the heating step and stress relaxations during the holding time). The material state of the wire (microstructure) changes in each step. The other program steps (6-12) were made to evaluate the presumably reversible stress-strain-temperature responses due to the martensitic transformation for current material state. Four ranges of maximum temperatures $T^{LTSS}$ in which the functional responses are different can be clearly distinguished in Figure 24 as follows:

A-B) the wire length changes minimally upon the constrained heating/cooling and the variation of functional response consists mainly in the decrease of the plateau stress,

B-C-D) the wire elongates sharply upon the constrained heating/cooling, the superelastic property is gradually lost and TWSME up to 3% appears,

D-E) the wire further deforms plastically upon the constrained heating/cooling and the superelastic stress-strain response similar to the virgin wire gradually reappears

E-G) the wire length changes minimally upon the constrained heating/cooling but functional properties degrades (plateau strain increases, hysteresis widens, cyclic instability and strain irreversibility appears).

It is essential to note that there is a difference between the stress-temperature responses presented in Figure 24 and stress-temperature responses observed in the individual continuous constrained heating tests up to various maximum temperatures $T^{LTSS}$ (Figures 20, 21, 22) consisting in that in the ex-situ test, the microstructure of the wire gradually evolves from A to G and starting microstructures of the wire in each step are thus different. This is the reason why stress maximum is not observed on the stress-temperature responses during the constrained heating/cooling (Figure 24, Col.1).

The key outcome from the ex-situ experiment is that the NiTi wire gets plastically deformed (Figure 25) upon the constrained heating within the LTSS temperature range B-C-D (Figures 24, 25), where the oriented martensite transforms to the austenite. Clearly, the hot strain increment (Figures 25, 26) is maximal around the state C within the LTSS temperature range, where the superelasticity of the wire is lost due to a high density of newly created lattice defects (Figures 24, 26). Plastic deformation, nevertheless, occurs also at higher temperatures in the range D-G (>200°C). Figure 26 helps the reader to obtain a complete view on the evolution of the functional responses of the wire during the constrained heating test.

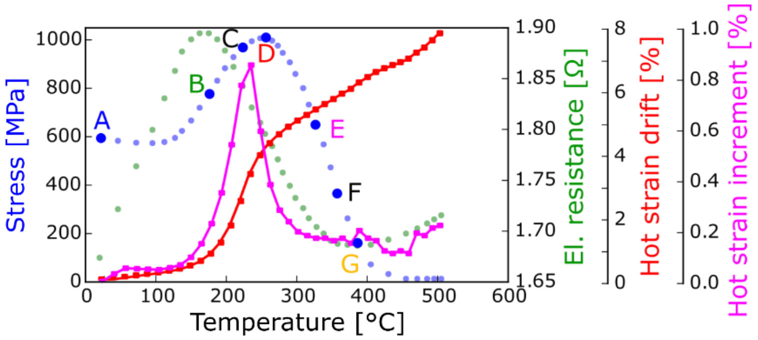

Figure 25. Ex-situ incremental LTSS experiment on Flexinol 90C actuator wire provide experimental evidence on the evolution of the Hot strain (red) and increment of hot strain (magenta) evaluated in austenite phase at 150°C [111].

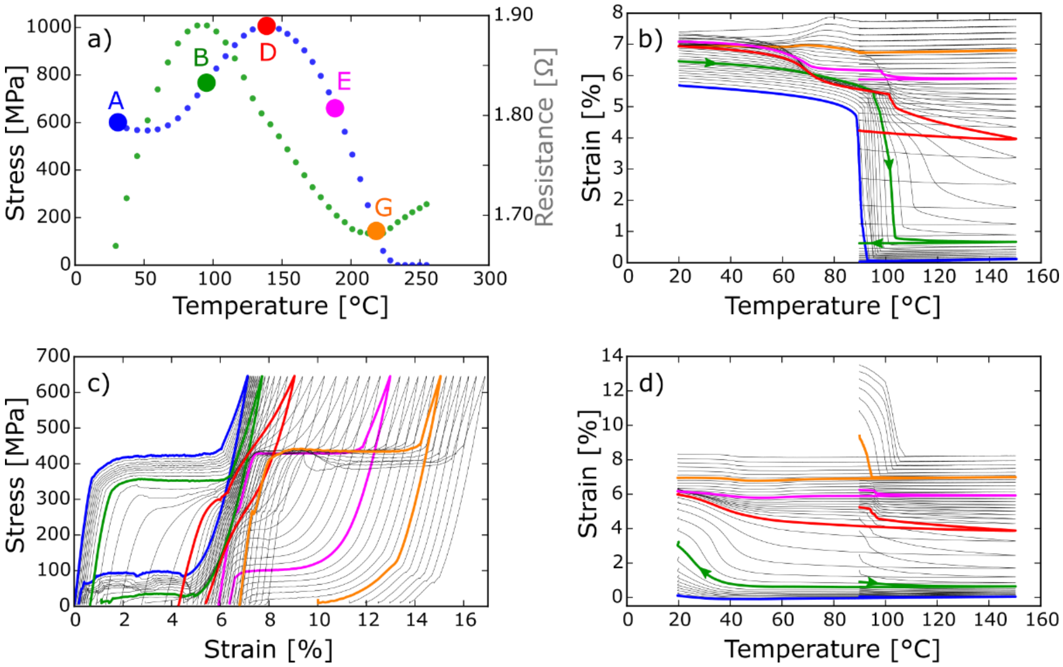

Figure 26. Ex-situ incremental LTSS experiment on Flexinol 90C actuator wire. Functional responses of the wire (see topside schema in Figure 24: b)2-3, c)3-4, d)4-5) evaluated during the constrained heating. Response recorded in 5 selected states A,B,C,D,E (a) are emphasized by color in graphs b-d [111].

## 3.6 TEM characterisation of microstructures in LTSS treated wires

It was concluded from the ex-situ experiment reported in the previous sections (Figures 24 - 26) that the density of defects within the microstructure of NiTi wire at first increases in the LTSS temperature range and later decreases during the constrained heating. In order to obtain a direct experimental evidence on this, the microstructure in the LTSS treated wire (Figure 27) was investigated by TEM. Thin foil specimens for TEM investigations were prepared from the LTSS processed wire as follows. A cross-sectional surface of the cut wire was carefully polished. Longitudinal slabs were extracted from the center of the wire using the focused ion beam (FIB) technique and subsequently thinned to electron transparency. TEM observations were carried out in a FEG TECNAI F20-ST and CM30 Ultra-Twin operated at 200kV and 300kV, respectively, at EMAT, University of Antwerp. An attempt to study dislocation microstructures in the LTSS processed straight annealed FWM#1 wire by TEM was impeded by the overlapping contrast of the grain boundaries in nanograined microstructure of this wire (Figure 18a) and similarly for the Flexinol 90C wire having similar grain size. Hence, the TEM investigation of microstructures was performed superelastic 125W/16ms electropulse treated NiTi wire having recrystallized microstructure with larger 500 nm grains as illustrated in Figure 27a.

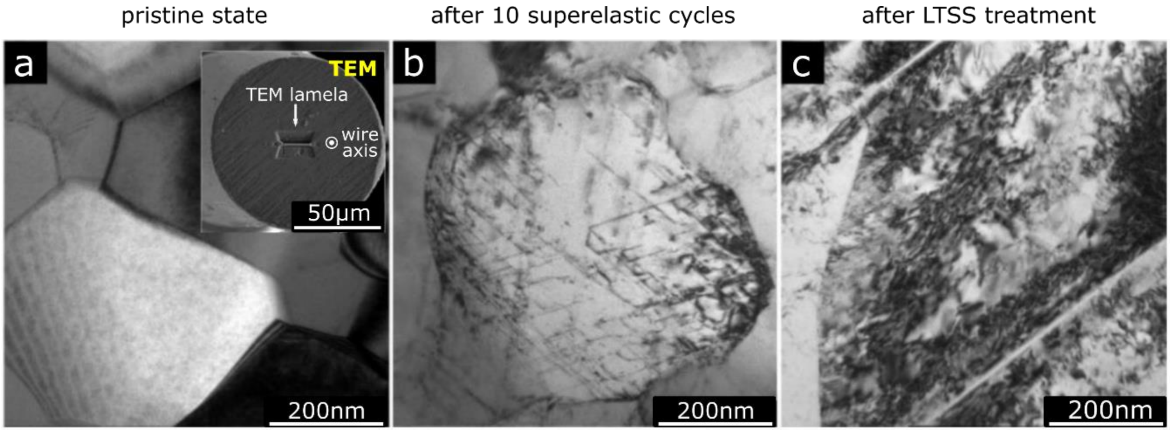

Figure 27. Microstructures in 125W/16ms electropulse treated FWM #1 NiTi wire in: a) virgin state, b) after 10 superelastic cycles at room temperature [48] and (c) after LTSS treatment [111].

The wire was prestrained to 9% and heated under constraint up to 300°C (Figure 28). After the treatment, the wire is 7% longer, austenitic and shows excellent superelastic behaviour (Figures 28c,d) – plateau strain is shorter, hysteresis smaller and the superelastic response is more stable on tensile cycling. TEM characterization was performed prior and after the LTSS treatment. The latter shows a microstructure characterized by a much higher density of entangled dislocations, internal strain, lamellar defects and no residual martensite (Figure 27c). This microstructure is remarkably different from that created by cyclic superelastic loading [48], where dislocations were clearly associated with {011}/<100> slip systems (Figure 27b). This means that LTSS deformation/transformation mechanism is completely different from that acting on cyclic superelasticity.

Details of this microstructure are shown in Figures 29, 30. Unlike after the superelastic cycling (Figure 27b), single dislocations could hardly be resolved in 2-beam analysis due to the very dense network of entangled dislocations and strong strain contrast (Figure 29).

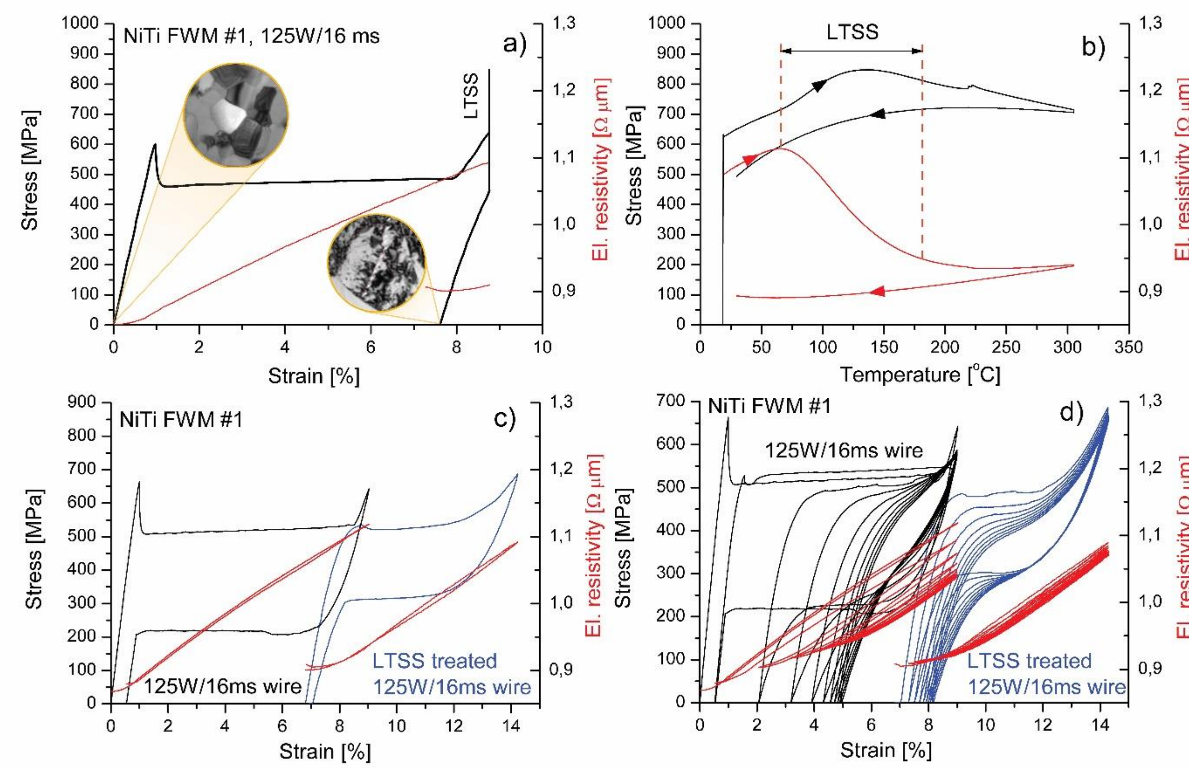

Figure 28. LTSS experiment on 125W/16ms electropulse treated NiTi FWM #1 wire (prestraining to 9%, constrained heating/cooling to 300C, unloading). Superelastic stress-strain responses prior and after the LTSS treatment are compared (c,d). TEM Microstructures before and after treatment (a) are reported in Figures 27 - 29 [111].

The activity of a plastic deformation upon the constrained heating is evidenced by the formation of dislocation cells and walls (Figure 30). Lamellar defects with a high density of dislocations inside them, a feature that was never observed in the superelasticaly cycled 125W/16ms wires, were abundant throughout the thin slabs. Bright field (BF) image in Figure 30a shows several such lamellar defects. Their crystallographic relationship with the grain matrix was investigated by selected area diffraction (SAD) acquired over the circled areas. The pattern obtained over area (b) shows two sets of reflections in {110} orientations (Figure 30b), one originating from the grain matrix (circular red dot in Figure 30c) and one from the planar defect (blue hollow dots in Figure 30c). They are in mirror orientation along the $(114)_{B2}$ twinning plane suggesting {114} compound twins. The same pattern was found for the other parallel lamellar defects seen in the grain. The second SAD pattern acquired over area (d) contains additional reflections from another lamellar defect oriented differently. They are schematically represented by green dots in Figure 30d. Relative to the grain matrix a $(-1-14)_{B2}$ twin orientation was again found. Within a single grain, two different deformation {114} twin planes were therefore activated. Other examples of lamellar defects, likely to be also deformation twins, are shown in Figures 30f,g,h. Large number of twins in the LTSS microstructure suggest they are relicts of an important deformation mechanism acting during the constrained heating and bear significant part of the plastic strain (7%) (Figure 28).

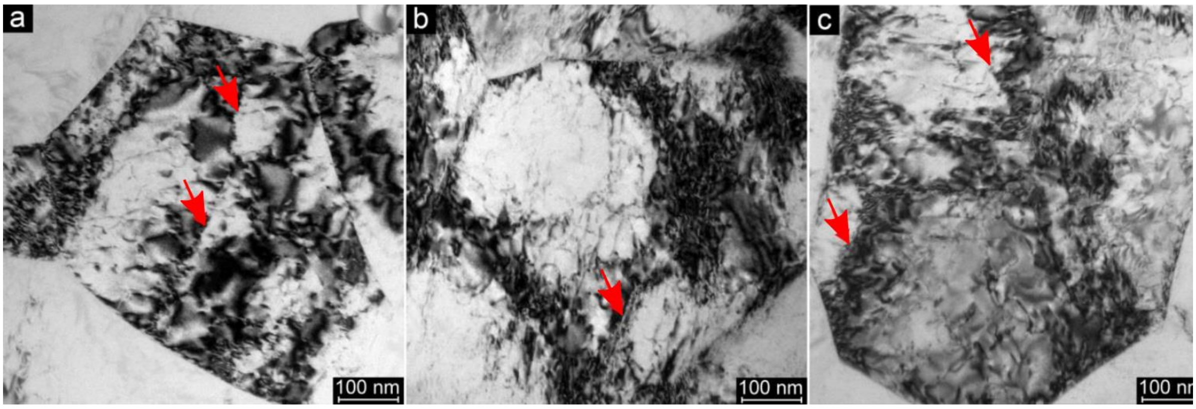

Figure 29. Microstructure in 125W/16ms FWM #1 wire after LTSS treatment (Figure 28). BF TEM micrographs show the evidence of dislocation activity during the LTSS inside grains (same grain in different tilts): dislocation tangles, strong strain contrasts, formation of dislocation walls (red arrows) [111].

It comes out from TEM investigations that the fully recrystallized microstructure of the 125W/16ms wire (Figure 27a) was converted into the heavily dislocated and twinned microstructure of the LTSS treated wire (Figures 29, 30). Although only the LTSS microstructure after constrained heating to 300°C, cooling and unloading (Figure 28b) was observed, it is expected that the 7% plastic elongation took place only during the constrained heating when the stress was rising towards the maximum in the denoted LTSS temperature range (Figure 28b). Although only indirect evidence is available to verify this, it is likely that more and more dislocations appear in the microstructure upon heating until the stress maximum is reached. Upon further heating beyond the stress maximum, the dislocated microstructure gradually recovers. The above mentioned generation and recovery of dislocations can be indirectly deduced also from the evolution of the electrical resistance and peak broadening and narrowing (FWHM) upon heating in Figures 22, 23.

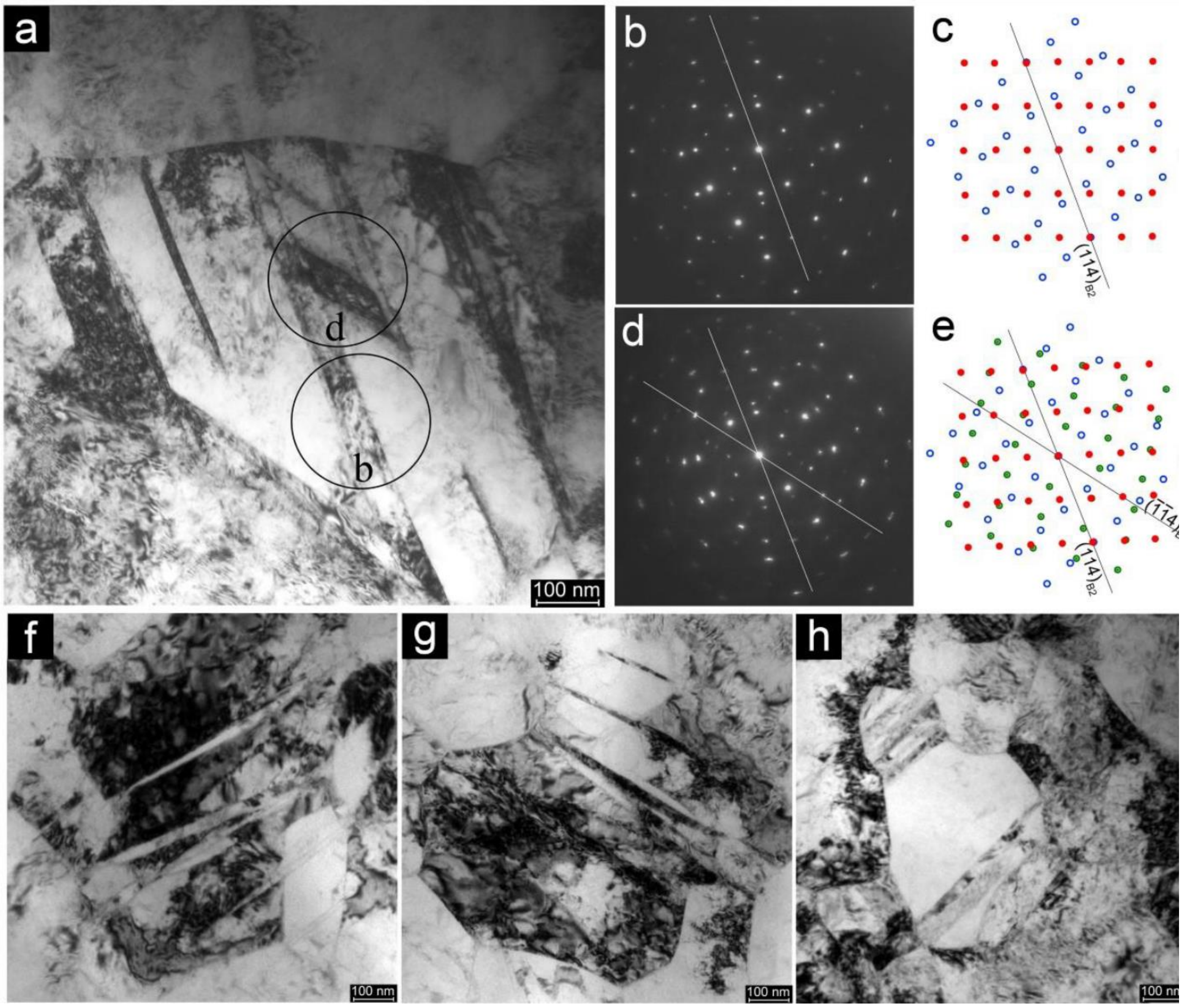

Figure 30. Microstructure in 125W/16ms FWM #1 wire after LTSS treatment. Another prevalent mode of plastic deformation during LTSS is twinning. Lamellar defects (a) were identified as {114} deformation twins (b-e) using SAD. Lamellar defects were found abundant throughout the sample (f-h) [111].

The maximum temperature reached upon the constrained heating hence matters. If the heating would continue up to 450°C, the microstructure and the functional properties similar to that of the original 125W/16ms wire would be most likely obtained. But if the heating would stop somewhere at 140°C (Figure 28b), much higher dislocation density and quasilinear elastic stress-strain response would be observed (as for the Flexinol 90C wire in Figure 24). The role of maximum temperature in the LTSS treatment will be further discussed in section 3.8.1. Note that the cyclic superelastic behaviour of the 125W/16ms NiTi wire (Figure 28d) is very unstable due to its fully recrystallized microstructure [89]. LTSS treatment till 300°C significantly improves the cyclic deformation stability of this wire. After 10 superelastic cycles (Figure 28d), the LTSS treated wire shows relatively stable 6% transformation strain and 100MPa hysteresis. This improvement in cyclic stability and decrease of stress hysteresis is a direct consequence of the change of microstructure by the LTSS. An appealing question thus appeared whether the functional response of the 125W/16ms wire can be further modified/improved by additional electropulse treatment. Particularly, whether the microstructure and functional properties similar to that of the straight annealed wire (Figure 18a) can be restored. Hence, the LTSS treated 125W/16ms NiTi wire was exposed to an additional 125W/12ms electropulse treatment. As the maximum temperature reaches ~ 700°C [51], this treatment is expected to further modify (recover) the microstructure of the LTSS treated wire. The stress-strain response of this wire (Figure 31a) was evaluated and its microstructure analysed by x-rays (Figure 31b) and by TEM again (Figure 32).

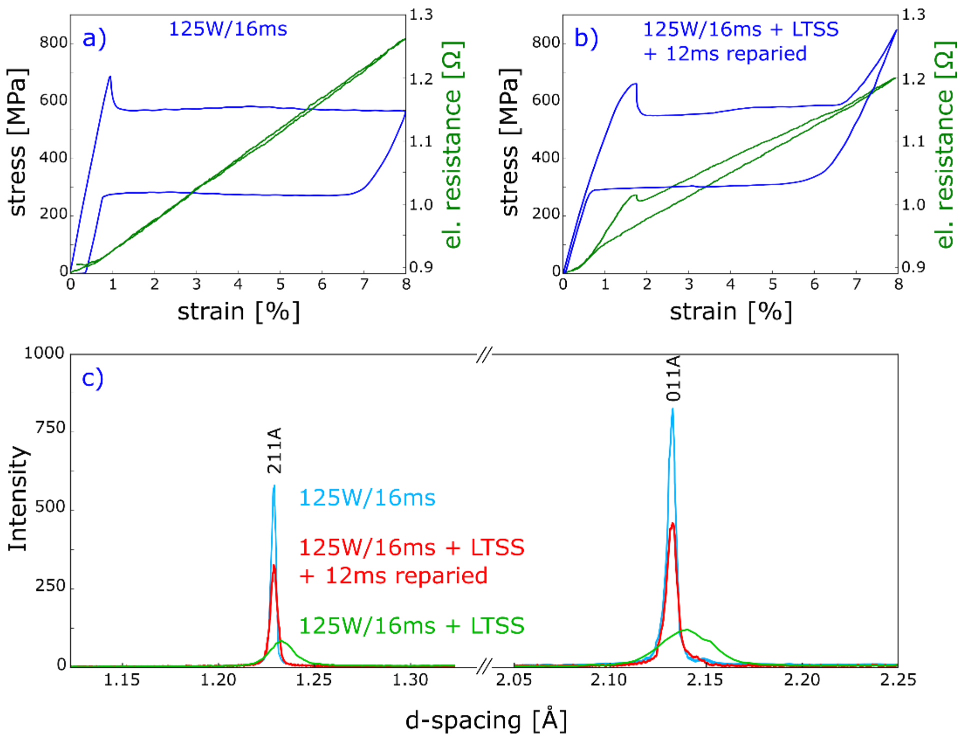

Figure 31. Effect of additional 125W/12ms repair pulse treatment on superelastic stress-strain response of LTSS treated 125W/16ms NiTi wire [111].

It was found that functional properties of the “repaired” wire were indeed remarkably improved by the additional 125W/12ms electropulse treatment (Figure 31a). The large transformation strain, sharp transformation yield point, R-phase and cyclic stability typical for straight annealed or 125W/12ms wire [51] were indeed restored – compare Figures 21, 28a and 31a. This was rather surprising. Recall that the starting NiTi wire is already “soft” with recrystallized microstructure. The impact of the additional 125W/12ms electropulse treatment on the microstructure of the LTSS treated wire (Figure 32) consists mainly in that the contrast caused by internal strains disappeared and that the dislocation density significantly decreased.

The tangles of dislocations have condensed into sharp subgrain boundaries (red arrows in Figure 32). Misorientation between neighboring subgrains is evidenced by split reflections spots in the SAD pattern taken over the circled area in Figure 32d. This microstructure is evidently different from the nanograined microstructure of the straight annealed wire but the grain size refinement caused by the successive actions of the LTSS-driven deformation and the electropulse-activated recovery brings it closer to it, as confirmed by TEM as well as x-ray diffraction (Figure 22b). The FWHM of the (011A) austenite reflection (scales with density of lattice defects) obtained from the 125W/12ms repaired wire fells in between that of the recrystallized 125W/16ms and LTSS treated microstructures. Texture changes could be due to the austenite twinning.

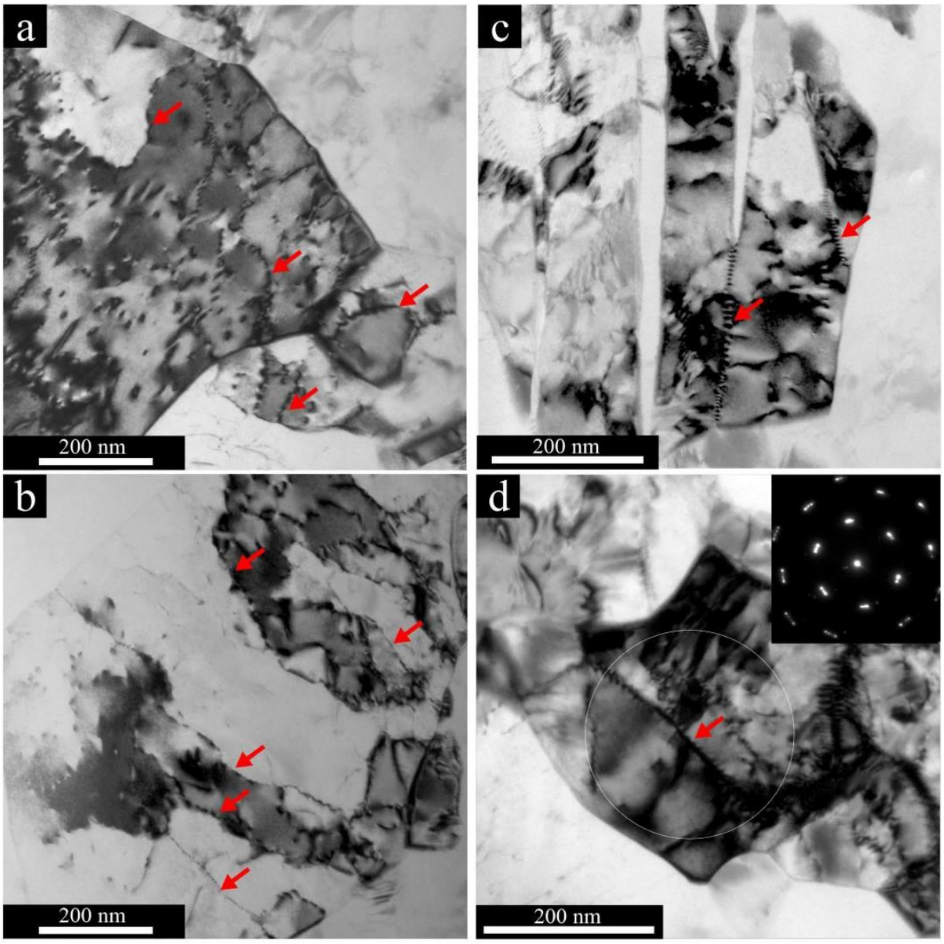

Figure 32. Microstructure in LTSS processes 125W/16ms FWM #1 wire subjected to additional 125W/12ms electropulse treatment. Microstructure underwent significant recovery; dislocations were annealed out or migrated to form sharp low angle grain boundaries (red arrows). Decrease of dislocation density and division of grains into subgrains with sharp boundaries characterizes the recovered microstructure yielding the wire excellent stable superelasticity [111].

Detailed analysis of the microstructure changes occurring during the supplemental 125W/12ms restoration treatment are beyond the scope of this work. Let us limit ourselves only to the simple statement that significant recovery of dislocation defects and internal stresses taking place during the additional 125W/12ms “repair” treatment lead to the formation of subgrains (Figure 32) which brings a stable superelastic behaviour (Figure 31a) comparable to that of the straight annealed NiTi wire (Figure 18a).

## 3.7 Localized LTSS characterized by DIC

As discussed above, the LTSS process takes place only in the part of the wire, where martensite phase is present upon heating (Figure 21). Nothing happens within the austenitic part of the wire elsewhere. If this is the case, plastic deformation of NiTi wire stretched into the mid of the stress plateau in tension by LTSS would be localized into the martensitic band only and hence the plastic deformation would be distributed heterogeneously in the LTSS treated wire. Since an experimental evidence to prove this assumption was needed, dedicated 1D DIC experiments on FWM NiTi#1 wire and Flexinol 90C wire capable of registering the homogeneity of strain along the wire have been performed. Results of the experiments are presented in Figure 33.

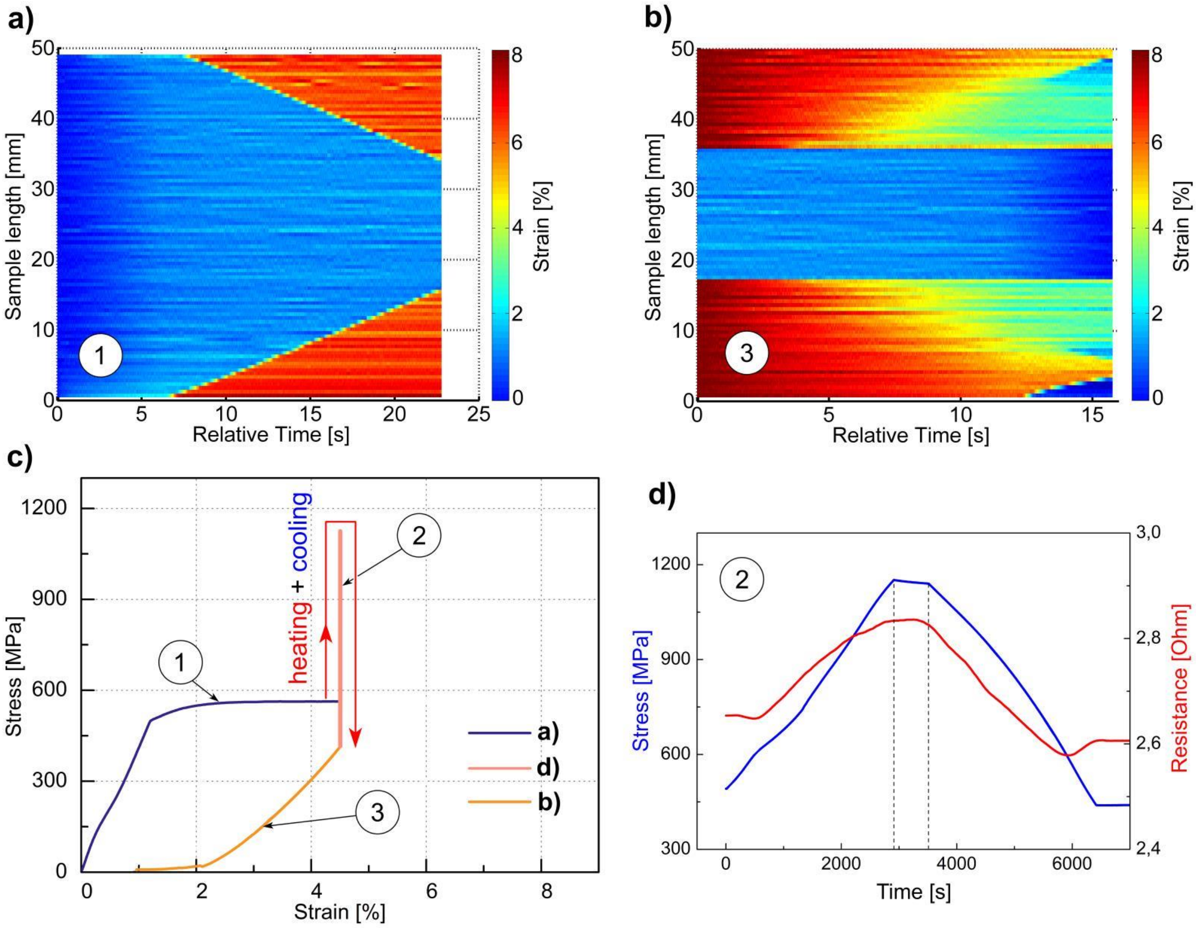

Figure 33. LTSS process within the martensite band observed by DIC. FWM #1 straight annealed wire is prestrained to 4.5% (1), subjected to constrained heating/cooling to 180°C (2) and unloaded (3) as shown in (c). Evolution of stress and electric resistance of the wire during the heating/cooling (2) is shown in (d) In-situ 1D DIC experiment during loading (a) and unloading (b) confirms that only the part of the wire that was in the martensite band during the constrained heating/cooling deformed plastically [111].

The straight annealed NiTi wire was deformed in tension to 4.5% strain at room temperature (curve 1 in Figure 33c), constrained, and heated to 180°C (temperature within the LTSS range), held 10 minutes at 180°C at constant length, cooled back to room temperature (curve 2) and unloaded (curve 3). Evolution of 1D DIC patterns observed during the tensile loading (Figure 33a) clearly evidences two martensite bands propagating from both ends of the sample mounted in a capillary towards the wire center. When the tensile loading stops at 4.5% strain (beyond the mid of the transformation plateau), two martensite bands cover both end parts of the wire, while the central part of the wire remains austenitic (Figure 33a). During the constrained heating/cooling, the wire thus contains two martensite bands and a virgin austenite in between. Upon subsequent unloading (curve 3), the central austenitic part of the wire where nothing had happened during the heating/cooling excursion shortens elastically, while the rest of the wire, where LTSS proceeded, undergoes reverse martensitic transformation with 1% strain remaining unrecovered after unloading (Figure 33c). The reverse transformation upon unloading is nearly homogeneous. It starts from the martensite band fronts near the center of the wire and continues towards the gripped ends. Since the gripped ends of the wire attached were cooled by the grips, the material there was heated to lower temperature and hence less affected. As a result, new martensite band nucleated in that volume and moved from one of the grips towards the center during unloading in relative time 12.5 s. The DIC results thus clearly confirmed the suspicion expressed in the context of Figure 21, that LTSS takes place only in parts of the wire, where the martensite bands were located during the constrained heating/cooling, while no structure change happens in the central austenitic part of the wire (Figure 34b).

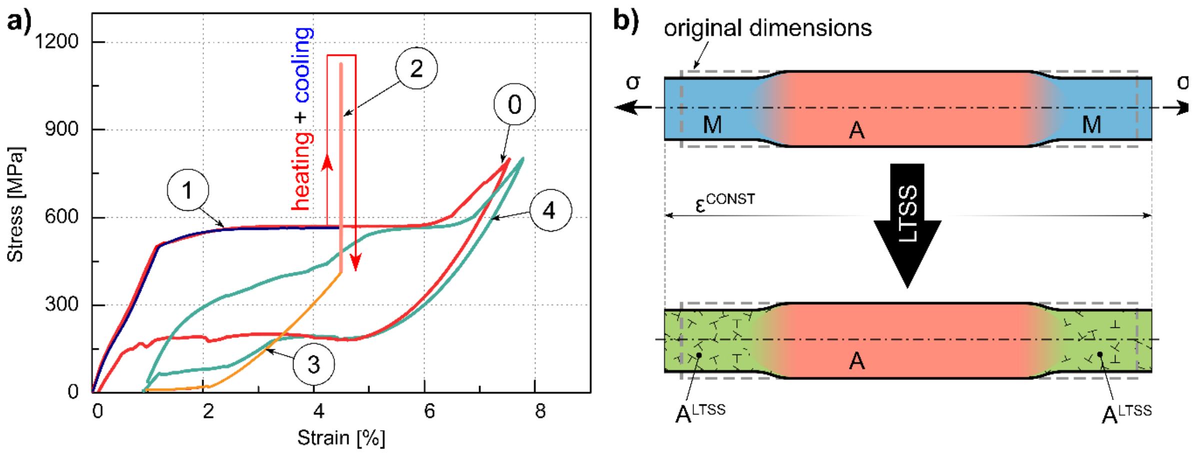

Figure 34. Superelastic stress-strain curve of straight annealed superelastic wire (a) before (0) and after (4) the LTSS treatment in partially deformed state (1-2-3). Schematic figure in (b) demonstrates that the LTSS process occurs homogeneously only in parts of the NiTi wire, where martensite bands are during the constrained heating when the temperature reaches the LTSS range [111].

Following the LTSS treatment, the austenitic wire thus consists of two different austenitic microstructures which is the reason why it exhibits a complex two plateau superelastic stress-strain response in a subsequent tensile cycle (Figure 34a). Looking at the DIC pattern (Figure 35b) recorded in the subsequent tensile cycle (strain scale set to zero at the start), one can see that the deformation proceeds homogeneously within the parts having the LTSS modified microstructure and in a localized manner by two martensite bands at the wire ends moving towards the grips. Later at relative time about 20s two martensite bands are created in the central part and move towards the center so that the wire becomes completely martensitic and deforms elastically at relative time around 35s. Similarly, the reverse transformation upon unloading can be analyzed from the results in Figure 35b. With the DIC method, local stress-strain responses of distinct parts of the LTSS treated wire can be beneficially evaluated. While the central part shows the original localized superelastic functional behaviour of the original NiTi FWM NiTi #1 straight annealed wire (Figure 35d), the volume next to it on both sides shows steep stress-strain response without plateau (Figure 35e), since the microstructure there was modified by the LTSS treatment. The parts of the wire attached to the grips, where temperature gradient existed during the heating/cooling, show localized deformation with different stress plateaus (Figure 35f) reflecting different microstructures existing there because the maximum temperature reached during the LTSS treatment was lower there. Since the stresses needed to drive martensitic transformation in different parts of such wire are different, these parts transform in different stage of the test (Figure 35a) and the stress-strain response of the wire becomes multistep (Figure 35c). In conclusion, the results of the DIC experiments prove that the LTSS occurs only in parts of the NiTi wire where martensite bands are located during the constrained heating and that the microstructure evolving locally in those place during the LTSS treatment gives rise to complex multistage functional superelastic behaviour of the NiTi wire (Figure 34).

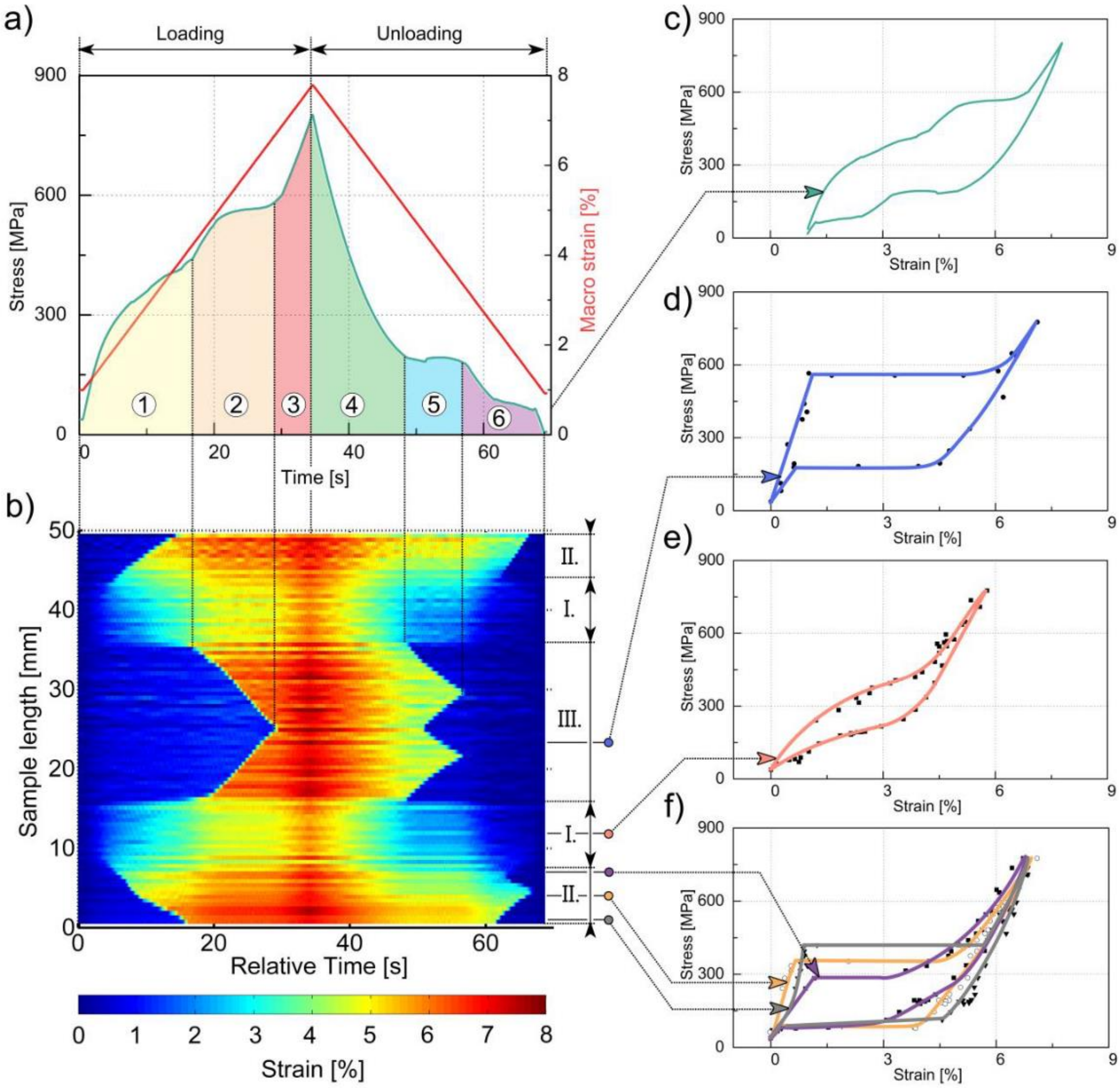

Figure 35. DIC analysis of the superelasticity of the LTSS treated partially transformed FWM #1 straight annealed NiTi wire. Parts of the wire where LTSS took place transform at lower stresses (e) than the central austenitic part (d) and the parts near grips (f), where the maximum temperature upon heating was lower. Complex macroscopic stress-strain curve (a) of partially LTSS processed NiTi wire is due to the microstructure inhomogeneity stemming from the selective LTSS process [111].

## 3.8 LTSS deformation mechanism

The experimental results presented above provide a new information on the TRIP like deformation/transformation mechanism acting upon the constrained heating of NiTi wire elongated due to the oriented martensite in it. Let us summarize what happens upon the constrained heating. As the temperature rises, the wire elongates due to thermal dilatation. At the same time, however, the oriented martensite is driven towards the reverse transformation to the parent austenite phase implying shortening of the wire, which is, however, prevented by the applied constraint. As a result, tensile stress in the wire increases (transformation strain due to reverse transformed oriented martensite is substituted by the elastic strain due to rising stress). Under such conditions, assuming that only transformation or elasticity occur, either the oriented martensite fully retransforms back to the austenite, which stops the stress from increasing, or the heated wire breaks when the rising stress exceeds its strength. The experiment however shows that the stress in fact reaches a maximum at certain temperature and decreases down to zero upon the further constrained heating (Figures 21, 26 and 28). Since 6% transformation strain cannot be compensated by the elastic strain, it means that some sort of plastic deformation had to occur in the heated material. Let us assume that, as the temperature and stress increase, TRIP like deformation proceeds involving reverse martensitic transformation coupled with dislocation slip in austenite and twinning in the martensite phase takes place. This deformation mechanism brings about the plastic deformation which in turn allows the material to transform back to the austenite phase, which is however plastically deformed (wire is austenitic and longer after constrained heating/cooling + unloading). This is what we call the LTSS deformation/transformation mechanism here.

In case of a small volume fraction of the oriented martensite in the wire prior to the constrained heating, stress maximum can be also reached when this oriented martensite fully retransforms back to the parent austenite upon constrained heating (transformation strain is compensated by the elastic strain only when the reverse transformation is completed). In case of larger prestrain (larger volume fraction of oriented martensite prior the constrained heating), however, the stress maximum is much larger and its appearance is clearly due to the LTSS deformation introduced above (transformation strain is compensated by both elastic and plastic strains). Because of that, the stress maximum increases with increasing prestrain at low prestrains but does not depend on it at larger prestrains (Figures 21e,h).

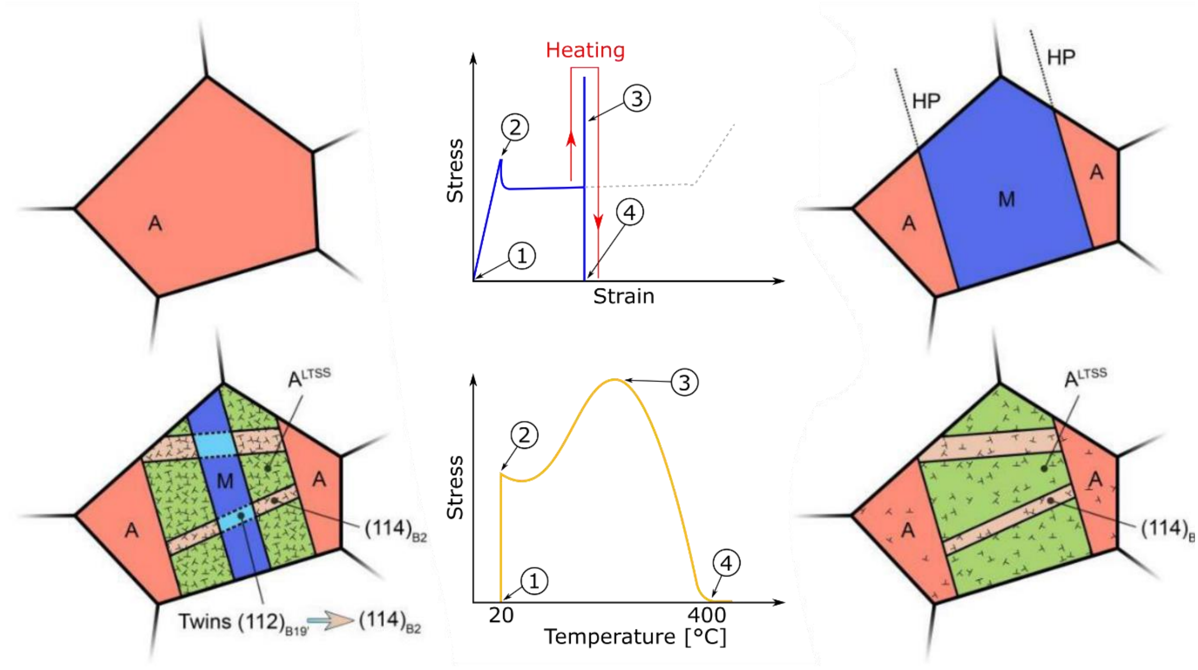

Figure 36. LTSS deformation mechanisms on the crystal lattice level. As the austenite/martensite habit plane moves during the reverse transformation, {112} martensite twinning taking place in martensite is inherited as {114} austenite twinning and dislocations are created at the propagating habit plane move in austenite phase. Both twinning and slip yields plastic deformation in tension. On the macroscopic level, the integrated effect of the coupled reverse martensitic transformation and plastic deformation is that the microstructure of the LTSS processed wire is converted from martensite to austenite between 2-3 and further recovers between 3-4 [111].

An essential point is that the reverse martensitic transformation and plasticity are thus coupled within the LTSS temperature range – i.e. the reverse transformation cannot proceed without the plasticity and vice versa. If the reverse martensitic transformation takes place under a large tensile stress during the constrained heating, the strain compatibility at the habit plane has to be established between the detwinned martensite and austenite, since the martensite cannot form the type II twins at high stress. We assume [111] that habit plane interfaces of the reverse martensitic transformation propagate at high stress and temperatures with the assistance of dislocations slip at the austenitic side (between 2-3 in Figure 36) and produce plastic deformation already during the heating step. The higher the stress, the more difficult is the formation of martensite type II twins required for martensite reversion. Note that the martensite twins a habit planes operating during the reverse transformation under stress can be generally different from the habit plane/type II twins typical for self-accommodated martensite in NiTi. The essential point is that such plastic deformation occurs neither in martensite nor in austenite but at the propagating habit plane. It needs to be understood as a TRIP like deformation mechanism distinct from dislocation slip.

The dislocation tangles, strong strain contrasts, dislocation walls and no slip planes observed by TEM in the austenite phase after the constrained heating (Figures 27, 29) seem to be in very good agreement with this scenario.

There is however a second deformation mechanism capable of assuring simultaneous reverse martensitic transformation and plasticity upon the constrained heating. The presence of the high density of lamellar defects identified as {114} austenite twins in the microstructure (Figure 30) after the LTSS treatment can be ascribed to the twinning in austenite (very large twinning shear of 0.425) [91]. However, as the LTSS process occurs only in the martensite band and not in the surrounding austenite, deformation twinning in the austenite phase has to be excluded. According to [91,92,93], the {114} austenite twins may form in the highly stressed martensite phase as {20-1} martensite twins and be retained in the austenite phase after reverse martensitic transformation as suggested in Figure 36. The mechanism of the unusual compound {20-1} twinning in the B19' structure [93] was identified in the literature [81] as one of the mechanisms enabling the NiTi martensite to deform plastically at high stresses [85,94]. When combined with reverse transformation we end up with {20-1}M/{114}A deformation twinning [111] which is the second LTSS deformation mechanism involved in LTSS. In this case, the plastic deformation occurs by twinning in the martensite and reverse transformation into a different "variant of austenite phase" (twinning instead of dislocation slip). As will be shown below, the {20-1}M/{114}A twinning deformation mechanism dominates over dislocation slip at large stresses in NiTi wires with strong matrix. Both mechanisms may proceed together. In summary, plastic strain at the habit plane due to the dislocation slip and {20-1}M/{114}A twinning allows for the reverse martensitic transformation during the constrained heating and leaves behind the modified austenitic microstructure $A^{LTSS}$ characterized by dislocation tangles and austenite twins as schematically suggested in Figure 36.

### 3.8.1 Effect of the maximum temperature

As the temperature and stress increase upon heating within the LTSS range, the density of defects in the microstructure of the wire increases (Figure 23d). As a result, superelastic stress-strain response of the wire evolves as shown in Figure 24A-D. Because of the increasing density of defects, the superelastic property is gradually lost from A to D. However, beyond the stress maximum, after all martensite in the wire have transformed to the austenite (Figure 22), microstructure recovery proceeds, density of defects now decreases (Figure 23e) and functional properties are gradually restored (Figure 24E-G), though microstructure is different from that of the virgin austenite. The dynamically evolving density of lattice defects in the heated wire in the wire is thus assumed to be highest at the temperature corresponding to the stress maximum (Figure 24D).

The material state and functional properties of LTSS treated wire (Figures 24-26) thus depend on the maximum temperature reached during the constrained heating/cooling. Compare the results of two LTSS treatments of 125W/16ms NiTi wire performed with different maximum temperatures (Figure 37). The superelastic stress-strain responses are clearly different after these two LTSS treatments (Figure 37b). Note that the above presented TEM microstructures (Figures 27-32) correspond to LTSS treatment with maximum temperature of 300 °C (Figure 28b). The dislocation density would be much higher if heating is stopped at 150°C and much lower if it continues till 450°C. The selection of maximum temperature is the key to the microstructure and functional property tuning by LTSS.

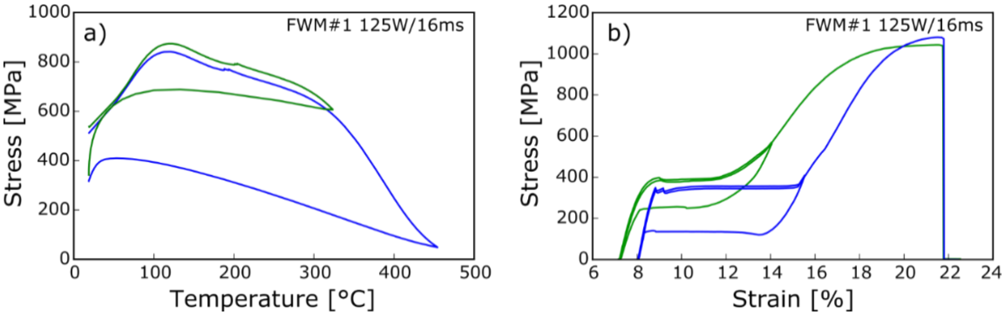

Figure 37. Effect of maximum temperature in the LTSS treatment on functional superelastic behaviour of 125W/16ms NiTi wire. The maximum temperature affects the superelastic response but not the strength and ductility [111].

### 3.8.2 Effect of the original microstructure of the wire

The straight annealed FWM#1 NiTi wire with nanosized grains and partially recrystallized microstructure subjected to the LTSS shows stress maximum 1400MPa at 200°C (Figure 21). In a contrast, the 125W/16ms NiTi wire with fully recrystallized microstructure subjected to the LTSS shows stress maximum 900 MPa already at 150°C (Figure 28b) . This means that the LTSS temperature and stress depend significantly on the original microstructure of the virgin wire. One of the key advantages of the LTSS over the shape setting of cold worked NiTi wire is that the LTSS can be performed at much lower temperatures (compare Figures 20 and 21), if the wires are properly heat treated to establish a suitable original microstructure.

In order to investigate the effect of original microstructure of the wire on the LTSS, the same LTSS constrained heating tests (deformation beyond the end of the plateau followed by constrained heating to 500°C) were applied to five NiTi wires with different microstructures (Figure 38). All five NiTi wires are superelastic, although their microstructures and functional properties are different [51] – grain size increased from 20nm in case of 125W/12ms up to ~6μm in case of 125W/16ms wire. The evolution of stress and electric resistance recorded during the constrained heating are mutually compared in Figure 38a. Clearly, the electric resistance and stress maxima decrease and shift to lower temperatures with decreasing strength of the original microstructure (from 125W/12ms to 125W/20ms). This proves that the LTSS stress-temperature range and stress maximum depend on the original microstructure as suspected. The reason is the varying propensity of the microstructure to the TRIP like deformation mechanism of the LTSS. Functional responses of the wires prior and after the LTSS treatment are compared in Figure 38b. Note that after LTSS treatment, all 125W/12-20ms wires are 7-10% longer and superelastic. Stress strain responses changed after the treatment (lower forward plateau stresses, longer plateaus and lower stress hysteresis). The strength of the wires, however, was not affected.

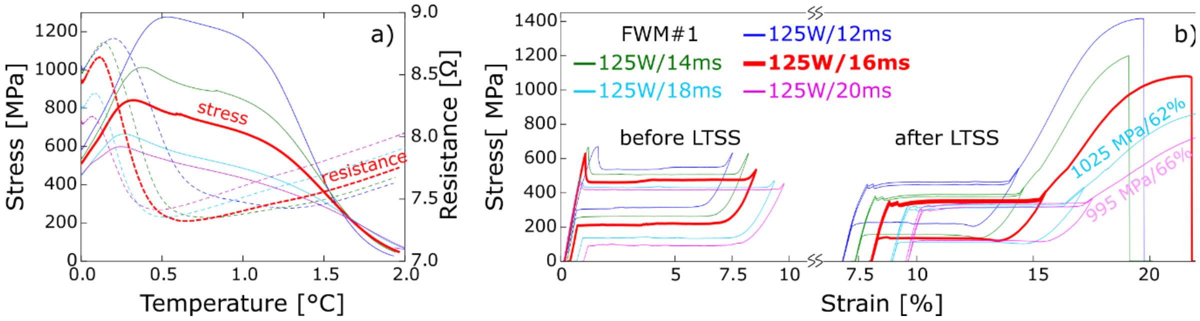

Figure 38. Effect of original microstructure on functional superelastic behaviour of LTSS processed NiTi wire. a) stress-temperature response during the constrained heating of 125W/12,14,16,18,20ms wires with different original microstructures. b) After the constrained heating/cooling, the wires are ~7-10% longer, have different microstructures and their superelastic functional responses are modified [111].

Further very important information was obtained from the analysis of in-situ synchrotron x-ray diffraction experiments (Figure 39). The analysis of individual austenite and martensite reflections Figure 39c) clearly documents the reverse martensitic transformation upon heating. While the martensite phase persists up to 300°C in 125W/12ms wire, it disappeared at 150°C in 125W/20ms wire. Partial segments of the diffraction patterns are shown in Figure 39d. Note the variation of the 020M reflection with increasing temperature.

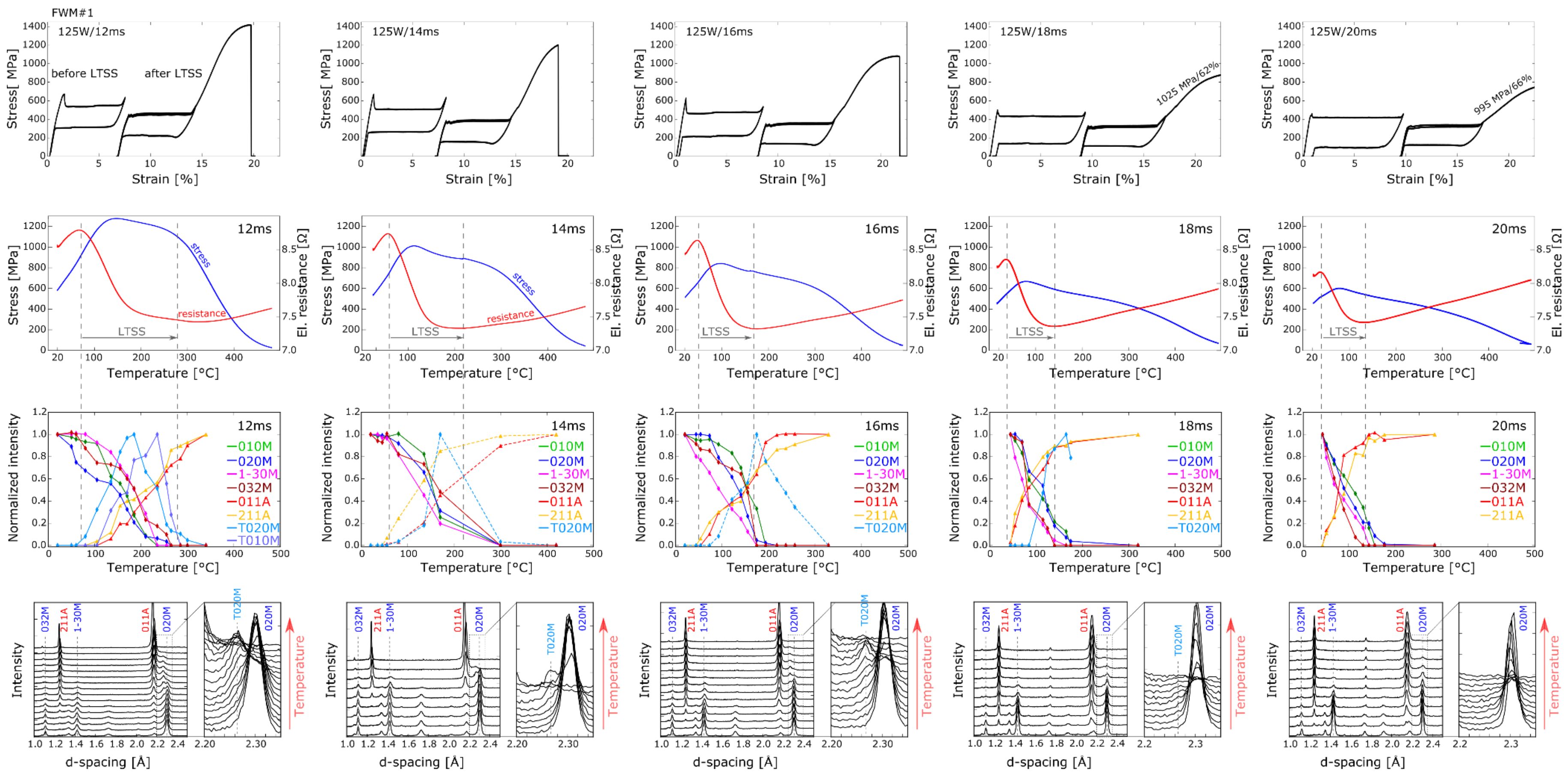

Figure 39. Effect of original microstructure on functional superelastic behaviour of LTSS processed NiTi wire. a) LTSS treatment of 125W/12,14-20ms wires with different original microstructures. The LTSS temperature range shifts to lower temperatures from 125W/12ms to 125W/20ms, b) After the constraint heating/cooling, the wires are ~7% longer, have modified microstructures and superelastic functional responses. Evolution of integrated intensity of austenite and martensite reflections upon heating c) 125W/12ms, d) 125W/16ms (synchrotron x-ray diffraction experiment, axial geometry). See text for details[111].

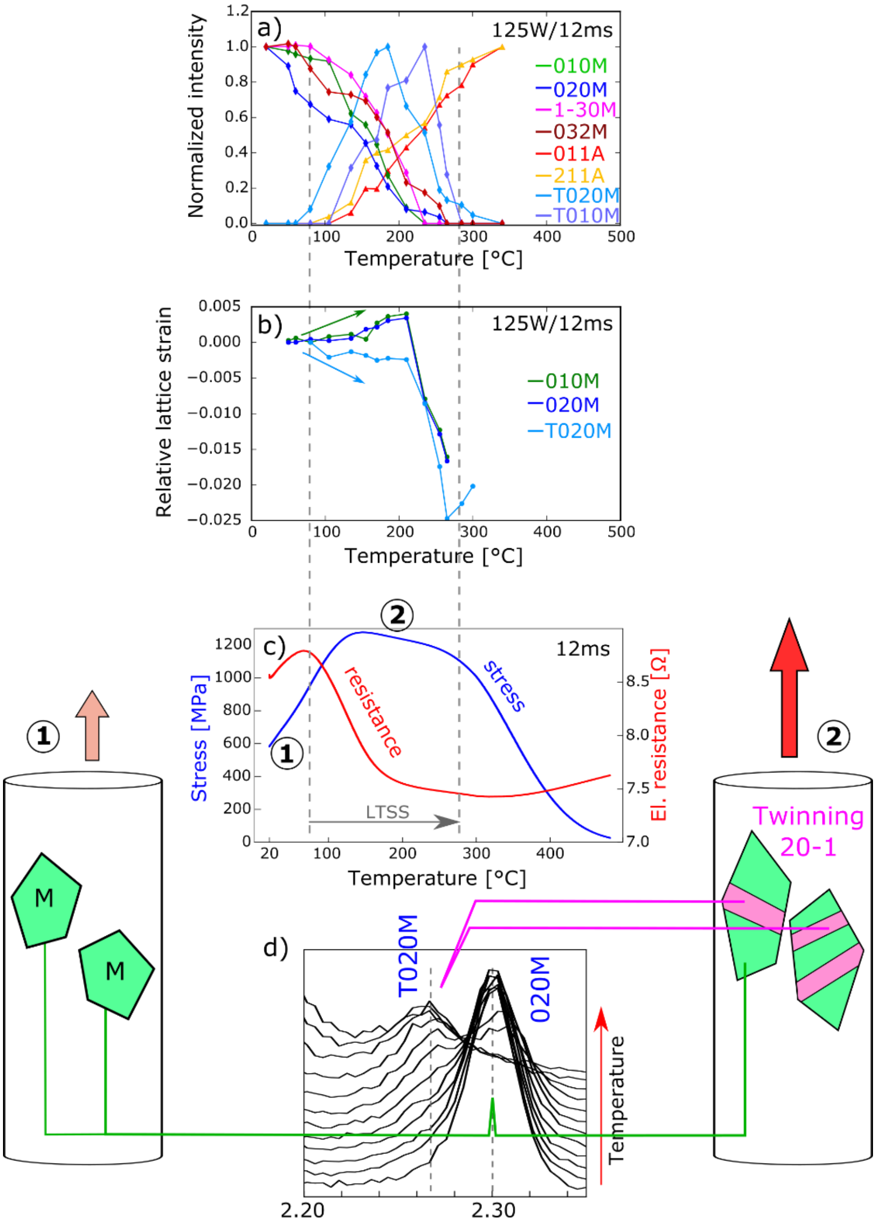

Figure 40. Microstructure evolution during constrained heating of 125W/12ms superelastic wire captured by in-situ synchrotron x-ray diffraction. Evolution of: a) Intensities of individual hkl reflections, b) Internal lattice strain c) stress, electric resistance with increasing temperature upon heating, d) lattice strain partitioning due to the 20-1 martensite twinning. The peak splitting is due to twinning deformation mechanism, however, both peaks belong to the same reflection. Such difference in interplanar d-spacing is caused by enormous difference in the stress in grains in which twinning did not yet take place and in grains which already did undergo twinning [111].

In high strength 125W/12ms and 125W/14ms wires, the 020M intensity decreases upon heating but there is an additional reflection T020M appearing at lower d-spacing, the intensity of which rises and falls with increasing temperature. This peak splitting was curious since there is no martensite reflection at the T020M peak position and structure change of B19’ martensite was extremely unlikely. We concluded that this 020M peak splitting upon heating is due to the {20-1} deformation twinning. The 020M plane is parallel in both martensite twins, however, the stress is very different prior and after the {20-1} deformation twinning. The T020M intensity comes from the {20-1} twinned lattice in grains where the stress is low while the 020M intensity comes from grains prior twinning, where the stresses are high (see detailed picture of 125W/12ms wire in Figure 40). The phenomenon was thus interpreted as diffraction evidence for the activity of {20-1}M twinning in the martensite. {20-1}M twinning is most likely accompanied by dislocation slip in martensite and provides the plastic deformation at high stresses above 800MPa in nanograined microstructure of 125W/12-14ms wire. There is no 020M peak splitting in case of the 125W/20ms wire suggesting that no {20-1}M twinning occurs. This is ascribed to the fact, that dislocation slip proceeding easily in the soft recrystallized microstructure assures the compatibility at the habit plane during the reverse martensitic transformation upon heating and the reverse transformation takes place at low stress. Both slip and twinning takes place in 125W/16-18ms wires and reverse transformation occurs at medium stress. The splitting could be resolved only thanks to the application of axial diffraction geometry in the diffraction experiment and excellent resolution of the ID22 diffractometer. Neutron diffraction experiment with lower instrumental resolution would show only peak broadening.

In summary, with decreasing matrix strength, the LTSS temperature range shifts to lower temperatures and the stress maximum decreases. After the LTSS treatments, all the 125W/12-20ms wires are ~7.5% longer (Figures 38b, 39a), show excellent stress-strain superelastic behaviour and maintain their original strength and ductility. The cyclic superelastic responses of LTSS treated wires are more stable compared to the original wires prior the LTSS treatment. The {20-1}M/{114}A twinning dominates the LTSS of high strength 125W/12ms wires at large stress, while it does not occur in soft 125W/20ms reverse transforming at low stress.

### 3.8.3 Increments and relaxations of stress and electric resistance

So far, the experimental results were discussed as if the stress-temperature response of the material to the constrained heating was instantaneous, as appropriate for the martensitic transformation. However, this is clearly not the case for the LTSS as evidenced by the stress and electric resistance responses recorded during the incremental constrained heating test (Figures 22, 23). The stress and electric resistance change with the increasing temperature during the heating step (increments $\Delta\sigma$, $\Delta\rho$ in Figure 23e,f) as well as during the subsequent holding at constant temperature (relaxations σ_relax and ρ_relax in Figure 23e,f). Note that the increments and relaxations are very different along the constrained heating tests (Figure 23). They provide supplemental information about the material state of the wire evolving during the constrained heating, which is however very difficult to interpret properly.

Think about the response of the prestrained martensitic wire to the heating step (Figure 23b). In case of a conventional elastic metal, the stress shall fall and electric resistance shall increase instantly with increasing temperature with no subsequent relaxation. This is indeed approximately the case for the austenitic wire (Figure 20a,b). However, the prestrained NiTi wire containing oriented martensite transforms to the austenite upon the constrained heating which makes a difference (Figures 20 - 26). If the temperature is below $A_s$, there is no transformation and the martensitic wire behaves like a common metal (the increment of stress is low and increment of resistance is large with negligible relaxations). However, once the temperature rises above the $A_s$ temperature, the stress increment in the heating step starts to increase, since higher stress is needed to keep the oriented martensite in the wire at higher temperature (Clausius-Clapeyron relationship). At the same time, however, the temperature increasing in the heating step triggers incremental reverse martensitic transformation (Figure 23). The transformation proceeds at first at the expense of elastic deformation and later, within the LTSS stress-temperature range, also at the expense of plastic deformation (Figures 24, 26). The plastic deformation processes presumably take place both during the heating step and subsequent holding time. This in turn affects the stress increment in the heating step.

The increment of electric resistance in the heating step, after the initial increase in martensite state, reaches its maximum at the $A_s$ temperature and starts to decrease. The decrease is due to the massive reverse martensitic transformation (electric resistance of austenite is less than that of the martensite). Since the habit planes moving in the LTSS temperature range are assumed to generate lattice defects, this also potentially affects the electric resistance change in the heating step. On the other hand, the newly created lattice defects annihilate during the subsequent holding time at high temperature, which results in relaxation of the electric resistance.

The electric resistance of the constrained NiTi wire increases with increasing temperature due to: i) conventional temperature effect on electric resistance of a metal, ii) generation of lattice defects by reverse martensitic transformation and decreases due to i) martensite to austenite transformation and ii) defect recovery at high temperature. Let us note that electric resistance of the wire in martensite state increases more steeply with increasing temperature than in the austenite state [87].

The stress increases with increasing temperature due to the intrinsic Clausius-Clapeyron dependence and decreases due to the instantaneous thermal elongation of the wire, as well as in response to any incremental plastic deformation in tension taking place either during the heating step or during the subsequent holding time. Since both the annihilation of lattice defects and plastic deformation are rate dependent processes, we observe relaxations of electric resistance and stress, respectively.

Having this in mind, we can try to analyze the increments and relaxations recorded experimentally along the constrained heating test (Figure 23e,f). When the heating starts, increment of electric resistance is positive (Figure 23e) but that of the stress is negligible (Figure 23f), as shall be the case for a metallic alloy. When the increasing temperature exceeds the As temperature (martensite in the wire starts to transform to austenite), the increment of stress rises but the increment of electric resistance starts to decrease due to the phase transformation as explained above. The relaxation of the electric resistance starts to increase together with the increasing stress (Figure 23e). Recall that the relaxation of electric resistance is considered to be due to the annihilation of lattice defects created by the habit plane moving incrementally in the heating step. The more lattice defects and the higher the temperature, the more pronounced relaxation of electric resistance is expected. This is indeed the case. As the oriented martensite, however, gradually transforms to the austenite, the relaxation of electric resistance reaches a maximum and decreases upon further heating, as the source of the lattice defects gradually expires. The relaxation maximum is observed at temperature ~200 °C (Figure 23e), where the reverse martensitic transformation (Figure 22) as well as plastic deformation (Figure 25) show maximum progress. Stress increments increasing with increasing temperature reach a maximum at temperature ~170 °C (Figure 23f) which, according to the above introduction, denotes the onset of the LTSS. The stress increment decreases to nearly zero at temperature ~260 °C and stress ~600MPa. At this temperature, the electric resistance of the wire attains its minimum suggesting that all martensite in the wire has already transformed as supported also by the x-ray data (Figure 22). The stress relaxation is due to the activity of rate dependent plastic deformation processes during the holding time (dislocations created during the heating step continue to move under large stress and yield plastic deformation). Stress relaxations start to increase within the LTSS temperature range (Figures 23f, 25) and attain a maximum at temperature ~280 °C when the LTSS is over, simply because they naturally increase with increasing temperature but decreases with decreasing stress.

In summary, we have to admit that the offered interpretation of the increments and relaxations is only qualitative. Modelling is clearly necessary for detailed analysis and we already started to work in this direction. However, as the results were available and we believe that the increments and relaxations closely reflect the evolution of material state of NiTi wire during the constrained heating, we provided here this qualitative interpretation.

## 3.9 The role of LTSS in NiTi technology

As already pointed out, LTSS concerns phenomena encountered when reverse martensitic phase transformation is forced to proceed under conditions favouring plastic deformation processes as dislocation slip or twinning. This is, however, by far not limited to a constrained heating laboratory tests discussed above. It is in fact very often encountered in various engineering applications of NiTi wires (shape setting, actuation, NiTi wire reinforced smart composites etc.). Several important cases will be briefly discussed below.

### 3.9.1 Thermomechanical treatment and shape setting of NiTi

LTSS can be used to adjust the shape, microstructure, and functional properties of an already annealed NiTi element. In fact, engineers frequently shape set annealed and cold worked NiTi wires without understanding the differences. Since the LTSS processing involves combination of reverse martensitic transformation and plasticity, it is necessary to control the temperature and stress in the heated material. While the temperature control is easy, particularly when electropulse heating is employed, controlling the stress in the heated material is possible only in case of simple geometries such as a wire loaded in tension. One has to know the level of maximum stress for a given wire to shape set it properly via LTSS and the effect of heating rate has to be taken into account.

The key difference between the LTSS and conventional heat treatment without any constraint is that the LTSS combines the microstructure strengthening with the microstructure recovery in a single controlled heating/cooling cycle. High density of lattice defects is introduced to the microstructure when the material is heated through the LTSS stress-temperature range towards the stress maximum causing its strengthening. Note that the force is generated by heated material itself, no external mechanical deformation is imposed. Further heating to higher temperatures beyond the LTSS range brings about a recovery of functional properties (Figure 24). Based on the knowledge of the LTSS deformation, fully annealed soft NiTi wire can thus be LTSS processed to give it a new shape, high strength and new functional properties in a fast controlled manner.

The difference between shape setting of a cold worked NiTi wire and already annealed NiTi wire lies in the different mechanisms involved. In case of shape setting a cold worked wire, increasing temperature triggers recovery processes and recrystallization (and plastic deformation) driven by stored energy in the lattice defects of a cold worked microstructure. In case of annealed NiTi wire, the driving force of the LTSS deformation mechanism is the chemical energy of the oriented martensite. Conventional shape setting of a cold worked NiTi results in a new microstructure homogeneously distributed everywhere in the wire and eliminates internal stresses. In a contrast, LTSS modifies the microstructure and creates plastic deformation of the NiTi element selectively only in locations where oriented martensite existed when the temperature attains the stress maximum during the constrained heating, and introduces significant internal stress into the microstructure. LTSS shape set NiTi elements thus always display gradient microstructures with peculiar internal stresses which yield the wire its complex functional response and brings about TWSME effect. A disadvantage is that new shape adjusted by the LTSS is not set exactly to the constrained shape as in the case of shape setting the cold worked NiTi but significant springback due to the internal stresses always appears in case of the LTSS.

The constraint imposed during the heating (fixed length, dead load or biased spring) affects the microstructure and functional properties of the LTSS treated wire (Figure 41). First of all, if the imposed constraint is not sufficient to keep the oriented martensite in the wire until the LTSS range is reached upon heating, the self-accommodated martensite recovers around $A_f$ and no shape setting takes place. The kind of the applied constraint, however, matters too. Compared to the fixed length condition where the stress rises and falls, the large stress persisting at high temperatures under dead load or bias spring conditions favours the plastic deformation processes in the microstructure. It was found experimentally that very interesting microstructure and functional properties can be achieved by applying dead load constraint upon Joule heating of continuous superelastic NiTi wire during respooling of both cold worked as well as annealed NiTi wire [96]. Applying variable force and/or temperature during the respooling allows for preparing NiTi wires with gradient microstructure/properties [97].

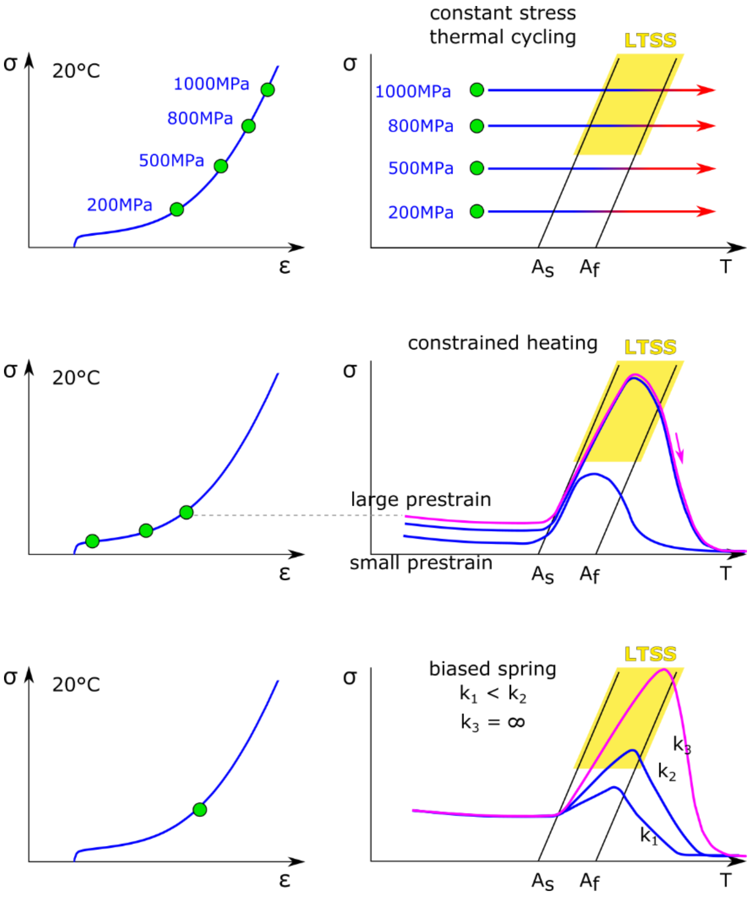

Figure 41**.** Three different modes of constrained heating. a) heating under constant applied stress, b) heating under fixed length, c) heating against biased spring. Note the importance of different prestress (a), prestrain (b) and mixed mode (c) constraint conditions. If the initial applied constraint is “weak” (low stress in (a), small prestrain in (b) or low $k_1$ in (c), the stress and temperature in the wire never reach the LTSS range. In that case, there is no drift upon thermal cycling and millions of thermomechanical loading cycles can be achieved.

When shape setting NiTi wires, there is often a choice between the environmental furnace treatment and joule heating which heats the material from inside. The specialty of the electropulse treatment is that heating can be very fast which disregards any diffusional processes such as precipitation [74]. It was found that the stress maxima observed in LTSS tests on the same wire do not depend on the used heating rate in the range 10 - $10^8$ °C/s. This means that the reverse transformation upon constrained heating is capable of following the rise of the temperature even during the fastest electropulse heating in a millisecond range. As this was somehow surprising (rate dependency of the LTSS mechanism was expected), further investigations are in progress.

The right approach to LTSS processing consists in adjustment of its microstructure prior the LTSS treatment (Figure 38), imposing suitable external constraint and applying suitable maximum temperature (Figure 37). LTSS processing can be applied repetitively to the same piece of wire without changing its functional properties if appropriate maximum temperature is selected. For example, the high strength FWM NiTi#1 superelastic wire (1500MPa strength, 14% ductility) was subjected to 10 subsequent LTSS treatments yielding net elongation ~60% while maintaining the same superelastic functionality.

### 3.9.2 Actuation

Besides the shape setting, the second area of NiTi technology, where the constrained heating is frequently encountered, is actuation. For the sake of clarity, Figure 17 is presented here once again as Figure 42. It is well known that NiTi actuator wires work reliably (no strain drift and millions of cycles till failure) only below a characteristic level of stress (typically ~300MPa for good quality NiTi actuator wire). When the applied stress exceeds this level, hot and cold strains (hot strain - strain reached at the highest temperature, cold strain –strain reached at the lowest temperature) start drifting and fatigue life decreases. Current state of art NiTi actuator applications respect this stress limit without really knowing the physics behind. This stress limit originates from the LTSS as explained below.

Figure 42 presents results of thermal cycling of Flexinol 90C actuator wire under 4 different levels of applied stresses. Strain response of the wire thermally cycled under 200 MPa stress is stable for millions of cycles. Problems appear when the applied stress increases - hot and cold strains start to drift, actuation strain starts to decrease and number of cycles till failure sharply decreases to tens of thousands. 500 MPa applied stress is already well beyond the stress limit for safe actuation. The role of LTSS is the following. Upon heating under 200MPa, the oriented martensite transforms to the austenite around 120 °C while the LTSS stress conditions (Figures 22-26) are not even met. With increasing applied stress, however, the temperature at which the martensite transforms to austenite increases according to the Clausius-Clapeyron equation and LTSS starts to take place upon heating. Essential difference with the previous constrained heating experiments is, that the stress does not decrease with the progress of the reverse transformation due to the applied dead load constraint. This means that the reverse transformation upon heating proceeds with accompanying plastic deformation (dislocation slip and {20-1}M/{114}A twinning) until the oriented martensite completely retransforms. As a result, the wire significantly elongates plastically in the first few cycles

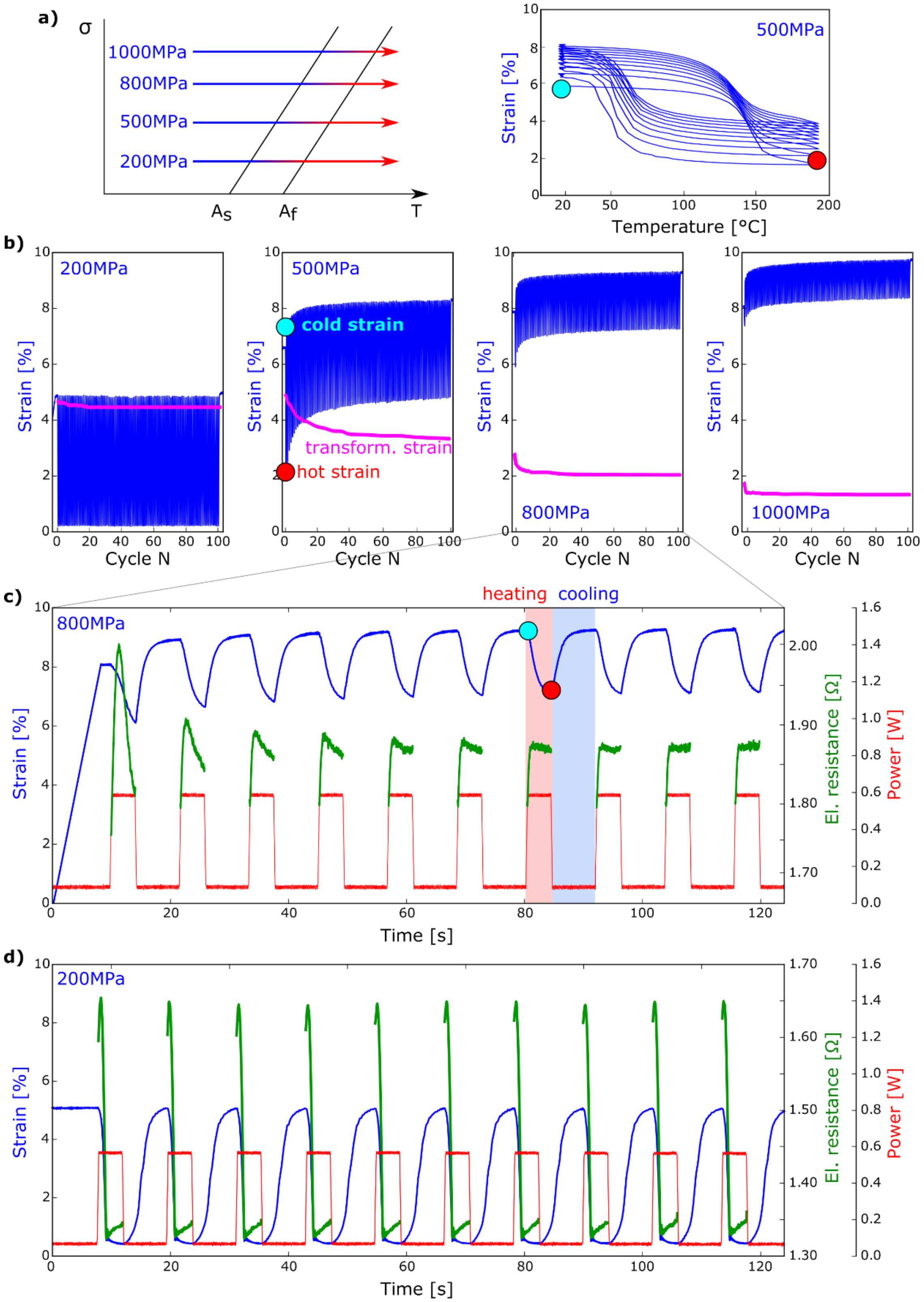

Figure 42. Thermal cycling of Flexinol 90C wire under constant applied stress. a) strain-temperature response under 500MPa. b) strain-No of cycles response in first 100 thermal cycles under different applied stresses, strain-time responses in first 10 thermal cycles under 800MPa (c) and 200MPa (d) stresses with electric resistance evolution [111].

(note the plastic strains 2%, 6% and 7.5% irrecoverable strains in the first cycle at 500MPa, 800MPa and 1000MPa, respectively). Upon further thermal cycling, hot and cold strains drift since the LTSS proceeds infinitesimally in each cycle. The actuation strain decreases with increasing applied stress due to the lattice defects. Note, however, that in spite of the LTSS, thermal cycling runs safely for more than 10000 cycles with actuation strain stabilized even under 1000 MPa applied stress.

The activity of the LTSS as the source of the strain instability during actuation is revealed by following the evolution of the electric resistance of the wire (Figure 42) during the thermal cycling. The electric resistance of the heated wire naturally increases with increasing temperature. But there is a local maximum appearing when the wire starts to shorten due to the reverse transformation. The resistance maximum appears also upon heating at low stresses 200MPa (Figure 42d). Note that the electric resistance drops and starts to increase again upon heating when the reverse transformation is over. The higher the applied stress, the larger is this resistance maximum and the higher is the temperature at which it appears. This is partially due to upward shift of the $A_s$ with increasing applied stress but partially also due to the creation of more lattice defects by the LTSS proceeding at larger stress. The electric resistance maximum at 800MPa (Figure 42c) is very large in the 1st cycle but quickly decreases and disappears in just 10 thermal cycles, since the resistance decrease due to the reverse transformation is balanced by its increase due to the incremental plastic elongation and lattice defects created upon the constrained heating (LTSS). There are small but constant drifts of hot and cold strains upon cycling at 500MPa, 800MPa and 1000MPa stress. Although the LTSS decreases and stabilizes upon further cycling, this incremental plastic elongation is the source of problems which cannot be avoided. Specific stress limit for each particular NiTi wire needs to be respected.

It shall be noted that the LTSS does not prevent the NiTi wire from the actuation functionality. In spite of the 2% irreversible elongation in the first cycle at 500MPa applied stress, the wire still exhibits 4% actuation strain and slightly less for higher applied stresses. It depends on the applied stress and matrix strength of the wire what will be the maximum allowable applied stress and how much the LTSS will affect the stability of the strain response upon the actuation cycling. If the applied force is large, the dead load constraint is even more severe than the fixed length constraint since the incremental plastic elongation does not assist the recovery of the oriented martensite as was the case under the fixed length condition. As a result, the strain drift upon thermal cycling at higher applied stresses can be hardly avoided. The only way how to minimize the impact of LTSS on the actuation performance of NiTi wires is to decrease the applied stress below the stress limit or to increase the stress limit by strengthening the microstructure of the wire.

In real actuator applications, the situation is frequently more complicated since the reverse martensitic transformation hardly occurs under constant applied force or constant strain but the NiTi wire typically acts against a bias spring - i.e. stress rises with increasing temperature more slowly and never fells down to zero. Although this gives some more space for the oriented martensite to recover compared to the fixed length condition, the problems with high stress persisting till highest temperature encountered under dead load condition largely remain. The LTSS is most likely the reason why the applied constraint and maximum temperature has a pronounced impact on the fatigue performance of NiTi actuator wires. It was reported by Scirè Mammano and Dragoni [24] that NiTi wire shows best fatigue performance upon thermal cycling under constant stress from among other constraints. Obviously, if the applied stress is sufficiently low (Figure 42), dead load is the safest way hot to avoid LTSS.

### 3.9.3 Two way SME

Although the two-way shape memory effect (TWSME) is probably the most spectacular phenomenon exhibited by NiTi, its applications are very limited. The main reason is that the TWSME is typically a small and unstable effect, which cannot provide a large work output against a bias load due to problems on cooling and has to be trained by a complex thermomechanical cycling. Conventionally, the TWSME is associated with dislocations introduced during the cyclic training [37]. In a contrast, the ex-situ experiment shows that significant TWSME of about 3% can be created by manipulating microstructure of the NiTi wire via a single constrained heating/cooling run (Figure 26).

To explain the origin of the large TWSME created via LTSS, let us consider a complex composite microstructure created by the concurrent martensitic transformation and plasticity proceeding upon heating in the constrained polycrystalline environment. We assume that the grain interactions play a key role. To explain that, the grain interactions in a polycrystalline environment are simulated using a simple conceptual bicrystal model introduced in Figure 43. The sequence of four steps 1-4 simulates deformation followed by constrained heating of a superelastic bicrystal consisting of two differently oriented grains A, B of the superelastic NiTi connected by a vertical grain boundary. While grain B transforms completely to the stress induced martensite, only partial transformation of grain A is sufficient to achieve the same strain (step 2) upon superelastic tensile loading due to the strong transformation anisotropy. White arrows suggest different internal stresses in adjoining grains due to the anisotropy and grain boundary constrain. LTSS taking place during constrained heating attacks selectively only the martensite phase (step 3). This means that plastic deformation proceeds in a different extent in the grains A and B. Since a strain compatibility has to be maintained at the vertical grain boundary after unloading (step 4), an opposite residual stress appears in the grains A, B (yellow arrows in 4) to compensate the strain mismatch at the grain boundary created by the LTSS. If the residual stress is high enough, a residual martensite may appear within the grain A experiencing tensile stress. When comparing the shape of the bicrystal in the austenite state after the LTSS treatment (step 4) with its original shape (step 1), it is longer and it contains dislocations and twin defects, oriented residual stress and potentially the residual martensite. Upon subsequent stress free cooling, the oriented residual stresses promote the growth of the tensile martensite variants, which gives a rise to the TWSME. It must be, however, emphasized that such conceptual bicrystal model was introduced only to explain qualitatively how the coupled martensitic transformation and plasticity acting in the constrained polycrystalline environment upon constrained heating brings about a large TWSME. The real situation is much more complex.

In case of the LTSS treatment of a real polycrystalline NiTi wire, the largest TWSME is observed at maximum temperatures around the stress maximum where a maximum residual stress and maximum defect density are introduced into the wire microstructure (Figures 24B-D, 26B-D). In the context of TWSME training, it shall be noted that the residual stresses responsible for TWSME are introduced by superelastic cycling [89] not by thermal cycling under constant load as described in chapter 0 [33]. In case of LTSS, the effect of martensitic transformation and plasticity coupling is most pronounced, therefore no cyclic deformation is needed. LTSS treatment is probably the most efficient way to imprint the TWSME into NiTi microstructure.

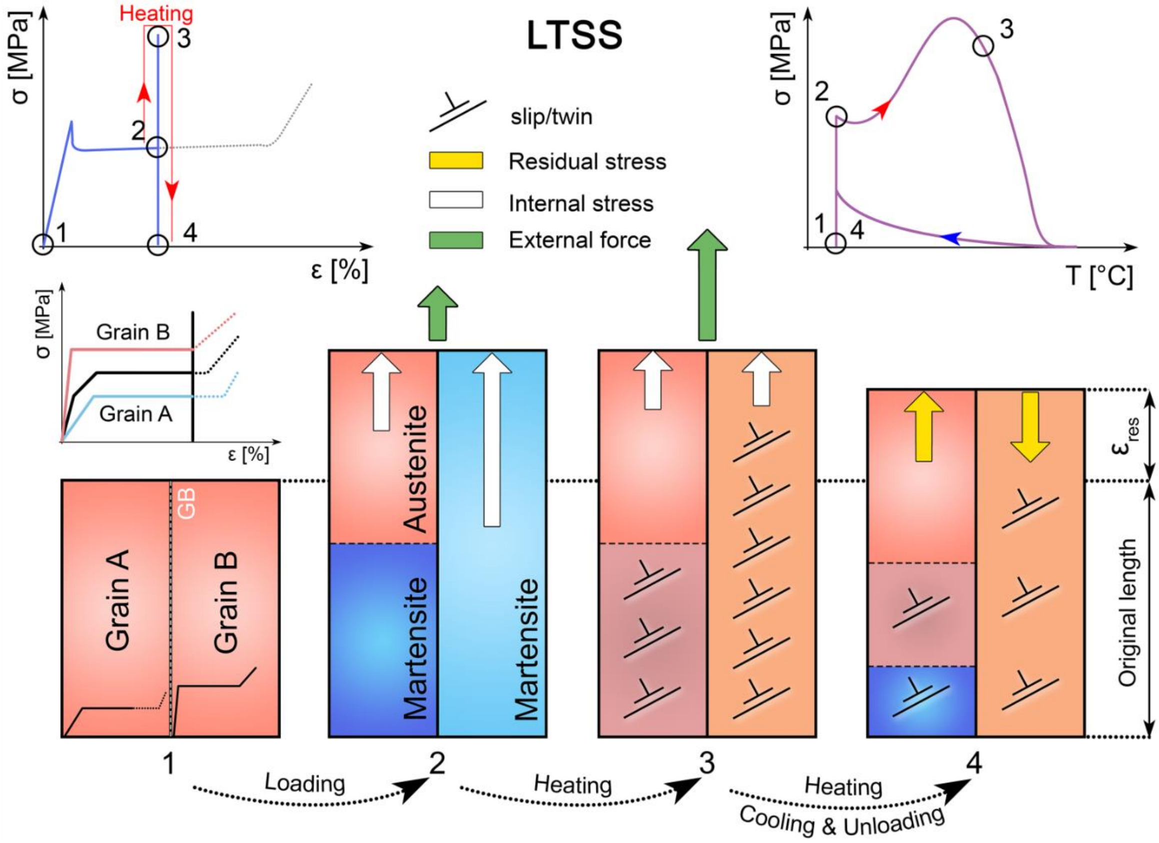

Figure 43. Bicrystal model of LTSS in constrained polycrystalline environment explaining the origin of residual stress and TWSME in LTSS treated NiTi wire. Conceptual bicrystal consisting of two differently oriented grains joined at a vertical grain boundary is subjected to constrained heating test. The oriented martensite is converted to longer austenite upon constrained heating (2->3) leaving residual stress and residual martensite in the unloaded microstructure (4), which are then source of the TWSME upon subsequent stress free cooling [111].

## 3.10 Conclusions

NiTi shape memory alloys, when deformed and heated under external constraint, undergo reverse martensitic transformation coupled with the plastic deformation due to dislocation slip and twinning. This deformation/transformation process, termed LTSS in this work, was systematically investigated by dedicated thermomechanical testing on superelastic and actuator NiTi wires with in-situ evaluation of electric resistance, synchrotron x-ray diffraction and digital image correlation of surface strains. Microstructures in LTSS treated wires were analyzed by TEM. Following main results were obtained.

- NiTi wire prestrained to oriented martensite and subjected to the constrained heating show a characteristic stress-temperature response with stress maximum somewhere in the temperature range 100°C-200°C depending on the starting microstructure of the wire.
- The stress-temperature response was interpreted as being due to gradual reverse martensitic transformation of oriented martensite into plastically deformed austenite (transformation strain of the vanishing martensite is compensated by plastic straining of the wire).
- LTSS selectively occurs only in the parts of the sample where oriented martensite exists, and has no effect on the parent austenite phase existing elsewhere in the wire sample.
- LTSS process converts the oriented martensite into the plastically deformed austenite with new microstructure containing high density of dislocation tangles, domain walls, internal strain and lamellar defects identified as {114} austenite twins.
- The kinematically incompatible {20-1} martensite twins retained by the reverse transformation into the austenite phase as {114} austenite twins constitute the {20-1}M/{114}A twinning mechanism of plastic deformation involved in LTSS.
- Dislocation slip at the reverse propagating habit planes and the {20-1}M/{114}A twinning upon heating represent the TRIP like LTSS deformation mechanism.
- While the {20-1}M/{114}A twinning operates at high stress in high strength 125W/12ms wires, dislocation slip at the habit plane prevails in soft 125W/20ms NiTi wires at lower stresses.
- LTSS is a thermomechanical treatment featuring strengthening followed by recovery of the microstructure.
- Depending on the starting microstructure, LTSS can be used to shape set NiTi components at temperatures as low as 150°C-300°C.
- LTSS treated wire has new shape and exhibits excellent functional properties.

- Functional properties of the LTSS treated wire depend on the starting microstructure, maximum temperature and applied constraint.
- NiTi wires with unique microstructures and functional properties can be prepared by the LTSS.
- Strain drift during thermal cycling of actuator NiTi wires originates from the LTSS.
- Two-way shape memory effect up to 4% can be created by a single constrained heating/cooling up to a carefully selected temperature.

# 4 Mechanical testing of NiTi wires

Part of my work in frame of the thesis concerning in-situ synchrotron x-ray diffraction study of cyclic superelastic deformation of NiTi wires was published in two recent articles; the first one deals with evolution of microstructure during cyclic superelasticity (*Instability of cyclic superelastic deformation of NiTi investigated by synchrotron X-ray diffraction – Paper I*) and the second one with unique 3D-XRD experiment (*Grain-resolved analysis of localized deformation in nickel-titanium wire under tensile load – Paper II*) in which propagation of localized martensite band in NiTi wire loaded in tension was analyzed with surprising results.

## 4.1 Superelastic cycling

As discussed in the chapter (1.3.2) there are numerous studies dealing with functional degradation upon superelastic cycling, but the link between macroscopic instability and microstructural processes during cycling was not understood until recently. To reveal this link, I have performed in-situ high resolution synchrotron X-ray investigation of cyclic tensile superelasticity of NiTi wire on ID22 ESRF beamline (*Paper I)*. All experiments were performed on Fort Wayne Metals NiTi#1 superelastic wires with custom treated microstructure by short electric current pulses [77]. Wires were annealed applying power pulse with 125W/100mm wire length and annealing times of 12, 14, 15, 16, 16.5, 18, 20ms. With increasing annealing time, grain size increases (from nano-grain size for 12ms, up to 5µm for 20ms) and matrix slip resistance decreases [48].

Instability of cyclic superelastic deformation of all these wires was systematically studied using synchrotron x-ray diffraction. The work reported in Paper I, however, is based on experiment performed on 125W/16.5ms heat treated NiTi wire only since it was easy to follow the degradation processes in this wire during first 10 cycles. In the case of shorter annealing times, same processes would need thousands of cycles to achieve same results, on the other hand, wires with longer annealing times showed complete change of functional behavior after first two cycles. It was found that cyclic instability of superelastic response of NiTi wire is due to gradual redistribution of internal stresses in the polycrystalline aggregate due to incremental plastic slip accumulation. With regard to the previous findings on thermomechanical loading, it follows that martensitic transformation is also accompanied by plastic deformation, the extent of which is given by microstructure slip resistance.

# Paper I

P. Sedmák, P. Šittner, J. Pilch, C. Curfs, Instability of cyclic superelastic deformation of NiTi investigated by synchrotron X-ray diffraction, Acta Materialia 94 (2015), 257 – 270.
DOI: https://doi.org/10.1016/j.actamat.2015.04.039

http://www.sciencedirect.com/science/article/pii/S1359645415002918

## 4.2 Localized deformation in NiTi shape memory alloys

Another issue preventing further growth of superelastic NiTi applications is the strain localization into macroscopic fronts propagating in NiTi wires under tensile load. The strain localization phenomenon is not unique to NiTi, it has long been known to engineers studying plastic flow in mild steels. In the case of NiTi, it has been called Lüders-like deformation and comprehensively studied in the last 20 years [11,36,98–105]. Because most of the experimental methods are based on surface observations, it was not clear what is the topology of martensite band front (MBF) in the bulk of NiTi wires. From the surface observations, the interface appears to be perpendicular to the wire axis, which is in conflict with observations on sheets or thin wall tubes where it is inclined by 55°.

I have employed synchrotron 3D XRD microscopy to reveal the topology of the martensite band front and internal stress field around it in NiTi wires deforming in tension at ID11 ESRF beamline. No other method can provide such topological information on the buried interface since the measurement must be carried out under applied stress and the information from the whole bulk of the material is needed. SEM, DIC or other methods record only the information from the surface of the sample. I was able to evaluate strain and stress tensors in thousands of micron sized grains and reconstruct internal stress field associated with propagating martensite band front.

# Paper II

P. Sedmák, J. Pilch, L. Heller, J. Kopeček, J. Wright, P. Sedlák, M. Frost, P. Šittner, Grain-resolved analysis of localized deformation in nickel-titanium wire under tensile load, Science. 353 (2016) 559–562, DOI: 10.1126/science.aad6700

http://science.sciencemag.org/content/353/6299/559.full?ijkey=Ar5p6MNOGevhk&keytype=ref&siteid=sci

# 5 Summary and outlook

## Summary

The main goal of this thesis was to investigate the deformation/transformation processes in the NiTi shape memory alloy wires subjected to the thermomechanical loading conditions favouring coupled martensitic transformation and plasticity by means of thermomechanical loading tests with in-situ synchrotron x-ray diffraction and electric resistance measurements. Four key tests studied include: i) localized deformation due to stress induced martensitic transformation in tension, ii) instability of cyclic tensile superelastic deformation, iii) instability of thermal cycling under constant tensile stress and iv) recovery stress tests consisting in constrained heating/cooling of the NiTi wire deformed in tension up to high temperatures.

Stress-strain-temperature responses of the NiTi wires determined in all performed experiments were due to the combined martensitic transformation and plasticity. The synchrotron x-ray diffraction and electric resistivity methods applied in-situ during the thermomechanical loading experiments enabled to obtain a supplemental structure sensitive information on the microstructure evolution during the thermomechanical tests. Based on the performed analysis, I was able to link the deformation mechanisms assumed to take place in the tested NiTi wires with the microstructure evolution. I obtained new information on the **localized superelastic deformation of NiTi wire in tension (*Paper II*),** on the **cyclic tensile superelasticity of NiTi (*Paper I*),** and on the **coupled martensitic transformation and plasticity in the thermomechanical loading tests under external constraint up to high temperatures (chapter 3)**. Key results can be summarized as follows.

### Localized superelastic deformation of NiTi wire in tension

Superelastic deformation of the NiTi wires in tension is localized into the macroscopic interfaces (martensite band fronts) propagating along the wire under constant applied stress. Although this phenomenon was thoroughly investigated in the literature before, it was not quite clear why the localization occurs, what is the topology of the propagating martensite band front and whether there are the internal stress gradients around it.

I performed a unique synchrotron x-ray diffraction experiment focused on the characterization of the martensite band front by means of 3D-XRD microscopy method using ID11 beamline at ESRF. I managed to determine strain and stress tensors in ~15000 austenitic grains within the martensite band front and reconstruct the macroscopic internal stress and strain fields in the wire from the grain resolved stresses. The martensite band front has a nose cone shape and there is an enormous internal stress inhomogeneity around it. As the martensite band front propagates through the wire, the stress states in the grains dramatically change when they appear within the martensite band front.

We revealed the mesoscopic mechanism by which the front of localized deformation propagates through the wire. The local stresses in grains ahead of the advancing front redistribute in such a way that the grains located at the buried conical interface experience much higher shear stresses compared to other grains far from the interface. Consequently, these grains transform collectively while very little is happening elsewhere in the wire. Because the maximum inelastic deformation via martensitic transformation is limited by the crystallography of the transformation, the martensite band front moves along the wire under constant applied force. Confronting the experimental results with results of FE simulation using thermomechanical model of NiTi polycrystal, we confirmed the earlier suspicion from the literature that the polycrystalline NiTi wire shows a softening type macroscopic response in tension. We found that the assumption that the martensitic transformation in polycrystalline NiTi wire loaded in tension takes place under nominal tensile stress frequently adopted in the literature is not quite correct – stress states in transforming grains are in fact very far from tensile and equivalent stresses are much higher than the nominal stress calculated from the applied force and wire cross-section.

### Cyclic superelasticity in tension

The cyclic instability of the superelastic stress-strain response of NiTi wires in tension was investigated using in-situ synchrotron x-ray diffraction and electric resistivity measurements.

We have found that the cyclic instability is due to gradual evolution of the microstructure in the cycled wire due to the incremental plasticity accompanying the stress martensitic transformation. We have determined how internal stresses in oriented grains are redistributed in constrained polycrystalline environment and described gradual accumulation of defects, residual martensite, internal stress and incremental plastic deformation accompanying the cyclic martensitic transformation. A mechanism linking the above mentioned experimental observations mutually together was proposed. We have explained that the resistance to dislocation slip is the key material characteristics affecting the instability is of cyclic superelastic deformation of NiTi wires. With decreasing matrix slip resistance, the coupling of martensitic transformation and plastic deformation becomes stronger and yields increasing irrecoverable strain.

### Constrained heating/cooling of deformed NiTi wire up to high temperatures.

Deformation processes in NiTi wires subjected to constrained heating/cooling after deformation into oriented martensite state were investigated by thermomechanical loading tests with in-situ electric resistance, in-situ synchrotron x-ray diffraction, in-situ digital image correlation of surface strains and ex-situ TEM observation of microstructures in tested wires.

It was found that deformed NiTi wire, when heated under external constraint, undergoes reverse martensitic transformation coupled with the plastic deformation due to dislocation slip and twinning. In other words, when heated, the constrained NiTi wire containing oriented martensite at room temperature, becomes gradually converted into a plastically deformed austenitic wire with new microstructure containing high density of dislocation tangles, domain walls, internal strain and lamellar defects identified as {114} austenite twins. The reverse martensitic transformation coupled with plastic deformation (LTSS deformation mechanism) taking place upon heating was interpreted as a unique TRIP like deformation mechanism acting in NiTi shape memory alloys at elevated temperatures and large stresses. This deformation mechanism involving dislocation slip at the reverse propagating habit planes and the {20-1}M/{114}A twinning is claimed to be very important for NiTi technology, particularly for the shape setting, actuation and two-way shape memory effect training.

### Thermal cycling under constant load

Reversible strain-temperature response of thermally cycled NiTi actuator wires is beneficially used in engineering applications and currently the actuation is a hot topic in the SMA field again. Key problem is the cyclic instability of the strain-temperature response and low fatigue performance in case larger applied stresses above ~300MPa (for a good quality actuator wire). The goal of my in-situ x-ray diffraction research was to determine the microstructure evolution in the thermally cycled wire, to find out what are the physical principles behind this sharp stress dependence of fatigue performance and whether the limiting stress can be potentially increased by manipulating the starting microstructure of the wire.

I have found that irreversible incremental microstructure changes and incremental plastic deformation occur mainly while the NiTi wire is reverse transforming from the oriented martensite to the austenite under stress beyond a critical level. Dislocation defects accumulate upon cycling but internal stresses (unlike superelastic cycling) do not. As a result, the strain-temperature response of the cycled NiTi wire drifts to larger strains but the actuator strain does not change upon cycling. The instability during the thermal cycling (drift) and the level of critical stress depend on matrix slip resistance of the NiTi wire.

I have concluded that the instability of the strain-temperature response upon thermal cycling is caused by gradual/incremental plastic deformation due to the TRIP like deformation mechanism. Whether stress and temperature in a particular thermally cycled NiTi wire reach the conditions where this deformation mechanism proceeds, depends on: i) the material state of the wire, ii) the maximum temperature upon heating and iii) externally applied constraint (level of the constant stress applied during thermal cycling under constant stress).

## Outlook

Results of the 3D-XRD experiment published in Science, in which the martensite band front in NiTi wire was described and mesoscale mechanism of localized deformation was for the first time explained, triggered a wave of further experimental and theoretical investigations by us as well as by others in the literature [106,107]. We have performed new experiment [108] focussing cycling tensile localized deformation, the results of which are currently being analysed. We managed to further progress with the analysis of the results of the 3D-XRD experiment by reconstructing the grain boundary network in the polycrystalline wire [109] and performing FE simulation of grains resolved strains and stresses. Thermomechanical model of NiTi adapted for non-local effects based on the results of the 3D-XRD experiment [110] is currently applied for localization phenomena in NiTi generally (NiTi springs, textiles, bending of tubes etc.).

What remains unknown is the stresses and strains in the martensitic part of the wire within the martensite band. An ideal tool for this purpose seems to be the new Nano-stage at ID11 ESRF beamline. This brand new stage offers a high energy beam with the minimum diameters of ~200x200nm so far. Diffraction tomography technique (focused x-ray beam with fine spaced point scanning across the wire diameter combined with rotation) will most probably solve the problem of overlapping reflections in the monoclinic martensitic phase (smaller beam = less grains fulfilling Bragg condition leading to less diffraction spots on 2D detector). However, the problem of the peak smearing along the eta (azimuthal) direction due to plastic deformation will still cause a lot of problems with the data analysis.

The work on instability of cyclic superelastic deformation of NiTi brought about a question whether the level of the cyclic instability is related to structural fatigue of NiTi. We believe the answer is YES and the team in Prague continues their research of NiTi fatigue along this line.

My low temperature shape setting research (chapter 3) lead to further experimental and theoretical investigations of the TRIP like deformation mechanism in NiTi in Prague. A theoretical framework for deformation/transformation of NiTi due to martensitic transformation with plasticity was proposed [111]. We managed to determine the unrecovered plastic strains generated by the forward and reverse martensitic transformations separately and explain why significant unrecovered strains are generated by the reverse martensitic transformation theoretically [112]. It was found that the TRIP like deformation mechanism does not occur only during the constrained heating but it is a general deformation mode of NiTi at elevated temperatures [113].

# 6 Bibilography

[1] W.J. Buehler, J.V. Gilfrich, R.C. Wiley, Effect of Low-Temperature Phase Changes on the Mechanical Properties of Alloys near Composition TiNi, J. Appl. Phys. 34 (1963) 1475. doi:10.1063/1.1729603.

[2] J. Mohd Jani, M. Leary, A. Subic, M.A. Gibson, A review of shape memory alloy research, applications and opportunities, Mater. Des. 56 (2014) 1078–1113. doi:10.1016/j.matdes.2013.11.084.

[3] M.H. Wu, L.M. Schetky, Industrial applications for shape memory alloys, Proc. Int. Conf. Shape Mem. Superelastic Technol. (2000) 171–182.

[4] K. Otsuka, T. Kakeshita, Science and technology of shape-memory alloys: new developments, Mrs Bull. 27 (2002) 91–100.

[5] K. Otsuka, X. Ren, Physical metallurgy of Ti–Ni-based shape memory alloys, Prog. Mater. Sci. 50 (2005) 511–678. doi:10.1016/j.pmatsci.2004.10.001.

[6] T.W. Duerig, ed., Engineering aspects of shape memory alloys, Butterworth-Heinemann, London ; Boston, 1990.

[7] C. Chluba, W. Ge, R.L. de Miranda, J. Strobel, L. Kienle, E. Quandt, M. Wuttig, Ultralow-fatigue shape memory alloy films, Science. 348 (2015) 1004–1007. doi:10.1126/science.1261164.

[8] D. Dye, Shape memory alloys: Towards practical actuators, Nat. Mater. 14 (2015) 760–761. doi:10.1038/nmat4362.

[9] ASTM. Standard test method for determination of the transformation temperature of nickel–titanium shape memory alloys by bend and free recovery. West Conshohocken, PA: ASTM International, (2010).

[10] Y. Liu, H. Yang, Strain dependence of the Clausius–Clapeyron relation for thermoelastic martensitic transformations in NiTi, Smart Mater. Struct. 16 (2007) S22–S27. doi:10.1088/0964-1726/16/1/S03.

[11] J.A. Shaw, S. Kyriakides, Initiation and propagation of localized deformation in elasto-plastic strips under uniaxial tension, Int. J. Plast. 13 (1997) 837–871.

[12] S. Suresh, Fatigue of Materials | Materials Science | Cambridge University Press, (n.d.). http://www.cambridge.org/us/academic/subjects/engineering/fatigue-materials-2nd-edition (accessed April 20, 2016).

[13] K.N. Melton, O. Mercier, Fatigue of NITI thermoelastic martensites, Acta Metall. 27 (1979) 137–144. doi:10.1016/0001-6160(79)90065-8.

[14] S. Miyazaki, K. Mizukoshi, T. Ueki, T. Sakuma, Y. Liu, Fatigue life of Ti–50 at.% Ni and Ti–40Ni–10Cu (at.%) shape memory alloy wires, Mater. Sci. Eng. A. 273–275 (1999) 658–663. doi:10.1016/S0921-5093(99)00344-5.

[15] Reinoehl, M., Bradley, D., Bouthot, R., Proft, J., The influence of melt practice on final fatigue properties of superelastic NiTi wires, SMST-2000 Proc. Int. Conf. Shape Mem. Superelasticity. (2000) 397–404.

[16] G. Kang, D. Song, Review on structural fatigue of NiTi shape memory alloys: Pure mechanical and thermo-mechanical ones, Theor. Appl. Mech. Lett. 5 (2015) 245–254. doi:10.1016/j.taml.2015.11.004.

[17] G. Eggeler, E. Hornbogen, A. Yawny, A. Heckmann, M. Wagner, Structural and functional fatigue of NiTi shape memory alloys, Mater. Sci. Eng. A. 378 (2004) 24–33. doi:10.1016/j.msea.2003.10.327.

[18] S. Miyazaki, Y. Igo, K. Otsuka, Effect of thermal cycling on the transformation temperatures of Ti・Ni alloys, Acta Metall. 34 (1986) 2045–2051.

[19] H. Matsumoto, Appearance of an intermediate phase with thermal cycling on the transformation of NiTi, J. Mater. Sci. Lett. 10 (1991) 408–410.
[20] H. Matsumoto, Transformation behaviour with thermal cycling in NiTi alloys, J. Alloys Compd. 350 (2003) 213–217.
[21] A.R. Pelton, G.H. Huang, P. Moine, R. Sinclair, Effects of thermal cycling on microstructure and properties in Nitinol, Mater. Sci. Eng. A. 532 (2012) 130–138. doi:10.1016/j.msea.2011.10.073.
[22] M.L. Bowers, Y. Gao, L. Yang, D.J. Gaydosh, M. De Graef, R.D. Noebe, Y. Wang, M.J. Mills, Austenite grain refinement during load-biased thermal cycling of a Ni49.9Ti50.1 shape memory alloy, Acta Mater. 91 (2015) 318–329. doi:10.1016/j.actamat.2015.03.017.
[23] C.N. Saikrishna, K.V. Ramaiah, S.A. Prabhu, S.K. Bhaumik, On stability of NiTi wire during thermo-mechanical cycling, Bull. Mater. Sci. 32 (2009) 343–352.
[24] G. Scirè Mammano, E. Dragoni, Functional fatigue of Ni–Ti shape memory wires under various loading conditions, Int. J. Fatigue. 69 (2014) 71–83. doi:10.1016/j.ijfatigue.2012.03.004.
[25] S.A. Padula, D. Gaydosh, A. Saleeb, B. Dhakal, Transients and Evolution in NiTi, Exp. Mech. 54 (2014) 709–715. doi:10.1007/s11340-013-9840-4.
[26] M.F.-X. Wagner, S.R. Dey, H. Gugel, J. Frenzel, C. Somsen, G. Eggeler, Effect of low-temperature precipitation on the transformation characteristics of Ni-rich NiTi shape memory alloys during thermal cycling, Intermetallics. 18 (2010) 1172–1179. doi:10.1016/j.intermet.2010.02.048.
[27] M. Mertmann, G. Vergani, Design and application of shape memory actuators, Eur. Phys. J. Spec. Top. 158 (2008) 221–230. doi:10.1140/epjst/e2008-00679-9.
[28] R. Casati, F. Passaretti, A. Tuissi, Effect of electrical heating conditions on functional fatigue of thin NiTi wire for shape memory actuators, Procedia Eng. 10 (2011) 3423–3428. doi:10.1016/j.proeng.2011.04.564.
[29] C.N. Saikrishna, K.V. Ramaiah, B. Vidyashankar, S.K. Bhaumik, Effect of Intermittent Overload Cycles on Thermomechanical Fatigue Life of NiTi Shape Memory Alloy Wire, Metall. Mater. Trans. A. 44 (2013) 5–8. doi:10.1007/s11661-012-1557-y.
[30] C.N. Saikrishna, K.V. Ramaiah, D. Paul, S.K. Bhaumik, Enhancement in fatigue life of NiTi shape memory alloy thermal actuator wire, Acta Mater. 102 (2016) 385–396. doi:10.1016/j.actamat.2015.09.034.
[31] B. Ye, B.S. Majumdar, I. Dutta, Texture memory and strain-texture mapping in a NiTi shape memory alloy, Appl. Phys. Lett. 91 (2007) 61918. doi:10.1063/1.2768899.
[32] B. Ye, B.S. Majumdar, I. Dutta, Texture development and strain hysteresis in a NiTi shape-memory alloy during thermal cycling under load, Acta Mater. 57 (2009) 2403–2417. doi:10.1016/j.actamat.2009.01.032.
[33] O. Benafan, R.D. Noebe, S.A. Padula, D.W. Brown, S. Vogel, R. Vaidyanathan, Thermomechanical cycling of a NiTi shape memory alloy-macroscopic response and microstructural evolution, Int. J. Plast. 56 (2014) 99–118. doi:10.1016/j.ijplas.2014.01.006.
[34] N.G. Jones, S.L. Raghunathan, D. Dye, In-Situ Synchrotron Characterization of Transformation Sequences in TiNi-Based Shape Memory Alloys during Thermal Cycling, Metall. Mater. Trans. A. 41 (2010) 912–921. doi:10.1007/s11661-009-0166-x.
[35] N.G. Jones, D. Dye, Martensite evolution in a NiTi shape memory alloy when thermal cycling under an applied load, Intermetallics. 19 (2011) 1348–1358. doi:10.1016/j.intermet.2011.03.032.

[36] Y. Liu, Y. Liu, J. Van Humbeeck, Two-way shape memory effect developed by martensite deformation in NiTi, Acta Mater. 47 (1998) 199–209. doi:10.1016/S1359-6454(98)00325-5.

[37] Y. Liu, G. Tan, S. Miyazaki, Deformation-induced martensite stabilisation in [100] single-crystalline Ni–Ti, Mater. Sci. Eng. A. 438–440 (2006) 612–616. doi:10.1016/j.msea.2006.02.130.

[38] S.W. Robertson, R.O. Ritchie, A. Mehta, X.-Y. Gong, A. Pelton, Ultrahigh resolution in situ diffraction characterization of the local mechanics at a growing crack tip in Nitinol, in: Proc. Int. Conf. Shape Mem. Superelastic Technol. Menlo Park CA SMST Soc. Forthcom., 2008. https://www.researchgate.net/profile/Robert_Ritchie/publication/242290502_Ultrahigh-Resolution_In_Situ_Diffraction_Characterization_of_the_Local_Mechanics_at_a_Growing_Crack_Tip_in_Nitinol/links/00463528cc2217f8af000000.pdf (accessed June 6, 2016).

[39] Z. Moumni, A.V. Herpen, P. Riberty, Fatigue analysis of shape memory alloys: energy approach, Smart Mater. Struct. 14 (2005) S287–S292. doi:10.1088/0964-1726/14/5/017.

[40] P. Sedmák, J. Pilch, L. Heller, J. Kopeček, J. Wright, P. Sedlák, M. Frost, P. Šittner, Grain-resolved analysis of localized deformation in nickel-titanium wire under tensile load, Science. 353 (2016) 559–562. doi:10.1126/science.aad6700.

[41] C. Maletta, E. Sgambitterra, F. Furgiuele, R. Casati, A. Tuissi, Fatigue properties of a pseudoelastic NiTi alloy: Strain ratcheting and hysteresis under cyclic tensile loading, Int. J. Fatigue. 66 (2014) 78–85. doi:10.1016/j.ijfatigue.2014.03.011.

[42] M. Kollerov, E. Lukina, D. Gusev, P. Mason, P. Wagstaff, Impact of material structure on the fatigue behaviour of NiTi leading to a modified Coffin–Manson equation, Mater. Sci. Eng. A. 585 (2013) 356–362. doi:10.1016/j.msea.2013.07.072.

[43] A.R. Pelton, J. Fino-Decker, L. Vien, C. Bonsignore, P. Saffari, M. Launey, M.R. Mitchell, Rotary-bending fatigue characteristics of medical-grade Nitinol wire, J. Mech. Behav. Biomed. Mater. 27 (2013) 19–32. doi:10.1016/j.jmbbm.2013.06.003.

[44] M. Rahim, J. Frenzel, M. Frotscher, J. Pfetzing-Micklich, R. Steegmüller, M. Wohlschlögel, H. Mughrabi, G. Eggeler, Impurity levels and fatigue lives of pseudoelastic NiTi shape memory alloys, Acta Mater. 61 (2013) 3667–3686. doi:10.1016/j.actamat.2013.02.054.

[45] K. Hirmanová, J. Pilch, J. Racek, L. Heller, P. Šittner, L. Recman, M. Petrenec, P. Sedlák, Physical Simulation of the Random Failure of Implanted Braided NiTi Stents, J. Mater. Eng. Perform. 23 (2014) 2650–2658. doi:10.1007/s11665-014-0916-9.

[46] K. Otsuka, C. M. Wayman, Shape Memory Materials, Cambridge university press, n.d. https://books.google.cz/books?id=DvItE9XUlN8C&redir_esc=y.

[47] Eucken S., Duerig T.W., The effects of pseudoelastic prestraining on tensile behavior and two was shape memory effect in aged NiTi, Acta Metall. 37 (1989) 2245–2252.

[48] R. Delville, B. Malard, J. Pilch, P. Sittner, D. Schryvers, Transmission electron microscopy investigation of dislocation slip during superelastic cycling of Ni–Ti wires, Int. J. Plast. 27 (2011) 282–297.

[49] A. Yawny, M. Sade, G. Eggeler, Pseudoelastic cycling of ultra-fine-grained NiTi shape-memory wires, Z. Für Met. 96 (2005) 608–618. doi:10.3139/146.101078.

[50] T. Simon, A. Kröger, C. Somsen, A. Dlouhy, G. Eggeler, On the multiplication of dislocations during martensitic transformations in NiTi shape memory alloys, Acta Mater. 58 (2010) 1850–1860. doi:10.1016/j.actamat.2009.11.028.

[51] R. Delville, B. Malard, J. Pilch, P. Sittner, D. Schryvers, Microstructure changes during non-conventional heat treatment of thin Ni–Ti wires by pulsed electric current studied by

transmission electron microscopy, Acta Mater. 58 (2010) 4503–4515. doi:10.1016/j.actamat.2010.04.046.

[52] X. Jiang, M. Hida, Y. Takemoto, A. Sakakibara, H. Yasuda, H. Mori, In situ observation of stress-induced martensitic transformation and plastic deformation in TiNi alloy, Mater. Sci. Eng. A. 238 (1997) 303–308.

[53] V. Novák, P. Šittner, J. Pilch, R. Delville, Effect of plastic slip on thermomechanical behavior of NiTi polycrystals investigated by micromechanics modelling, in: EDP Sciences, 2009. doi:10.1051/esomat/200903009.

[54] D.M. Norfleet, P.M. Sarosi, S. Manchiraju, M.F.-X. Wagner, M.D. Uchic, P.M. Anderson, M.J. Mills, Transformation-induced plasticity during pseudoelastic deformation in Ni–Ti microcrystals, Acta Mater. 57 (2009) 3549–3561. doi:10.1016/j.actamat.2009.04.009.

[55] A.W. Richards, R.A. Lebensohn, K. Bhattacharya, Interplay of martensitic phase transformation and plastic slip in polycrystals, Acta Mater. 61 (2013) 4384–4397. doi:10.1016/j.actamat.2013.03.053.

[56] Nitinol 1 - Fort Wayne Metals, (n.d.). http://www.fwmetals.com/services/resource-library/nitinol-1/ (accessed May 31, 2016).

[57] Y.C. Shu, K. Bhattacharya, The influence of texture on the shape-memory effect in polycrystals, Acta Mater. 46 (1998) 5457–5473. doi:10.1016/S1359-6454(98)00184-0.

[58] J. Pilch, L. Heller, P. Sittner, Heat Treatment of thin NiTi filaments by electric current, SMST E-Elastic Newsl. ASM Int. Online Publ. (2010). http://energia.moebius.com.br/oo/Energia/Nitinol/0107Pilc0110Heat.pdf (accessed June 26, 2015).

[59] B. Malard, J. Pilch, P. Sittner, V. Gartnerova, R. Delville, D. Schryvers, C. Curfs, Microstructure and functional property changes in thin Ni–Ti wires heat treated by electric current—high energy X-ray and TEM investigations, Funct. Mater. Lett. 2 (2009) 45–54.

[60] M.F.-X. Wagner, A. Schaefer, Macroscopic versus local strain rates during tensile testing of pseudoelastic NiTi, Scr. Mater. 63 (2010) 863–866. doi:10.1016/j.scriptamat.2010.06.038.

[61] Y.J. He, Q.P. Sun, Rate-dependent domain spacing in a stretched NiTi strip, Int. J. Solids Struct. 47 (2010) 2775–2783. doi:10.1016/j.ijsolstr.2010.06.006.

[62] H.F. Poulsen, Three-dimensional X-ray diffraction microscopy: mapping polycrystals and their dynamics, Springer Science & Business Media, 2004. http://books.google.com/books?hl=en&lr=&id=_jzrH20Qu6cC&oi=fnd&pg=PA1&dq=%22appear+on+the+atomic+scale.+To+reduce+their+associated+strain%22+%22its+interaction+with+neighboring+grains+or+by+the+emerging%22+%221.1.+Evolution+of+typical+structures+in+a+metal+during+deformation,+as%22+&ots=fsIz9gLZFP&sig=VDwrjVSP1qtvU87b3KkWGUDPfbk (accessed June 26, 2015).

[63] J. Oddershede, S. Schmidt, H.F. Poulsen, H.O. Sørensen, J. Wright, W. Reimers, Determining grain resolved stresses in polycrystalline materials using three-dimensional X-ray diffraction, J. Appl. Crystallogr. 43 (2010) 539–549. doi:10.1107/S0021889810012963.

[64] J. Oddershede, S. Schmidt, H.F. Poulsen, L. Margulies, J. Wright, M. Moscicki, W. Reimers, G. Winther, Grain-resolved elastic strains in deformed copper measured by three-dimensional X-ray diffraction, Mater. Charact. 62 (2011) 651–660. doi:10.1016/j.matchar.2011.04.020.

[65] B. Jakobsen, H.F. Poulsen, U. Lienert, J. Almer, S.D. Shastri, H.O. Sørensen, C. Gundlach, W. Pantleon, Formation and Subdivision of Deformation Structures During Plastic Deformation, Science. 312 (2006) 889–892. doi:10.1126/science.1124141.

[66] S.E. Offerman, N.H. van Dijk, J. Sietsma, E.M. Lauridsen, L. Margulies, S. Grigull, H.F. Poulsen, S. van der Zwaag, Phase transformations in steel studied by 3DXRD microscopy, Nucl. Instrum. Methods Phys. Res. Sect. B Beam Interact. Mater. At. 246 (2006) 194–200. doi:10.1016/j.nimb.2005.12.058.

[67] E. Jimenez-Melero, N.H. van Dijk, L. Zhao, J. Sietsma, S.E. Offerman, J.P. Wright, S. van der Zwaag, Characterization of individual retained austenite grains and their stability in low-alloyed TRIP steels, Acta Mater. 55 (2007) 6713–6723. doi:10.1016/j.actamat.2007.08.040.

[68] H. Abdolvand, M. Majkut, J. Oddershede, J.P. Wright, M.R. Daymond, Study of 3-D stress development in parent and twin pairs of a hexagonal close-packed polycrystal: Part II – crystal plasticity finite element modeling, Acta Mater. 93 (2015) 235–245. doi:10.1016/j.actamat.2015.04.025.

[69] P. Šittner, D. Vokoun, G.N. Dayananda, R. Stalmans, Recovery stress generation in shape memory Ti 50 Ni 45 Cu 5 thin wires, Mater. Sci. Eng. A. 286 (2000) 298–311.

[70] X. Yan, J. Van Humbeeck, Influence of pre-strain on recovery stress of annealed NiTi thin wire during isothermal holding, J. Alloys Compd. 509 (2011) 1001–1006. doi:10.1016/j.jallcom.2010.09.156.

[71] Petr Sittner, Veronique Michaud, Jan Schrooten, Modelling and Material Design of SMA Polymer Composites, Mater. Trans. 43 (2002) 984–993.

[72] D. E. Hodgson, Fabrication, heat treatment and joining of nitinol components, in: Proc. Int. Conf. Shape Mem. Superelastic Technol., SMST, The International Organization on Shape Memory and Superelastic Technology, Pacific Groove, CA, USA, 2000: pp. 11–24.

[73] D. E. Hodgson, in Medical Device Materials: Proceedings from the Materials & Processes for Medical Devices Conference 2003, 8-10 September 2003, Anaheim, California, in: ASM International, 2004: p. 226.

[74] B. Malard, J. Pilch, P. Sittner, R. Delville, C. Curfs, In situ investigation of the fast microstructure evolution during electropulse treatment of cold drawn NiTi wires, Acta Mater. 59 (2011) 1542–1556. doi:10.1016/j.actamat.2010.11.018.

[75] R. Zhu, Y. Jiang, L. Guan, H. Li, G. Tang, Difference in recrystallization between electropulsing-treated and furnace-treated NiTi alloy, J. Alloys Compd. 658 (2016) 548–554. doi:10.1016/j.jallcom.2015.10.239.

[76] V. Delobelle, G. Chagnon, D. Favier, T. Alonso, Study of electropulse heat treatment of cold worked NiTi wire: From uniform to localised tensile behaviour, J. Mater. Process. Technol. 227 (2016) 244–250. doi:10.1016/j.jmatprotec.2015.08.011.

[77] J. Pilch, L. Heller, P. Sittner, Heat Treatment of thin NiTi filaments by electric current, SMST E-Elastic Newsl. ASM Int. Online Publ. (2010). http://energia.moebius.com.br/oo/Energia/Nitinol/0107Pilc0110Heat.pdf (accessed May 31, 2016).

[78] J. Pilch, P. Sittner, Method of heat treatment and/or inspection of functional mechanical properties, particularly transformation strain and/or strength, of shape memory alloy filaments and apparatus for the application of this method, US20120018413 A1, 2012. http://www.google.com/patents/US20120018413 (accessed November 9, 2016).

[79] J. Pilch, L. Heller, P. Sittner, in Medical device materials V: proceedings of the Materials & Processes for Medical Devices Conference 2009, August 10-12, 2009, Minneapolis, MN, USA, in: ASM International, Materials Park, OH, 2010.

[80] J. Seibold, E. Müller, K. Volenec, P. Sittner, L. Heller, J. Pilch, Medical device, US9216100 B2, 2015. http://www.google.com/patents/US9216100 (accessed November 9, 2016).

[81] O. Benafan, S.A. Padula, R.D. Noebe, D.W. Brown, B. Clausen, R. Vaidyanathan, An in situ neutron diffraction study of shape setting shape memory NiTi, Acta Mater. 61 (2013) 3585–3599. doi:10.1016/j.actamat.2013.02.040.

[82] C. Yu, B. Aoun, L. Cui, Y. Liu, H. Yang, X. Jiang, S. Cai, D. Jiang, Z. Liu, D.E. Brown, Y. Ren, Synchrotron high energy X-ray diffraction study of microstructure evolution of severely cold drawn NiTi wire during annealing, Acta Mater. 115 (2016) 35–44. doi:10.1016/j.actamat.2016.05.039.

[83] O. Benafan, S.A. Padula, R.D. Noebe, D.W. Brown, B. Clausen, R. Vaidyanathan, An in situ neutron diffraction study of shape setting shape memory NiTi, Acta Mater. 61 (2013) 3585–3599. doi:10.1016/j.actamat.2013.02.040.

[84] I. Karaman, A.V. Kulkarni, Z.P. Luo, Transformation behaviour and unusual twinning in a NiTi shape memory alloy ausformed using equal channel angular extrusion, Philos. Mag. 85 (2005) 1729–1745. doi:10.1080/14786430412331331961.

[85] W.J. Moberly, J.L. Proft, T.W. Duerig, R. Sinclair, Deformation, twinning and thermo-mechanical strengthening of Ti50Ni47Fe3, Acta Metall. Mater. 38 (1990) 2601–2612. doi:10.1016/0956-7151(90)90272-I.

[86] O. Benafan, R.D. Noebe, S.A. Padula, D.J. Gaydosh, B.A. Lerch, A. Garg, G.S. Bigelow, K. An, R. Vaidyanathan, Temperature-dependent behavior of a polycrystalline NiTi shape memory alloy around the transformation regime, Scr. Mater. 68 (2013) 571–574. doi:10.1016/j.scriptamat.2012.11.042.

[87] V. Novák, P. Šittner, G.N. Dayananda, F.M. Braz-Fernandes, K.K. Mahesh, Electric resistance variation of NiTi shape memory alloy wires in thermomechanical tests: Experiments and simulation, Mater. Sci. Eng. A. 481–482 (2008) 127–133. doi:10.1016/j.msea.2007.02.162.

[88] P. Sedmak, P. Sittner, J. Pilch, L. Heller, J. Kopecek, J. Wright, P. Sedlak, M. Frost, Grain-resolved analysis of localized deformation in nickel-titanium wire under tensile load, Science. (2016).

[89] P. Sedmák, P. Šittner, J. Pilch, C. Curfs, Instability of cyclic superelastic deformation of NiTi investigated by synchrotron X-ray diffraction, Acta Mater. 94 (2015) 257–270.

[90] H.K. Yang, V. Doquet, Z.F. Zhang, Micro-scale measurements of plastic strain field, and local contributions of slip and twinning in TWIP steels during in situ tensile tests, Mater. Sci. Eng. A. 672 (2016) 7–14. doi:10.1016/j.msea.2016.06.064.

[91] E. Goo, K. T. Park, Application of the von Mises criterion to deformation twinning, Scr. Metall. 23 (1989) 1053–1056.

[92] M. Nishida, S. Ii, K. Kitamura, T. Furukawa, A. Chiba, T. Hara, K. Hiraga, New deformation twinning mode of B19′ martensite in Ti-Ni shape memory alloy, Scr. Mater. 39 (1998) 1749–1754.

[93] J.X. Zhang, M. Sato, A. Ishida, Deformation mechanism of martensite in Ti-rich Ti–Ni shape memory alloy thin films, Acta Mater. 54 (2006) 1185–1198. doi:10.1016/j.actamat.2005.10.046.

[94] T. Ezaz, H. Sehitoglu, W. Abuzaid, H.J. Maier, Higher order twin modes in martensitic NiTi—The (201¯) case, Mater. Sci. Eng. A. 558 (2012) 422–430. doi:10.1016/j.msea.2012.08.022.

[95] O. Benafan, Deformation and phase transformation processes in polycrystalline NiTi and NiTiHf high temperature shape memory alloys, University of Central Florida Orlando, Florida, 2012. http://etd.fcla.edu/CF/CFE0004496/Benafan_Othmane_201204_PhD_Final.pdf (accessed November 9, 2016).

[96] J. Pilch, L. Heller, P. Sittner, Final thermomechanical treatment of thin NiTi filaments for textile applications by electric current, in: EDP Sciences, 2009. doi:10.1051/esomat/200905024.

[97] J. Pilch, P. Sittner, Method of heat treatment and/or inspection of functional mechanical properties, particularly transformation strain and/or strength, of shape memory alloy filaments and apparatus for the application of this method, US20120018413 A1, 2012. http://www.google.com/patents/US20120018413 (accessed November 9, 2016).

[98] G. Tan, Y. Liu, P. Sittner, M. Saunders, Lüders-like deformation associated with stress-induced martensitic transformation in NiTi, Scr. Mater. 50 (2004) 193–198. doi:10.1016/j.scriptamat.2003.09.018.

[99] P. Sittner, Y. Liu, V. Novak, On the origin of Lüders-like deformation of NiTi shape memory alloys, J. Mech. Phys. Solids. 53 (2005) 1719–1746. doi:10.1016/j.jmps.2005.03.005.

[100]M.A. Iadicola, J.A. Shaw, Rate and thermal sensitivities of unstable transformation behavior in a shape memory alloy, Int. J. Plast. 20 (2004) 577–605. doi:10.1016/S0749-6419(03)00040-8.

[101]Q.-P. Sun, Z.-Q. Li, Phase transformation in superelastic NiTi polycrystalline micro-tubes under tension and torsion—-from localization to homogeneous deformation, Int. J. Solids Struct. 39 (2002) 3797–3809.

[102]E. Pieczyska, H. Tobushi, K. Date, K. Miyamoto, Torsional deformation and fatigue properties of thin niti sma strip, J. Solid Mech. Mater. Eng. 4 (2010) 1306–1314.

[103]D. Favier, H. Louche, P. Schlosser, L. Orgéas, P. Vacher, L. Debove, Homogeneous and heterogeneous deformation mechanisms in an austenitic polycrystalline Ti–50.8 at.% Ni thin tube under tension. Investigation via temperature and strain fields measurements, Acta Mater. 55 (2007) 5310–5322. doi:10.1016/j.actamat.2007.05.027.

[104]M. Kimiecik, J. Wayne Jones, S. Daly, Grain orientation dependence of phase transformation in the shape memory alloy Nickel–Titanium, Acta Mater. 94 (2015) 214–223. doi:10.1016/j.actamat.2015.04.026.

[105]M. Kimiecik, J.W. Jones, S. Daly, Quantitative Studies of microstructural phase transformation in Nickel–Titanium, Mater. Lett. 95 (2013) 25–29. doi:10.1016/j.matlet.2012.12.063.

[106] H.M. Paranjape, P.P. Paul, H. Sharma, P.Keneser, J.-S. Park, T.W. Deurig, L.C. Brinson, A.P. Stebner, Influences of granular constraints and surface effects on the heterogeneity of elastic, superelastic, and plastic responses of polycrystalline shape memory alloys, J. Mech. Phys. Solids, 102 (2017), 46-66. doi:10.1016/j.jmps.2017.02.007

[107] G. Winter, J.P. Wright, S. Schmidt, J. Odershedde, Grain interaction mechanisms leading to intragranular orientation spread in tensile deformed bulk grains of interstitial-free steel, Int. J. Plast. 88 (2017) 108-125, doi:10.1016/j.ijplas.2016.10.004

[108]P. Sedmak, P. Sittner, J. Pilch, MA2900 experiment at ID11 ESRF, 2017

[109] P. Shayanfard, L. Heller, J. Stanek, L. Petrich, V. Schmidt, P. Sittner, FEM simulation of mechanical behavior of polycrystalline materials based on realistic reconstruction of their grain boundaries from incomplete 3D-XRD data, 2017 ,in preparation.

[110] M. Frost, P. Sedlak, P. Sedmak, P. Sittner Experimentally motivated numerical reconstruction of macroscopic martensitic transformation front in NiTi superelastic wires, Proceedings of VIII ECCOMAS Thematic Conference on Smart Structures and Materials, SMART 2017, A. Guemes, A. Benjeddou, J. Rodellar and J. Leng (Eds), p. 1491-1501.

[111] P.Sittner, P. Sedlak, H. Seiner, P. Sedmak, J. Pilch, R. Delville, L.Heller, L. Kaderavek, On the coupling between martensitic transformation and plasticity in NiTi: experiments and continuum based modelling, Prog. Mater Sci., 2017, submitted

[112] L. Heller, H. Seiner, P. Sittner, P. Sedlak, O. Tyc, L. Kaderavek, On the plastic deformation accompanying martensitic transformation in thermomechanically loaded NiTi, 2017, in preparation.

[113] L. Heller, P. Šittner,P. Sedlák, O. Tyc, L. Kadeřávek, M.Klementová,, On the temperature dependence of NiTi mechanical behavior due to coupled transformation-plasticity, 2017, in preparation